UNIVERSIDADE DO PORTO

FACULDADE DE ENGENHARIA

Master's Thesis

All-solid-state sodium ion structural batteries

Henrique Carvalho Vaz Barreira

Supervisors:

Federico Danzi, PhD.

Prof. Joana Oliveira, PhD.

Masters in Mechanical Engineering - Aeronautical and Vehicular Structures

MEM

DEPARTAMENTO DE ENGENHARIA MECÂNICA

Faculdade de Engenharia

September, 2023

Candidate: Henrique Carvalho Vaz Barreira, No. 201806197, 201806197@up.pt

Scientific Guidance: Federico Danzi, PhD., fdanzi@inegi.up.pt

Scientific Co-Guidance: Joana Oliveira, PhD., jespain@fe.up.pt

U.PORTO

FEUP FACULDADE DE ENGENHARIA
UNIVERSIDADE DO PORTO

DEPARTAMENTO DE ENGENHARIA MECÂNICA

Faculdade de Engenharia

Rua Dr. Roberto Frias, Porto

September, 2023

Acknowledgements

I would like to begin by thanking my supervisors, Professor Federico Danzi and Professor Joana Oliveira, whose contribution and fuidance throughout the development of this thesis was essential for all stages of the developed work.

A special acknowledgment to INEGI and in particular the UMEC section, who was always available with materials essential to the experimental part of the work. Also, special thanks to the FEUP's Department of Physics Engineering and close collaboration with FCUP and IFIMUP's laboratory, where the work conducted by its associates was a valuable help to the development of this thesis.

I would also like to thank all of my friends and course colleagues who accompanied me throughout these five years of college, in particular to Sofia who provided much needed support.

At last, a big thank you for my family for providing me with all the necessary tools to accomplish academic success and fulfilment.

Abstract

The drive towards more sustainable and efficient energy storage systems has become a vital aspect of modern engineering, particularly in the aeronautical and transportation industries. The integration of structural batteries has been put forward as a promising solution to address the dual challenge of weight reduction and energy storage demands in these industries. Focusing on mobile applications, weight reduction plays a crucial role in achieving superior performance and efficiency. Conventional solutions based on separating energy storage and structural components often lead to increased weight and complexity. By incorporating sodium-ion structural batteries, a unified design can lead to significant weight saving and streamlined structures, which in its turn results in increased fuel efficiency and extended range of electric vehicles and aircraft. Beyond these advantages, the environmental benefits of sodium-ion structural batteries present a compelling case for their widespread use. Sodium, being an abundant and naturally occurring element in the earth's crust, offers a sustainable and cost-effective alternative to the resource-demanding materials used in traditional batteries. By getting rid of toxic elements and reducing the widespread use of rare earth metals, sodium-ion structural batteries mitigate environmental degradation and contribute to a greener energy landscape. Moreover, the advantage of having high-voltage sodium-ion structural batteries without the inclusion of metal sodium lies in the elimination of any safety risks. Metal sodium is highly reactive and can lead to hazardous side reactions, such as dendrite formation and electrolyte decomposition, which may result in battery instability and safety concerns. By eliminating the need for metallic sodium, these batteries can achieve higher levels of safety, reducing the likelihood of thermal runaway and potential fire hazards.

This work begins with a review on the current literature available for sodium ion batteries, as well as the state of the art in the development of all-solid-state batteries. An overview of the current progress on structural batteries was also done, to ensure a better understanding as to why specific materials were chosen in place of other possible candidates.

The experimental section focuses on developing a novel sodium-ion structural battery, with metal-free electrodes, encapsulated in high structural performance materials like structural resin and glass fibres. The binding agent at the interface between electrodes and solid-state electrolyte plays a key role in ensuring the functionality and long-term stability of solid-state batteries. This component acts as a cohesive agent, firmly bonding the electrodes to the solid electrolyte, which is crucial for maintaining excellent ionic conductivity and electron transport across the interface. From the structural standpoint, a weak binding

agent can lead to a compromised mechanical integrity of the battery, originating delamination and the loss of structural cohesion. Common solid-state batteries binding agents include polymers. In this work it was shown for the first time, to the best of our knowledge, that including structural resin in a polymer binding agent, depending on the composition percentage, provides not only electrochemical stability but also mechanical integrity, as well as an insulating role.

The feasibility and success of such innovations were assessed through a series of electrochemical tests, such as electrochemical impedance spectroscopy and charge and discharge cycles, as well as destructive tests to infer the state of the different contact surfaces. The results provided a clear understanding of the beneficial effect of the structural resin in the cell's electrochemical behaviour, as well as the advantages of utilising glass fibres as encapsulating agents.

In conclusion, this research boosts the development of high voltage all-solid-state sodium-based batteries with metal-free electrodes. Moreover, the success of including structural elements such as epoxy and glass fibres onto the structure opens a pathway for the enhancement of its mechanical properties, as well as enabling more sturdy and sustainable structural batteries.

Keywords: Nasicon, Structural Resin, Glass Fibres, Hard Carbon, SIB, Structural Battery, Vanadium Phosphate.

Resumo

A procura por sistemas de armazenamento de energia mais sustentáveis e eficientes tornou-se um aspeto crucial da engenharia moderna, especialmente nas indústrias aeronáutica e de transporte. A integração de baterias estruturais tem sido apresentada como uma solução promissora para enfrentar o duplo desafio de redução de peso e necessidade de armazenamento de energia nessas indústrias. No contexto de aplicações de mobilidade, a redução de peso tem um papel crucial para alcançar um desempenho e eficiência superiores. Soluções convencionais que se baseiam na separação do armazenamento de energia e dos componentes estruturais frequentemente resultam num aumento de peso e complexidade. Ao incorporar baterias estruturais de iões de sódio, um projeto unificado pode levar a uma significativa redução de peso e a estruturas mais simples, o que, por sua vez, resulta numa maior eficiência de combustível e aumento do alcance para veículos e aeronaves elétricas. Além dessas vantagens, os benefícios ambientais das baterias estruturais de iões de sódio apresentam um caso sólido para o seu uso generalizado. O sódio, sendo um elemento abundante e naturalmente presente na crosta terrestre, oferece uma alternativa sustentável e económica aos materiais que exigem recursos implementados em baterias tradicionais. Ao eliminar elementos tóxicos e reduzir o uso de metais raros, as baterias estruturais de iões de sódio contribuem para a uma maior redução da degradação ambiental e para um uso da energia de forma mais sustentável. Além disso, a vantagem de ter baterias estruturais de iões de sódio de alta tensão sem a inclusão do sódio metálico reside na eliminação de potenciais riscos de segurança. O sódio metálico é altamente reativo e pode levar a reações secundárias perigosas, como a formação de dendritos e a decomposição do eletrólito, o que pode resultar em instabilidade e problemas de segurança na bateria. Ao eliminar a necessidade de sódio metálico, essas baterias podem alcançar níveis mais altos de segurança, reduzindo a probabilidade de sobreaquecimento e potenciais riscos de incêndio.

O presente trabalho começa com uma revisão da literatura atual disponível sobre baterias de iões de sódio, bem como o estado-da-arte no desenvolvimento de baterias totalmente no estado sólido. Foi também realizada uma revisão geral dos avanços atuais em baterias estruturais, a fim de garantir uma melhor compreensão das razões pelas quais determinados materiais foram implementados em detrimento de outros possíveis candidatos.

A seção experimental concentra-se no desenvolvimento de uma nova bateria estrutural de iões de sódio, com elétrodos livres de metal, encapsulados em materiais de alta performance estrutural, tais como uma resina estrutural e fibras de vidro. O agente de ligação na interface entre os elétrodos e o eletrólito sólido desempenha um papel fundamental para

garantir a funcionalidade e a estabilidade de longo prazo das baterias no estado sólido. Este componente atua como um agente coesivo, ligando firmemente os elétrodos ao eletrólito sólido, o que é crucial para manter uma excelente condutividade iônica e transporte de elétrodos através da interface. Do ponto de vista estrutural, um agente de ligação fraco pode comprometer a integridade mecânica da bateria, originando delaminações e perda de coesão estrutural. Os agentes de ligação comuns para baterias sólidas incluem polímeros. Neste trabalho, foi demonstrado pela primeira vez, até onde o autor tem conhecimento, que a inclusão de resina estrutural como agente de ligação polimérico, dependendo da porcentagem de composição, proporciona não apenas estabilidade eletroquímica, mas também integridade mecânica e um papel isolante.

A viabilidade e o sucesso destas inovações foram avaliados por meio de uma série de testes eletroquímicos, tais como espectroscopia de impedância eletroquímica e ciclos de carga e descarga, bem como testes destrutivos para inferir o estado das diferentes superfícies de contato. Os resultados forneceram uma compreensão clara do efeito benéfico da resina estrutural no comportamento eletroquímico da célula, bem como das vantagens de utilizar fibras de vidro como agentes encapsulantes.

Em conclusão, esta pesquisa impulsiona o desenvolvimento de baterias de sódio no estado sólido de alta voltagem com elétrodos livres de metal. Além disso, o sucesso da inclusão de elementos estruturais, como resina epoxy e fibras de vidro, na estrutura, abre caminho para o melhoramento das suas propriedades mecânicas, além de possibilitar baterias estruturais mais robustos e sustentáveis.

Palavras-Chave: Nasicon, Resina Estrutural, Fibras de Vidro, *Hard Carbon*, Baterias de Ião de Sódio, Baterias Estruturais, Fosfato de Vanádio.

Contents

List of Figures

List of Tables

List of Acronyms

ASSSIB	All-Solid-State Sodium Ion Battery
CNT	Carbon Nano-Tubes
EIS	Electrochemical Impedance Spectroscopy
HC	Hard Carbon
ICE	Initial Coulombic Efficiency
LIB	Lithium Ion Batteries
NASICON	Sodium Ionic Super Conductor
PBA	Prussian Blue Analogue
SEI	Solid Electrolyte Interface
SIB	Sodium Ion Batteries
SSE	Solid State Electrolytes

Chapter 1

Introduction

Since the 19th century, starting with the Industrial Revolution, humanity has increasingly relied on non-renewable sources of energy to fulfill its daily requirements, ranging from basic gas-powered heaters to massive aircraft like the 285-ton *Antonov An-225 Mriya*. However, and as the name suggests, these sources are not infinitely available, with researchers predicting that oil, gas and coal will run out in 35, 37 and 107 years, respectively [1]. For these reasons, alternative sources of energy need to be employed. The electrification of the world, originating from renewable sources of fuel, is a step forward in the direction of preserving the planet's resources.

Replacing hydro carbonated fuels by electrical power is not something new, with the first electric vehicles appearing on scene around the beginning of the 19 $^{\text{th}}$ century. However, only recently this technology was employed at larger scales trying to be the alternative to fossil fuels, namely in the transportation industry. In 2010, the share of electric cars in the global market represented less than 0.1% of the world's car fleet, with the share increasing to 4.6% in 2020, according to the International Energy Agency [2], showing that despite the progress being made, it is still far from replacing fossil fuels.

An important step to achieve this electrification is the development and fabrication of batteries that can be considerably less harmful to the environment than fossil fuels, being used to store energy from clean sources. Lithium Ion Batteries (LIB), so far, have been the most used energy storage systems implemented to achieve this objective, due to their presented high energy density, durable and reliable cycle lives and also high electrical potential difference [3]. Despite providing a short term solution for an alternative to fossil fuels, in the long turn, the extraction of lithium to manufacture these batteries may be just

as detrimental to the planet's resources as is the use of fossil fuels. The major problem with lithium extraction is that, due to its diminished presence in the earth's crust (0.002-0.006 wt%), the methods for extraction are harmful to the environments where it is located. With the main drawbacks being the immense water consumption (for a tonne of lithium, up to 2 million of liters of water may be needed [4]), lithium extraction has an intrinsic high risk of leaving the soil unusable and also toxic spillage to the surrounding environment being all real possibilities. For these reasons, more sustainable alternatives need to be found.

With this in mind, the introduction of Sodium Ion Batteries (SIB) may be a viable solution to overcome the issues related with lithium mining. With sodium belonging to the same main group as lithium in the periodic table, alkali metals, they share most of the their electrochemical properties and also behaviour in terms of battery properties. Adding to these, sodium is the sixth most abundant element on earth, with a content of 2.74 wt%, it makes it infinitely more feasible to extract than lithium. However, sodium ions possess larger atomic radius than lithium ones, meaning that larger resistances will need to be overcome during the migration process of the ions in the SIBs [5], resulting in slower kinetics and the need for different strategies so that sodium-based batteries can match the performances of lithium-based ones. For this to be possible, extensive work and research needs to be done to develop electrodes capable of providing said performances and as well to have an electrolyte that is compatible with the developed electrons and also meets safety requirements in terms of working conditions.

In this thesis, the use of a Sodium Ionic Super Conductor (NASICON) as a solid-state electrolyte will be explored for the development of an All-Solid-State Sodium Ion Battery (ASSSIB) with metal-free electrodes that can aspire to be a viable alternative for the conventional, but environmentally harmful, LIB. ASSSIB have already shown potential in form of improved safety, energy density and packaging efficiency when compared to lithium-ion and liquid-based sodium-ion batteries [6]. The first stages of the experimental procedures will consist on assessing the internal resistances of the solid state electrolyte, binding agent, carbon electrodes and current collectors in asymmetric capacitors to identify the most promising electrochemical cell design. With agreeable results, the full sodium-ion solid state cell was designed, assembled and tested, with a nasicon electrolyte and high voltage nasicon-type cathode. Finally, the use of a structural resin and fiber encapsulation underwent electrochemical tests and a full working solid-state sodium-ion structural battery was achieved and tested, with optimized design and assembling methods.

Due to the sequential nature of the experimental tests and the diversity of intermediary steps to be tested, in a completely new cell configuration from scratch, the results will be displayed following the logical sequence of events used throughout the testing and development phase.

Chapter 2

Sodium-Ion Structural Batteries

From a conceptual point of view, the functioning principles of a battery are simple. One needs electrons flowing from one electrode to another, as well as a separate channel for the flow of ions, in order for electricity to be generated. However, in practice, the process is extremely complex. A great deal of variables will affect the final performance of each energy storage system. In this section, a summary of the latest technology and developments to improve the performance of sodium-ion batteries will be displayed, as well as a look into the mechanical characterization of solid electrolytes, all-solid-state and structural batteries.

2.1 Battery Performance

Different tests are usually performed to obtain the battery performance parameters, with varying degrees of complexity and most of them can be performed using a potentiostat. A potentiostat is an analytical instrument, containing multiple internal circuits, designed to control the potential of a given cell's working electrode, generating and measuring potentials and currents. The main battery parameters are listed in Table 2.1.

2.1.1 Electrochemical Impedance Spectroscopy

One of the most used and most important tests performed is the Electrochemical Impedance Spectroscopy (EIS). EIS, as the name suggests, measures the internal impedance of a given electrical circuit. As is known, a circuit's electrical resistance is its resistance to the flow of

Table 2.1: Performance evaluating parameters

Parameter	SI Units	Description
Capacity	mAh g^{-1}	It allows to quantify how much energy is stored in the battery.
Energy Density	Wh kg^{-1} or Wh L^{-1}	Quantifies the amount of energy a given cell can store per unit of volume or weight.
Power Density	W kg^{-1} or W L^{-1}	Similar to the previous parameter, but instead of energy it is related to power.
Cycle Life	N	Measures the number of charge and discharge cycles a battery can undergo before having its capacity decrease to a certain predefined threshold.
Ionic Conductivity	S cm^{-1}	Parameter that characterizes the ion transport mechanism within the cell. It is expressed in Siemens per meter and is used to measure the true bulk resistance of the cell and depends on factors such as the cross sectional area of the polymeric film (A), the thickness (t) and the resistance of the polymeric film (R).

electrical current. It can be given through Ohm's law, being the ratio between the voltage, E, and current, I [7].

$$R = \frac{E}{I} \tag{2.1}$$

In battery research and development, however, utilizing complex impedance analysis is crucial, as opposed to solely considering real resistance, as it provides a more comprehensive understanding of battery behavior. Batteries exhibit dynamic electrical responses, encompassing not only resistive losses but also capacitive and inductive elements. Complex impedance spectroscopy captures these complexities, offering insights into charge transfer resistance, double-layer capacitance, and diffusion processes within the electrodes and electrolytes. By looking beyond real resistance, one can gain vital insights into the intricate electrochemical battery performance

EIS is in most cases quantified by measuring the current through a cell after having applied an AC (Alternate Current) potential to the said cell. Different elements of the cell can contribute to the EIS' observed spectrum, such as the electrode kinetics and the behaviour of the diffusion layer. The excitation applied is normally a sinusoidal potential wave, with the cell responding with an AC current signal. The sinusoidal excitation signal has the

following structure.

$$E_t = E_o \sin \omega t \tag{2.2}$$

where E_t represents the potential at time t, E_o is the amplitude of the signal and ω is the radial frequency. The corresponding AC current signal will be shifted in phase (ϕ) and possesses a different amplitude, I_t, than the initial one, I_o, depending on the excited electric component.

$$I_t = I_o \sin \omega t + \phi \tag{2.3}$$

Using Ohm's law once again, it is possible to extract the new formula for the impedance (Z) of a given cell.

$$Z = \frac{E_t}{I_t} = \frac{E_o \sin \omega t}{I_o \sin \omega t + \phi} = Z_o \frac{\sin \omega t}{\sin \omega t + \phi} \tag{2.4}$$

By doing some mathematical manipulations, one can obtain the impedance as a complex number, where Z_0 is the impedance's magnitude and ϕ the phase shift.

$$Z(\omega) = \frac{E}{I} = Z_o exp(j\phi) = Z_o(\cos \phi + j \sin \phi) \tag{2.5}$$

In terms of visual representation, due to the impedance having a real and an imaginary part, a Nyquist plot or a Bode diagram are typically employed. In a Nyquist plot the real part of the impedance plotted on the X-axis and the imaginary part on the Y-axis. Each point in the plot is the impedance at a given frequency, with it increasing from the right to the left of the diagram. Depending on the cell's configuration, the plot can consist of one or several semicircles. These semi-circles result from a predefined modeled equivalent circuit. One major drawback of this type of representation is that the user cannot determine at which given frequency a dot is obtained just by looking at the plot. Nonetheless, the nyquist plot can provide crucial information regarding the interface layers and diffusion mechanisms within the electrical component. For this reason, the nyquist plot is the best option for visual representation when leading with battery configurations.

The other alternative is to use the Bode Diagram. This representation does allow the user to have information about the frequency that a given point was subjected to, being therefore useful in applications where one wants to know when the system becomes unstable. The impedance is displayed using a logarithmic scale on the X-axis and both the phase shift (ϕ) and the absolute value of the impedance shown in the Y-axis.

Despite being a quick experiment to conduct an EIS, post-processing phase can be more complex and require high level of experience. There is the need to model an equivalent circuit that represents the entire system of the electrochemical cell [8] in order to infer and understand the mechanisms going on in the said electrochemical cell. Electrical circuit elements need to be implemented in order to fully simulate mechanisms happening in the

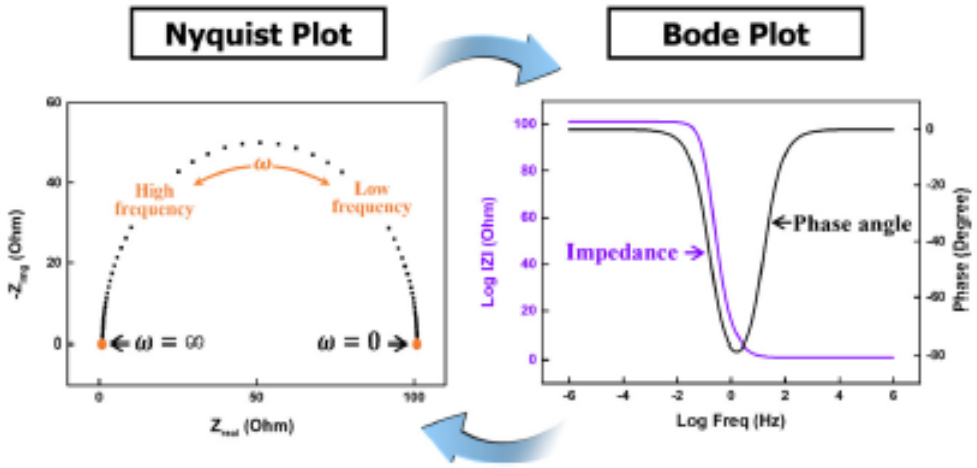

Figure 2.1: Representation of an EIS through the Nyquis pot (left) and the Bode plot (right) [8].

cell. Table 2.2 lists the equivalent elements typically used to model the equivalent circuit of the electrochemical cell.

Table 2.2: Circuit elements used in the equivalent circuit model

Equivalent Element	Formula
R (Resistance)	R
C (Capacitance)	$1/(j\omega\ C)$
W (Warburg Impedance)	$\sigma\ \omega^{-1/2}$ - $j\sigma\ \omega^{-1/2}$
CPE (Constant Phase Element)	$1/Q(j\omega)^{\alpha}$

Where the resistance (R) is used to represent inter-facial resistance between the solid electrolyte and the bulk ionic resistance of the electrolyte. The capacitor (C) models the charge accumulation and depletion happening at the electrolyte/electrode inter-face. Constant phase elements (CPE) are used for non-ideal capacitors, mainly due to possible porosity of the electrochemical materials. Finally, the warburg (W) element is used for resistances that occur due to diffusive processes [9].

Elements such as the constant phase element (CPE) and the Warburg (W) impedance need to be implemented to describe more complex mechanisms of the cell. The CPE is used to model behaviours that have a non ideal capacity characteristics, such as the electric double layer present in the interface between the electrode and the electrolyte. The Warburg impedance is used to represent the diffusion processes.

2.1.2 Galvanostatic Charge and Discharge Process

This type of test consists in charging an electrochemical cell to a predefined plateau of tension and/or charging time, using constant current, and then letting the cell discharge

until it reaches its minimum threshold,with a constant charge, in a so-called galvanostatic process.

The test will allow the cell's cycle life and efficiency to be measured, as well as the quantification of the number of cycles of charge/discharge a cell can withstand before starting to experience a notorious decrease in its performance.

2.2 Sodium-Ion Batteries

As previously mentioned, the recent surge in interest for sodium-ion batteries, Fig. 2.2 displays an illustration of the system, stems from the need for alternatives to lithium-ion batteries for large-scale energy use. In terms of the storage mechanisms for the ions and also the intercalation chemistry regarding cathode materials, SIB shares most of its characteristics with the lithium-based counterpart, making it possible to utilise some of the existent technology of the lithium-based batteries. On the other hand, glaring differences can be observed between the two concepts, that will in its turn require a different approach to the methods employed to manufacture the cells.

Na^+ ions (1.02 Å) present a considerably larger ionic radius when compared to Li^+ ions (0.76 Å), which in turn results in disturbances in the phase stability, transport properties and inter-phase formation [10]. Adding to this, sodium itself is heavier than lithium (23 g/mol versus 6.9 g/mol) and has a higher standard electrode potential (-2.71V vs. SHE (standard hydrogen electrode) versus -3.02 vs. SHE, for lithium), meaning that SIBs will have difficulties matching LIBs in terms of energy density [10].

The development of cathodes, anodes and electrolytes capable of yielding similar results to LIBs have seen an exponential rise in the past few years in terms of resources and time devoted to its study. In terms of cathode materials, the industry has been able to achieve satisfactory results by employing, for example, Prussian Blue Analogue (PBA) cathodes, Layered Oxide cathodes and Nasicon-type cathodes such as vanadium phosphate (NVP) based ones. However, in terms of anodic materials, there is a struggle to achieve compounds capable of satisfactory Na voltage storage and high structural stability. For example, recent studies discovered that graphite, the most commonly used material for LIBs, does not allow the intercalation for Na [11]. For this reason, non-graphitic components, such as Hard Carbon, have been subject of extensive research as possible anodes for SIBs [11]–[13]. In terms of electrolytes, research is steering towards solid eletrolytes in order to address the safety issues arisen by the use of organic liquid eletrolytes, such as $NaClO_4$ or $NaPF_6$ [10]. All of these topics will be further detailed on the following sections.

2.2.1 Anode Materials

In a battery, the anode is where the oxidation reactions occur when the battery is discharging and it is responsible for providing the electrons that will subsequently flow through an

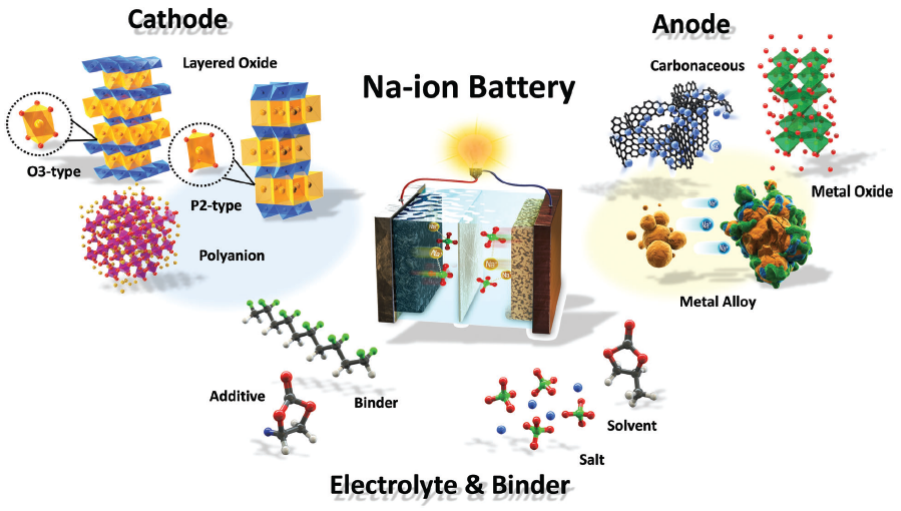

Figure 2.2: Illustration of a Na-ion battery system [10].

external circuit. For SIBs, the most common mechanism involved in anode oxidation/reduction is the desodiation/sodiation process. There are three major processes responsible for the desodiation/sodiation process: insertion, conversion and alloying reaction.

2.2.1.1 Oxide Based Materials

The first category of anodes for sodium ion batteries materials are based either on intercalation mechanisms, or on conversion based mechanisms. In intercalation based anodes, the metal based atoms are always transitioning between the inside and the outside of the crystal lattice. Fig 2.4 displays the difference between sodium and potassium based cells with intercalation-based mechanisms. In conversion based anodes, the reactions occurring in the structure lead to chemical transformations of the atom species into host lattices to form new compounds [10]. Some oxide based materials combine both intercalation and conversion mechanisms.

Titanium Based Oxides

The use of oxide-based material as anodes has some disadvantages due to the low operational potential used. Safety issues in the form of metallic sodium plating and dendrite formation led to the use of titanium-based oxides, which are part of the insertion-based materials, becoming more attractive and investigated. The use of these compounds arise from the redox couple ($Ti^{4+/3+}$) present in sodium cells, as well as their reasonable operating voltage and relative cost.

I. **Titanium dioxides**

   Titanium dioxides (TiO_2) have been researched as possible anodes for SIBs due to their high theoretical capacity (335 mAh g^{-1}), high rate performance, low cost and

non-toxicity [14]. These dioxides can be divided into Rutile and Anatase, its crystalline structures displayed on Fig. 2.3, with the latter receiving increased attention due to the fact that its activation barrier for sodium ion insertion into the lattice is comparable with the values observed for lithium-based cells [10].

Experimental evidence shows that the sodium storage mechanisms for titanium oxides experience stagnant kinetics due to the aforementioned larger ionic radius of the sodium-ions. To address this issue, several strategies were developed, such as the modification of the nano-scale architecture by employing metallic titanium and also the introduction of carbon additives that improve overall conductivity. For example, Chen's group [15] was able to synthesize a chemically bonded graphene-TiO_2 that displayed the best rate capability when compared to available literature based on titanium anodes.

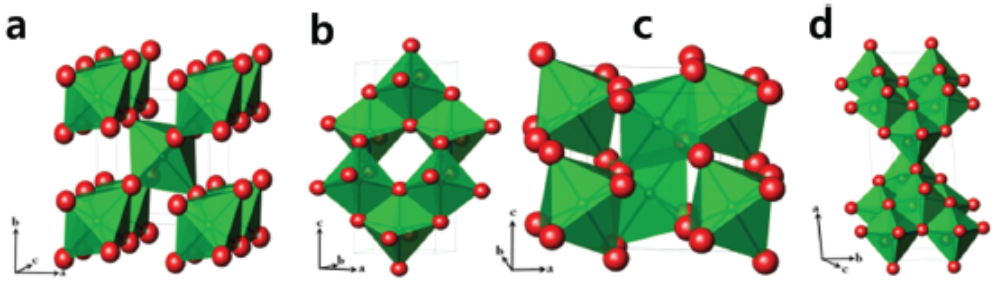

Figure 2.3: Crystal structures of Titanium dioxide. (a) Rutile, (b) Anatase, (c) Bronze and (d) Brookite [10].

II. **Lithium Titanite**

Lithium titanite ($Li_4Ti_5O_{12}$), also known at the "zero-strain" anode material, has already been deeply investigated for long-life stationary LIBs and is considered to be one of the most promising anodes for use in SIBs. When incorporated in sodium-ion batteries, studies have shown that lithium titanite shows a relatively stable specific capacity (155 mAh g^{-1}) with great coulombic efficiency (>99%), sodium storage voltages of 0.93V and current rate of 0.1C [15]. The experienced sodium storage voltage is higher that the one where there is deposition of sodium metal, therefore making this anode safer than HC.

However, there are drawbacks when incorporating lithium titanite in SIBs. It is observed a three-phase separation that will cause the anode to crack and delamination from the current collector to occur, leading to poor cycle life.

III. **Sodium Titanite**

There are different compounds of sodium titanite, with the most investigated one being $Na_2Ti_3O_7$. The main advantage of this compound comes from its ability to operate at low potential levels. Xu *et al.* [16] shed some light on the mechanisms

for this type of sodium titanite and reported that this oxide based material could exchange, in a non-permanent way, sodium-ions to provide the low voltage operating potential mentioned before. Structural instability was also discovered due to electrostatic repulsion stemming from the intercalation of sodium ions in the layered oxide structure.

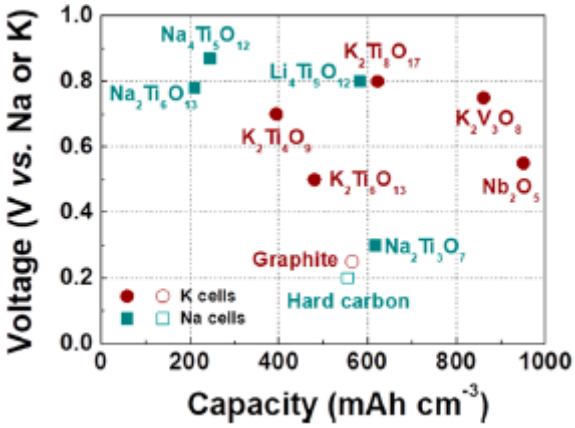

Figure 2.4: Capacity-voltage plot for intercalation-based anodes for Sodium and Potassium-Ion cells [17].

Optimizing strategies, such as carbon coating of the oxide have been developed and yielded satisfactory results, with improvement of the cyclability and coulombic efficiency.

Transition Metal Based Oxides

These types of oxides are inserted in the category of conversion materials. The main feature linked to these materials is the potential for high specific capacities. In practice, these materials suffer from phenomena like large volume expansion and contraction during the sodiation/desodiation process leading to deterioration of the electrodes and consequent rapid capacity fading [10]. There have been recently proposed methods to overcome these issues, such as carbon coating of the materials and improvements in the nano-scale structure.

I. **Iron Oxides**

Komaba and colleagues [18] first reported the use of iron oxides as anodes back in 2010, when they conducted the electrochemical insertion of sodium ions into nanocrystalline structures of Fe_3O_4, in the voltage range of 1.2-4.0V. The authors presented, by cycling tests, that the structure displayed excellent capacity retention for the transferred sodium ions. More recent studies achieved better performances using hybrid carbon-nanosheets [19]. The sodium storage mechanism in iron oxides is believed to be achieved by the reversible conversion reaction, with the Na_2O matrix being impregnated by iron nanoparticles [10].

II. **Cobalt Oxides**

Cobalt oxides (Co_3O_4) have been demonstrated to suffer the reversible conversion reaction mechanism through the formula: $Co_3O_4 + 8\,Na^+ \longrightarrow 4\,Na_2O + 3\,CO$. Research done by Rahman *et al.* [20] highlighted the possibility that the previously mentioned conversion reaction is not fully completed in the first observed discharge to 0.01V. After 50 cycles, the results obtained showed a reversible capacity of 447 mAh g^{-1} and about 86% capacity retention after 50 cycles.

Strategies for the optimization of the structures were also employed, mainly through using Carbon Nano-Tubes (CNT) as additives for the anode material. The main advantages observed were the reduction in the times of ion transfer paths, the decrease in the overall stress/strain during the sodiation/desodiation process and the enhanced electrical conductivity [10], being however every time and cost consuming.

III. **Tin Oxides**

The use of tin oxides, such as SnO and SnO_2, have been proposed in recent years. Research has shown that, when the sodium-ions are inserted onto the tin oxide's structure, a displacement-reaction occurs, and Na_xSn amorphous particles are formed. This will lead eventually to the volume expansion of the nanowires present in the structure during sodiation. These factors will lead later on to the rise of the total electrical impedance, contributing to the downfall of the cell's performance.

To overcome this, strategies such as N-doped graphene coupled with SnO_2 [21] were developed to improve the overall behaviour. This specific method was able to achieve excellent capacity retention and good initial reversible capacity (339 mAh g^{-1} at 20 mA g^{-1}).

IV. **Copper Oxides**

The final oxide proposed is the copper based oxide (Cu_xO). The attractions for its use originate from the copper's abundant presence in the earth's crust, meaning relative low costs of manufacture. Also, it has been reported that these oxides present good chemical stability and theoretical capacity.

Studies conducted by Liu *et al.* [22] observed the changes and the evolution of CuO nanowires during the sodiation process. Based on the results obtained, the authors were able to discern that the sodiation process is made up of three steps. Each step consisted of different sodiated products, such as Cu_2O and Na_2O for the first step, NaCuO for the second and $Na_6Cu_2O_6$, Na_2O and Cu for the final step.

Copper based oxides suffer the same problem as the other oxides. They are severely affected by the volume changes during the sodiation process, with solutions such as the incorporation of carbon in the structures being proposed to address this issue.

2.2.1.2 Alloy Reaction Based Materials

Another possible subcategory for anodes is based on the alloying reaction to the sodiation/desodiation process. Alloying materials share the same advantageous feature of the conversion-based materials, in the ability to store a considerable amount of sodium ions using a relatively low operating voltage. Several materials have been identified as possible candidates, and Antimony (Sb), Phosphorous (P) and Tin (Sn) are amongst the most promising alloy-based anode materials for SIBs.

Antimony (Sb)

If engineered correctly, the use of antimony as anode can originate an excellent theoretical capacity of 660 mAh g^{-1}. For this is required to be verified the formation of Na_3Sb at the fully sodiated state [10].

Darwiche's group [23] discovered that the process of alloying/dealloying in sodium-based cells is much more complex that of their lithium counterpart. The intermediate phases encountered for Na cells revealed to be mostly amorphous and could not be identified precisely. However, the authors developed the theory that these undefined intermediate phase may be responsible for the improved cycling of the Na-Sb reactions. This is due to the intermediate phase acting as a buffer and henceforth alleviating the strain experienced. The downside is the enormous volume changes experienced during the alloying processes, with changes coming at around 390%. To overcome this issue, research over the past few years has focused on developing nanostructures of the active materials and incorporating carbon-based additives in order to improve conductivity [24], [25].

Phosphorous (P)

Theoretically, among the high-capacity anodes for SIBs, phosphorous in the form of Na_3P presents the highest theoretical capacity of 2596 mAh g^{-1} [26], making its use as anode very appealing.

Phosphorous exists in the form of three allotropes: Black, Red and White (see Fig 2.5). White phosphorous is extremely volatile with the atmosphere, as well as toxic, making it not a good candidate for anode applications. Nonetheless, the other two allotropes show remarkable characteristics.

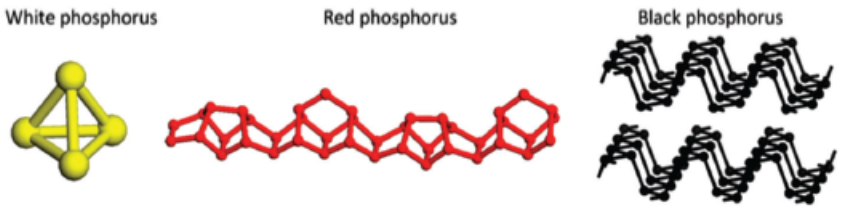

Figure 2.5: Illustration of the structure for each allotrope of Phosphorous [10].

I. **Red Phosphorous**

This allotrope possesses the advantage of being commercially available and is environmentally friendly. However, it suffers from low electrical conductivity and, being an alloying material, experiences massive volume changes (around 400%) which leads to the growth of the SEI.

These issues can be tackled by incorporating carbon composites into the red phosphorous' nanostructure. The inserted carbon matrix can therefore increase the poor electrical conductivity and limit the volume changes. Liu *et al.* [27] proposed the encapsulation of red phosphorous nanoparticles into porous nitrogen-doped carbon nanofibres. The results obtained were highly satisfactory, with an ultra long cycle life (81% retention over 1000 cycles), high-rate capability (637 mAh g^{-1} at 500mA g^{-1}) and great reversible capacity. Despite the good results, the practical feasibility of employing these strategies to large-scale use are low, due to highly costly carbon nanomaterials used. For this reason, the other phosphorous allotrope, black-P, may be a more suitable solution.

II. **Black Phosphorous**

Black phosphorous presents itself as the most stable, thermodinamically wise, allotrope. It has the advantage of possessing a relatively high bulk electronic conductivity. To enhance its performance, some strategies have been defined.

Mulder *et al.* [26] fabricated a high-performance anode based on a black phosphorous and carbon composite. Unlike in the example for the red phosphorous, the authors were able to synthesize the composite using a cost-effective mechanical ball milling process. The choice of incorporating carbon comes from evidence suggesting that the intimate contact between carbon and black-P leads to high cycling stability in SIBs and therefore better overall performance of the cell. The results obtained showed excellent capacity retention and cycling stability (1381 mAh g^{-1} in 100 cycles accounting for 90.5% of the initial reversible capacity), as expected. These results when coupled to the overall cost and practicality of the whole sintering process, makes carbon and black-P composites very attractive as use for anodes in SIBs.

Tin (Sb)

Over the past few years, the use of tin as an anode material for sodium-ion batteries has received increased attention. After progressing through the different steps in the sodiation process ($Sn \longrightarrow NaSn_5 \longrightarrow NaSn \longrightarrow Na_9Sn_4 \longrightarrow Na_{15}Sn_4$) [10], it is expected that, on the fully sodiated state, tin-based anodes can achieve theoretical specific capacity values in the orders of 847 mAh g^{-1}. As is the case as the two alloying-based anodes seen previously, tin will also suffer from debilitating volume changes during the alloying and dealloying phases.

For this reason, optimizing strategies are focusing on buffering and preventing volume changes. Incorporating carbon nanostructures have been proven as efficient techniques to address this issue. Liu's group [28] was able to introduce nanometer-sized tin nanodots into porous nitrogen-doped carbon nanofibres, using thermal based techniques and electrospinning. The results achieved impressive reversible capacity (633 mAh g^{-1} at current density of 200 mA g^{-1}). Moreover, the use of the porous nitrogen-doped carbon matrix proved to be effective in the prevention of large volume variation in the tin nanodots. The use of carbon also has the advantage of functioning both as conductive material and current collector, improving the energy density by lowering the total assembly's weight.

2.2.1.3 Carbon Based Materials

The most promising sub-category of anodes is based on the insertion reaction. Anodes composed of carbon materials are among the most widely used anode materials for SIBs and other alkali-based batteries due to their relative low cost [17]. Carbon based anodes consist of three different types of materials: graphite, soft carbon and hard carbon.

Graphite

When the process of identifying possible anodes for SIBs began, graphite was thought to be one of the most suitable candidates. This is due to the fact that it is the most widely applied anodic material for LIBs [11]. However, when tests were performed, researches reached the conclusion that sodium ions do not intercalate with graphite. A possible explanation for this phenomena may be related to the ionization energy of the sodium metal [17], as well as the larger ionic radius of Na^+ when compared to its lithium counterpart.

Some solutions have been found, such as the use of sodium-ion based solvents combined with pseudo-capacitive behaviours, with use of ether-based electrolytes [29]. However, the properties achieved using graphite based anodes can't compete with hard carbon based anodes, meaning that the employing of graphite for large-scale energy uses is less likely.

Soft Carbon

Soft Carbon is a type of amorphous carbon, manufactured through process of *pyrolisis*. It is a well suited candidate for anode material due to its low-cost, acceptable electrical conductivity and adjustable layer spacing [11]. For example, Li *et al.* [30] managed to develop a soft carbon anode derived from anthracite for room temperature SIBs and managed to achieve high sodium storage performance with superior cycling stability, as well as a reversible capacity of 222 mA g^{-1}. However, in practical application, this type of amorphous carbon experiences low energy density when employed in a full battery assembly. This is due to the fact that high operating voltage during the batteries' cycling can reduce

the working potential of the anode [11], making it a not so attractive candidate for anodes in SIBs.

Hard Carbon

As has been possible to see so far, the other two carbon based anode materials may not be well suited for the large-scale industrial use that will be required for SIBs. For this reason, hard carbon has attracted a lot of attention, and is by far the most promising anode for sodium ion based applications. The electrochemical performance and microscopical structure of the hard carbon is heavily influenced by the type of material it was originated by, as well as the carbonization temperature used. Hard Carbon (HC) can be synthesizes using the following materials.

I. Carbohydrate or other organic polymers, for example, sucrose and sugarcane bagasse.

II. Biomass source, such as algae, rice-husk or shaddock peels.

III. Resin carbon, with the likes of phenolic resin being used.

Another factor that influences the behaviour of the carbon-based anode is the structure of the hard carbon. HC can be generated through a form of thermosetting precursor that undergoes solid phase carbonization during the pyrolisis process [11] (see Fig. 2.6), with pyrolisis being the process of converting biomass to an intermediate product through the heating of the biomass in the absence of oxygen [31]. When using carbohydrates as the thermosetting precursor, the hydrogen and oxygen present will evaporate in form of water vapor, yielding an interconnected network of carbons to form the hard carbon. Another method of synthesizing hard carbon is through hydrothermal carbonization. It consists in heating biomass in a water suspension at relatively low temperatures (no more than 250 ºC) in a saturated pressure environment, being seen as a good procedure due to its low cost and light synthesis condition [12].

In terms of the mechanism for storing sodium in HC materials, there is still extensive debate as to which one is the best suited to explain the phenomena, with no definite answer having been yet defined. The first studies dedicated to explain these mechanisms were presented by Dahn *et al.* [32], where the now known theory of "house of card" was presented to explain the Intercalation-Adsorption mechanism, with the sodium ions being intercalated between the parallel graphene sheets with the consequence of a change on the insertion potential as the sodium-ion content increases. This change in the potential explained the inclined potential curve observed on Figure 2.7b.

A few years later, another mechanism was proposed by Cao *et al.* [34] to explain the sodium-ion storage in hard carbon materials. It presented an opposite approach to the "house of card" method, by explaining the Adsorption-Intercalation mechanism. The authors simulated, theoretically, the energy change when sodium-ions are incorporated into

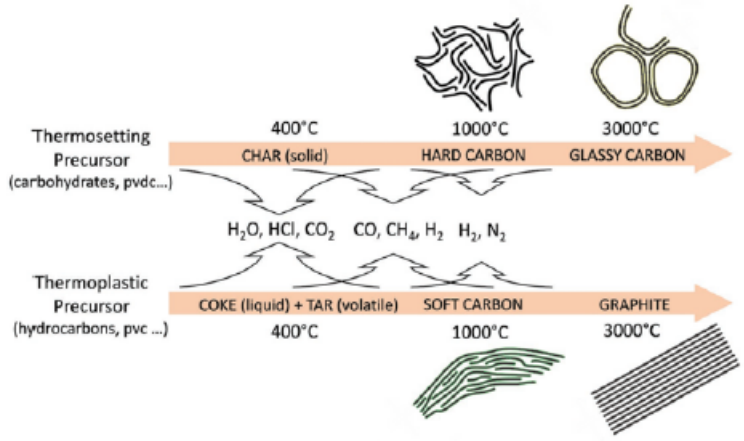

Figure 2.6: Process of carbonization through pyrolisis of the thermosetting and thermoplastic precursors [11].

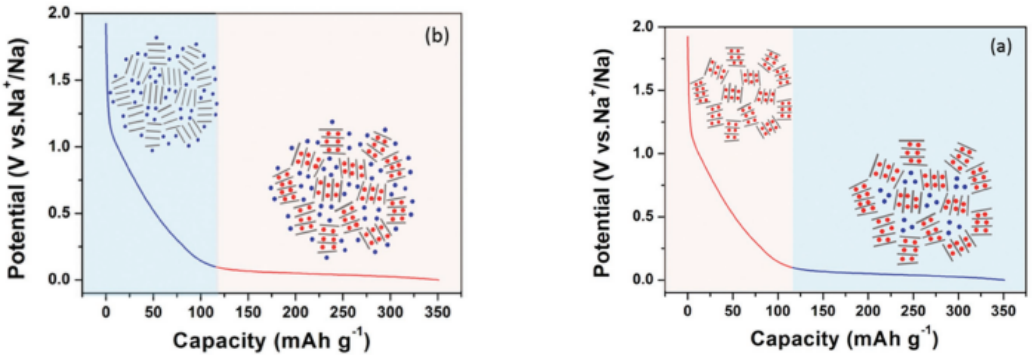

(a) (b)

Figure 2.7: Illustration of the (a) Adsorption-Intercalation and (b) Intercalation-Adsorption mechanisms for the storage of sodium-ions in hard carbon [33].

the hard carbon material. The results showed that when a low potential platform is observed, there is a reversible extraction and insertion of the ions in the hard carbon structure.

Notwithstanding the results achieved for the two already mentioned theories, other storage mechanisms were proposed. The work conducted by Xu's group [35] helped elucidate the mechanism of Adsorption-Pore Filling, that states that there is no intercalation of sodium-ions in-between the graphite layers, but instead there is a filling of micropores in the structure during the low potential plateau region of the cell's behaviour [11], as illustrated in Fig. 2.8. Using sulfur-infused hard carbon composites and well-engineered hard carbon structures, Xu's group was able to discern that during the charge/discharge cycles, the sodium-ions would first be adsorbed by the HC surface at regions where defect sites or heteratoms were present in the high-voltage plateau region. On the other hand, during the low-voltage plateau regions, the ions would fill the micro/nanopores of the structure.

As it is possible to see, there is still quite a debate regarding the storage mechanism for sodium-ions in hard carbon structures, with the micro-structures of the HC having a huge

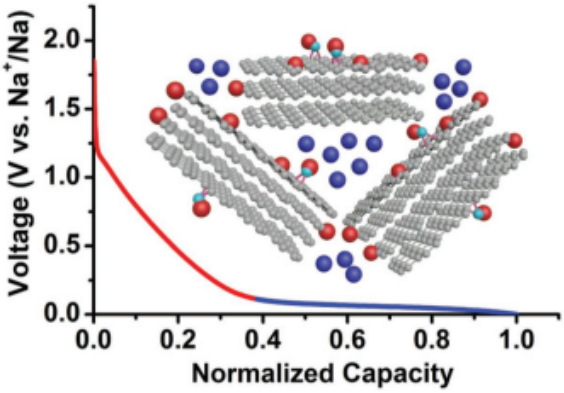

Figure 2.8: Illustration of the Adsorption-Pore Filling mechanism for the storage of sodium-ions in hard carbon [35].

influence on the experienced behaviour. More research is needed to fully comprehend these mechanisms.

In more practical terms, the use of hard carbon is still plagued by the likes of its low-rate capability, cycle stability and low Initial Coulombic Efficiency (ICE) [11]. Hard carbon when used as an electrode with liquid electrolytes, due to its high specific area, will strengthen the contact between itself and the electrolyte, forming what is known as the Solid Electrolyte Interface (SEI). This layer is the product of reduction processes that are deposited at the electrode surface in very thin layers (10^{-5} m or less). This film consists of polymer or oligopolymer products of a solvent reaction [36]. In terms of ionic conductivity, the SEI does allow ionic movement and doesn't block ionic intercalation, however, it does deteriorate over time the connection between the electrode and the electrolyte, meaning an irreversible capacity loss. With this in mind, some optimization strategies were developed for the manufacturing of HC structures, in order to improve its performance. It can be seen as optimal strategies to be implemented as future works for the electrochemical cell developed within this work.

I. **Heteratom Doping**

This mechanism consists on substituting an electron/ion of the active material by another and henceforth improve the sodium-ion storage in the hard carbon's structure. The preferred sources for doping are non-metallic atoms. B, O, N, F, P and S are the most used ones. This mechanisms proves useful due to the fact that they modify the intrinsic structure of the hard carbon material. For example, a study conducted in 2017 [37] showed that by employing P or S atoms in the structure leads to a dilation of the interlayer spacing and therefore facilitating the diffusion of the sodium-ions or that using P or B atom doping there is an increase in the sodiation sloping capacity. However, there are some drawbacks of heteratom doping, such as low initial coulombic efficiency and possible structural deformation during the charge/discharge

process caused by atoms such as S, P and F [11]. For this reason, caution must be employed when choosing the doping atoms.

II. **Structure and Morphology Designing**

Changing the morphological design of the HC materials will yield different structural characteristics which, when engineered correctly, can improve the performance of the electrode materials. There are a number of different structural designs that can be employed, such as 2D carbon sheets, 3D carbon microspheres and so on. Sun *et al.* [38] developed a unique structure of mesoporous hollow carbon spheres couples with sulfur and nitrogen heteratom doping as can be seen in Figure 2.9. The results showed that this structure was able to improve the kinetics of electron transport which in its turn led to an improvement of the capacity cycles.

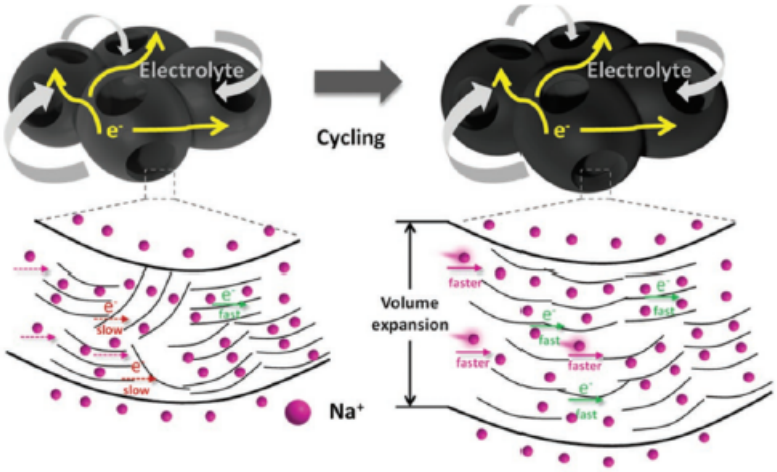

Figure 2.9: Illustration of the mesoporous hollow carbon spheres and effects after volume expansion [38].

III. **Preparation of Composite Materials**

The previous two strategies were based on improving preexisting carbon materials with newly developed strategies. In recent research, the focus has been on developing, from scratch, carbon composite materials that can intrinsically improve their performance as electrodes and not depend on external sources such as heteratom doping. By coupling soft and hard carbon, Titirici's group [39] was able to obtain acceptable reversible capacity (282 mAh g^{-1}) at a current density of 30 mA g^{-1} with a high initial coulombic efficiency of 80%. The authors believe the results were due to the blockage of selected pores in the HC structure by the soft carbon, which led to a decreased rate of SEI formation. This shows that coupling hard and soft carbon may be a viable option to improve anode performance. Notwithstanding, the whole process of manufacturing and industrialization cannot be overlooked, as it plays an important role in the development of the anode's characteristics.

IV. **Optimization of Battery Conditions**

Adding to the strategies of improving the anode by itself, there is also the possibility of optimizing the battery conditions in order to extract the best possible performances of the carbon-based anodes. The electrolyte can be optimized in order to prevent the inconvenient loss of irreversible capacity of the hard carbon anode [11].

Pre-oxidation of the anode can also be a solution, with studies demonstrating that it can enhance the electrochemical properties of the HC as anode material. Based on the pre-oxidation of the anode, Hu's group [40] was able to improve the sodium storage capacity from 94.0 up to 330.8 mAh g^{-1}, as well as the initial coulombic efficiency from 64.2 to 88.6%.

2.2.2 Cathode Materials

Developing and selecting the appropriate cathode material for the SIB configuration is crucial to obtain the best performance possible. Different redox couples used will yield different performances, as seen in Fig. 2.10. As it's known, the electrochemical performance of the sodium-based batteries is mainly dictated by the electrochemical performance of its cathode, as well as by the cathode's overall weight.

These cathodic materials are divided into two main categories, them being the layered oxides and the polyanions.

2.2.2.1 Layered Oxide Based Materials

Layered oxide cathodes, who consist of the chemical formula Na_xMO_2 where M represents one or several transition metals (M = Ti, V, Cr, Mn, Fe, Co, Ni), are composed of repeated sheets of edge-sharing transition metal octahedra structures (MO_6) with sodium ions intercalated in between them [17]. They can be categorized through their respective sodium content with nomenclature such as P2 or O3 being representative of their coordination (O-Octahedral or P-Prismatic) and the number of layers in the elementary cell (2 or 3) [36].

The attraction of these layered metal oxides arises from the high theoretical capacity of about 240 mAh g^{-1} and their relative cost-effective synthesis methods. However, there is the disadvantage of the seen tendency of mono-metallic layered oxides (Fe, Ni, Mn, Cr, etc.) to suffer from irreversible changes on its structure, leading to low coulombic efficiency and rapid capacity decay [5].

The choice of what crystalline structured cathode to be used is not a linear process. O3 type structures are usually stable when the layered transition metal oxide presents a compound $Na_{1-x}MO_2$ where x is close to a null value. Examples of this structure are cobalt and nickel ($NaCoO_2$ and $NaNiO_2$, respectively) based oxides. During the sodiation/desodiation process, this structure suffers a reversible transformation into prismatic structures. Sodium ions can be extracted from this crystal structure, meaning that vacancies are formed and

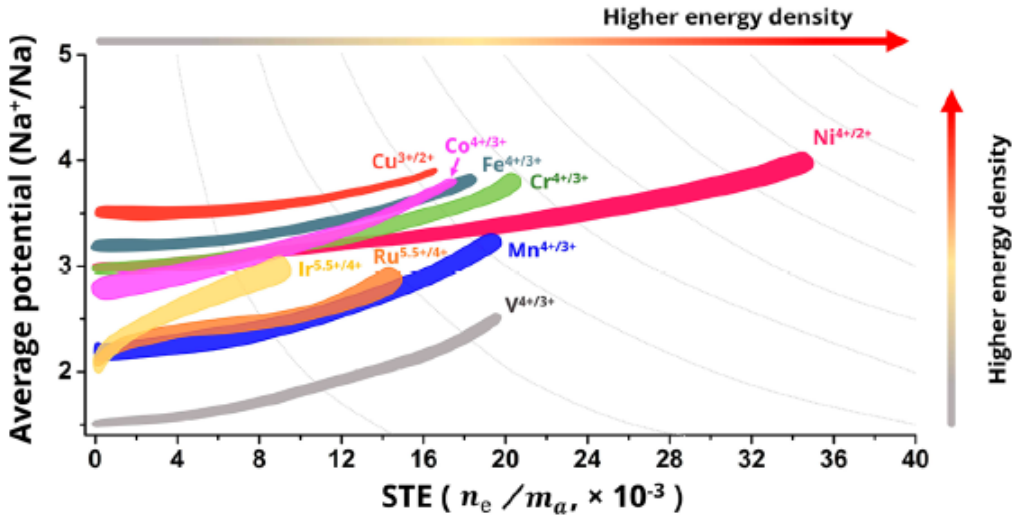

Figure 2.10: Comparison between the average working potential, specific transferred electrons (STE) and specific energy density of different redox couples used in cathodes [41].

diffusion is improved. However, the aforementioned extraction will make the sodium layers extremely repulsive to oxygen.

In terms of the P2-type morphology, it has some fundamental differences when compared to the octahedral structure. The structure is more stable when the "x" value for the sodium content is between 0.3 and 0.7. Once again, when voids are present, there is a strong repulsion of the oxygen by the sodium layers, which will in turn increase the interlayer distance [36], with the sodium ions occupying the available prismatic sites. The most well known example of this structure is the iron based oxides ($Na_{1-x}FeO_2$).

2.2.2.2 Polyanion and PBA Based Materials

Layered sodium compounds present voltage profiles that have considerable sloping angles. For this reason the use of materials who enable enhanced distances between intercalating sodium ions may be good candidates for cathodic materials in sodium-based batteries, making the process more efficient.

The first proposed use of polyanionic and Prussian Blue Analogue (PBA) based materials for SIBs was received with some skepticism due to previous experiences in lithium-based cells, mainly due to the low energy density presented. However, this may not be the case with SIBs. Studies have shown that, when the alkali-ion size increases, the gravimetric and volumetric energy densities of the layered oxide-based materials show a significant decrease (see Fig. 2.11). On the other hand, when polyanionic and PBA compounds are used, the effect of the ion size and molecular weight is much less pronounced.

Prussian Blue Analogue Compounds

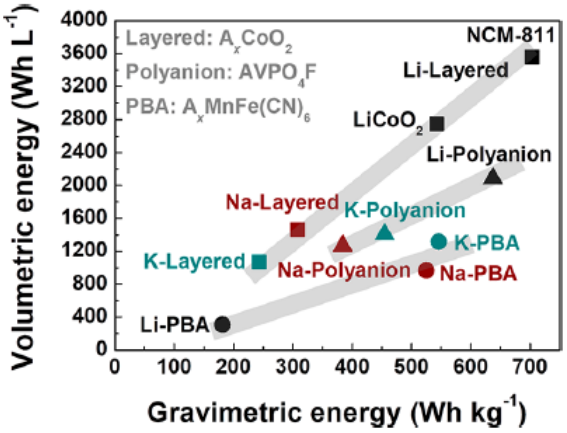

Figure 2.11: Comparison of the gravimetric energy and volumetric energy density of layered oxides, polyanionic and PBA compounds [17].

Prussian Blue Analogue (PBA) compounds, for use in SIBs, belong to what is known as the cyano-bridged coordination polymers family [42]. Their typical chemical formula can be expressed as $NaM_A[M_B(CN)_6]_y$, with M representing transition metals such as Fe, Mn, Co, Ni, Cu and so forth. These transition metal based ions ($M_A{}^{2+}$ and $M_B{}^{3}$) will be positioned on alternate corners of the octahedral structure (ses Fig. 2.12). PBAs, as is the case of polyanionic compounds, possess an open framework structure. This three-dimensional rigid framework, containing open ionic channels and interstitial sites, provides fast diffusion channels for the sodium ions [17].

The sintering process is done through a wet chemistry route at low temperature. This process will result in a structure composed of hydrated PBA lattice with an increased number of $M_B(CN)_6$ vacancies. The presence of H_2O in the structure will heavily influence the electrochemical properties. During cycling, if there are water molecules being released onto the structure, they can cause a side reaction with organic-based electrolytes, leading to its eventual deterioration. As a consequence, a low H_2O content is desired for long-term cycling of PBA based cathodes.

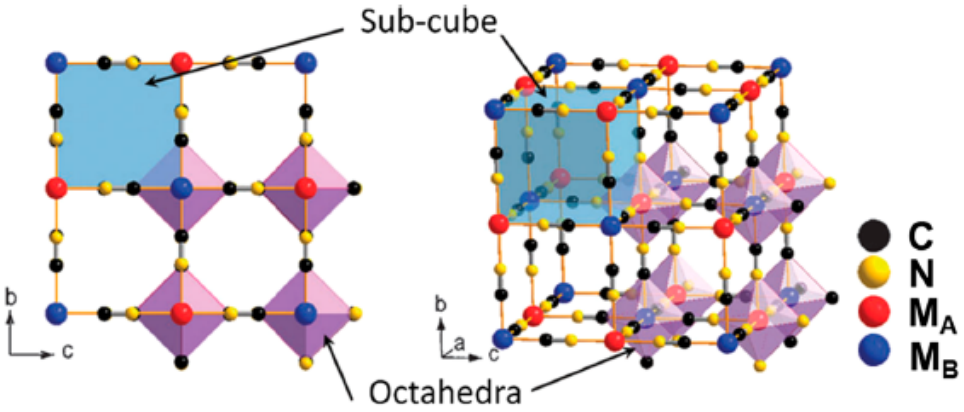

Figure 2.12: Framework of PBAs [17].

In the past few years, researchers have been able to develop PBA based cathodes for SIBs with electrochemical performances similar to iron phosphates based cathodes in LIBs, which is impressive. For example, Wang *et al.* was able to synthesize a rhombohedral $Na_{1.92}Fe[Fe(CN)_6]$ that achieved long-life time (750 cycles), good energy density (490 Wh kg^{-1}) and high capacity of about 160 mAh g^{-1} [43].

The use of polyanionic and PBA based cathodic materials has tremendous potential in the field of SIBs, with numerous combinations and applications not yet fully explored.

Polyanionic Compounds

When compared to layered oxides, the use of transition metal based polyanionic compounds has demonstrated to exhibit excellent thermal stability [36]. Its structure is based on tetrahedral or three-sided motifs, such as XO_4 and XO_3 (X = P, S, B, Si, and more). The main advantages from these compounds arise from the versatility of its structure, making it possible to employ materials that can improve faster diffusion mechanisms for the sodium ions, due to its open framework. Another interesting feature is the possibility to engineer and modify the working voltage of the cathode by altering the chemical composition of the compound.

There are three main sub-categories for these compounds: phosphates, sulfates and silicates. Each of them possess unique features, as will be seen next.

I. **Sulfates**

In theory, the substitution of the phosphate compound $(PO_4)^{3-}$ by $(SO_4)^{2-}$ leads to higher operating voltage due to the greater ionicity [10]. Since the output voltage of the cell is mainly governed by the redox potential of the cathodic material [44], sulfates have received further attention due to their increased potential of the redox couple. If engineered correctly, the incorporation of sulfate based compounds may improve the operating voltage. The use of fluorosulfates (SO_4F) and hydroxysulfates (SO_4OH) can increase even higher the potentials of the cell. Barpanda *et al.* [45] was able to synthesize a Fe-based cathode $Na_2Fe_2(S_{04})_3$ that demonstrated a reversible capacity with values well over 100 mAh g^{-1} using the $Fe^{3+/2+}$ redox couple with a potential located at 3.8V, the highest appeared for this specific reaction. This confirms the theoretical affirmation with which this paragraph started, showing the strong ionicity of $(SO_4)^{2-}$ when compared to the phosphate based compound.

II. **Silicates**

The use of Silicates (SiO_4) as cathodic materials in SIBs has the potential to introduce high structural stability in the cathode due to tetrahedral open frameworks structure inherent to these silicate compounds.

As far as promising polyanionic cathode material goes, orthosilicates (Na_2MSiO_4, M = Fe, Mn) are right at the top of the list. These compounds' great potential arise from

their very low cost (Si, Fe and Ne are among the most abundant elements on earth) and also their theoretical specific capacity which present interesting values due to the possibility of having two electrons exchanged per formula unit [46].

Li *et al.* was able to produce, through solid state and sol-gel method, iron based orthosilicates (Na_2FeSiO_4) with cubic based structures [47]. An acceptable reversible capacity of 106 mAh g^{-1} was achieved at 30ºC between 1.5 and 4.0V. On top of this, great impressive cycling performance was achieved due to its structural stability. This structural stability stems from the rigid three dimensional open framework of the orthosilicates. Moreover, no significant cell volume change was observed during the charge/discharge process. All of these factors make this particular cathode very interesting for sodium-ion batteries.

III. **Phosphates**

The use of phosphates ($(PO_4)^{3-}$) as cathodes for sodium-based batteries has received great attention the last few years due to numerous factors. The strong P-O covalent bonds present in these compounds, as well as the low thermal expansion coefficient verified, leads to very high structural stability of the framework [48]. Moreover, the 3D framework of the phosphate compounds present an abundance of spacious interstitial vacancies for the diffusion of the sodium ions, leading to a decrease in the volume changes during the insertion/extraction process.

There are different types of structures for sodium storage in the phosphate category. Olivine ($NaFePO_4$) and Maricite ($NaFePO_4$) are what is known as single-phosphate materials for the storage of sodium. They are different phases of the same compound, with maricite appearing during the high-temperature synthesis of olivine. This is not desirable, as maricite suffers from poor electrochemical performance. Henceforth, efforts have been done to develop sintering process able to create pure olivine. For example, Fang and colleagues were able to synthesise olivine-based structures coated with carbon through scalable spray drying method and achieved excellent electrochemical performances [49].

Another single-phosphate material is the Sodium Ionic Super Conductor (NASICON) type phosphate with the formula $Na_xM_2(PO_4)_3$ (M= V, Ti, $1 \leq x \leq 3$). These type of materials have received great attention recently due to its unique crystal structure. NASICON structures possess three dimensional interconnected tunnels and two types of positions where the sodium ions are distributed (M1 and M2) where the sodium ions are diffused at a relatively high working voltage (higher than 3.5V).

$Na_3V_2(PO_4)_3$ is one of these compounds and presents a very promising use due to the possible reversible cycling of two sodium ions per formula unit, giving it an interesting energy density of 400 Wh kg^{-1} [36]. Despite this, and as is expected with NASICON type electrodes, $Na_3V_2(PO_4)_3$ suffers from poor electrical conductivity.

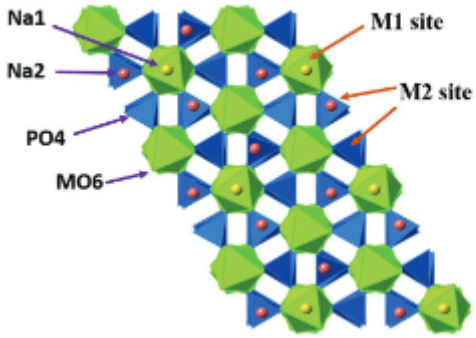

Figure 2.13: Illustration of the vanadium-based NASICON phosphate structure [48].

To overcome this, several strategies have been put into place, such as surface modification and elemental doping [50]. Surface modification comes in the form of incorporation of carbon materials, such as CNT, amorphous carbon and so on, onto the cathodic material and also in the design of three dimensional porous architectures. Elemental doping is another viable strategy to improve the electrochemical performance (electronic and ionic conductivity) by using, for example, Mn^{3+}, Fe^{3+}, Al^{3+}, Ti^{4+} and other dopants onto the NVP structure. The results achieved have been satisfactory, however, there is still the need to enable the use of these cathodic materials in full-scale energy demand operations.

In this work, a carbon coated $Na_3V_2(PO_4)_3$ cathode material was used due to the distinct advantaged that NVP-C offers over NVP as a cathode material in sodium-ion batteries. The incorporation of a carbon coating in NVP-C enhances the electrical conductivity, facilitating more efficient electron transfer during charge and discharge cycles. This in turn results in improved battery performance, higher rate capability and faster sodium-ion diffusion kinetics. Furthermore, the carbon coating acts as a protective layer, reducing unwanted side reactions at the electrode-electrolyte interface and enhancing the overall cyclability and longevity of the battery. With its higher specific capacity and enhanced structural stability, NVP-C was the chosen cathode material for the full cells at this stage.

2.2.3 Electrolyte Materials

In the configuration of a battery, the electrolyte has the critical function of conducting ions from one electrode to the other, while being electronically insulated. It should also possess acceptable chemical and electrochemical stability, and an appropriate mechanical strength to prevent the transportation of redox species, as well as dendrite growth [51]. Two types of electrolytes can be employed, liquid and solid state.

2.2.3.1 Liquid Electrolyte Systems

In liquid electrolytes, the ion transport mechanisms consists of two main elements. A given number of solvents are used as a transport medium, and salts as charge carriers. In sodium based cells, the most common solution is to use $NaPF_6$, $NaCF_3SO_3$, $NaBF_4$ or $NaClO_4$ as the salts, and use carbonate ester solvents, like propylene carbonate (PC) or butylene carbonate (BC), among others. Not less important, there are also additives and binders in play to ensure a good liquid electrolyte structure. The additives have the function of improving the stability of the SEI and also for safety features such as reducing the flammability of the cell. In its turn, binders are employed to enhance and make more efficient the process of storage of the sodium ions [10].

Liquid electrolytes can provide excellent wettability of the electrode surface and therefore high ionic conductivity. However, the disadvantages can outweigh the benefits. The possibility of fire outbreak due to high flammability creates safety concerns for these types of electrolytes. Moreover, liquid electrolytes provide null mechanical strength and structural stability, and have difficulties in forming stable SEI, making its use in high-energy structural batteries not attractive. For these reasons, the use of solid state electrolytes for SIBs have been seen as the sane approach for the development of an all-solid-sate sodium ion structural battery.

2.2.3.2 Solid State Electrolytes

Using electrolytes in solid state solves the safety issues concerning liquid based ones. Solid State Electrolytes (SSE) possess very low flammability, with no risk of leakage and very low chance of volatilization. Moreover, these systems possess higher thermal stability and allows for simpler all-solid-state structural battery designs.

There are however some concerns when employing SSE. They possess intrinsic low conductivity at room temperature applications, weak electrochemical stability and there are struggles in improving the inter-facial compatibility between electrode and electrolyte, which leads to poor Na^+ diffusion processes [52]. Despite this, SSE possess attractive potential, with several methods used to solve the aforementioned issues.

Solid electrolytes can be identified through three main categories: inorganic ceramic, organic polymers and hybrid structures composed of both organic and inorganic electrolytes.

Organic Polymer Electrolytes

Organic polymer SSEs can be seen as a solution to some of the problems experienced with other solid-state electrolytes. They are, in general, substantially cheaper than ceramic electrolytes due to their simple manufacturing processes. Moreover, they present acceptable mechanical strength (10^6-10^8 Pa) [51] which makes them an effective structure to suppress the growth of dendrites in the electrolyte/electrode interface. The main issue with

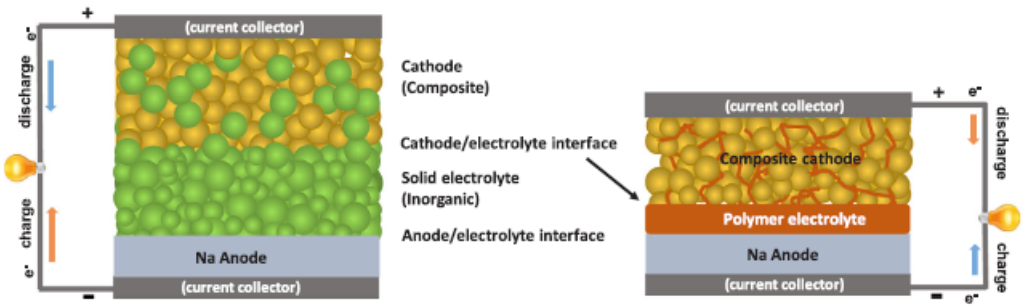

Figure 2.14: Illustration of SIBs with an inorganic (left) and organic (right) solid electrolytes [52].

solid polymer electrolytes is their low ionic conductivity at room temperature. In polymer structures, ion transport is conducted through amorphous chain segments. However, these structures are only available above the glass transition temperatures (T_g) of polymers, at around 60-80 ºC, making them only interesting to work with around that temperature region. Moreover, the fact that these compounds are not in all-solid form makes them mechanically unstable, being a potential source of weakness when employed in structural batteries.

Polyethylene oxide (PEO) was the first solid polymer to be studied as an electrolyte, first for lithium based batteries in the 1970s [53] and later for sodium-ion batteries. Since then, more organic polymers have been employed as SSE for SIBs such as polyvinil alcohol (PVA), poly(vinyl pyrrolidone) (PVP) or polyacrylonitrile (PAN).

Despite the advantages presented, using electrolytes made solely of organic polymers is not feasible for room temperature due to their ionic conductivity. For example, the ionic conductivity of PAN at room temperature is between 10^{-5} and 4x10^{-4} S cm^{-1}, while PEO exhibits even lower values, between 10^{-9} and 10^{-7} S cm^{-1} [54] For this reason, combining organic solid polymers with one another or even ceramic based structures to create hybrid/-composite electrolytes has been seen as a promising technology to extract the best possible results.

Inorganic Ceramic Electrolytes

This type of solid electrolyte has attracted interest due to its ability to prevent uneven electrodeposition of anode material in the electrode/electrolyte interface due to its high modulus. Moreover, they present acceptable room temperature ionic conductivity, before any optimizing strategies were applied. This shows that the ceramic's ionic transportation mechanisms possess interesting features. It is known that ionic conductivity heavily relies on the existence of mobile ions and connected vacancies that allow for the ions to realize extraction and diffusion processes [52].

There are still some unwanted characteristics, such as high cost and brittleness, that make its large-scale use a challenge as of yet, but strategies to minimize these issues are

already developed and implemented. Inorganic ceramics are further divided into oxide-based, sulfide-based, and NASICON type structures.

I. **β-Al_2O_3 and β''-Al_2O_3**

This compound, which possesses a two dimensional framework structure, belongs to the oxide-based electrolytes for SIBs. They consist of alternating stacking sequences of oxygen with aluminium ions in the octahedral and tetrahedral interstices, with the conduction plane being composed of conglomerates of oxygen and sodium ions [55], as seen on Fig. 2.15.

β-Al_2O_3 and β''-Al_2O_3 present different stacking sequences, in the conduction plane, from each other.

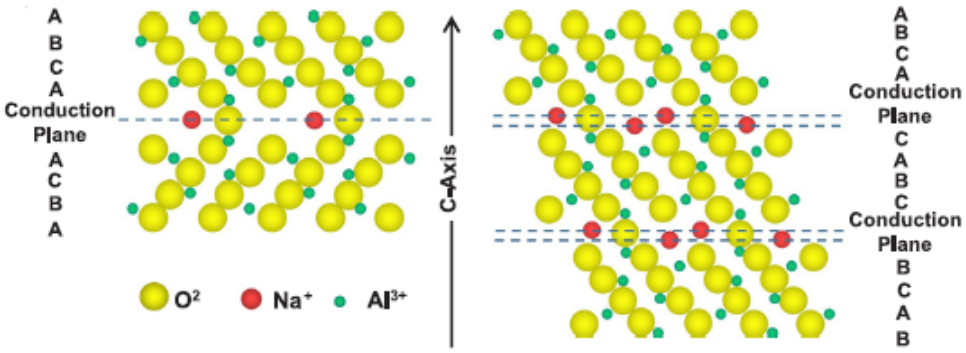

Figure 2.15: Stacking sequence of β-Al_2O_3 (left) and β''-Al_2O_3 (right) [52].

In terms of electrochemical performance, β''-Al_2O_3 has shown to possess higher ionic conductivity (1 S cm^{-1} at 300ºC for a single crystalline structure [55]) than its counterpart on account of its higher concentration alkali-based ions on the conduction plane. Its unit cell is also 50% more spacious than β-Al_2O_3 because of differences in the oxygen stacking sequence, making it easier to conduct ions through its structure. Several processes have been reported for the synthesis of alumina based electrolytes, such as sol-gel, solution combustion and co-precipitation method.

As mentioned, single crystalline structures of β''-Al_2O_3 present great ionic conductivity at 300ºC. However, at room temperatures, the conductivity decreased to 2.0 x 10^{-3} Scm^{-1}. To improve these values, some strategies have been proposed. Altering the concentrations of the sodium ions and/or substituting aluminium ions with mono or divalent ions, such as cesium, are possible solutions. Modifying the micro structure of the electrolyte can also improve the conductivity [56]. Notwithstanding the issues with ionic conductivity, these are not the only ones. Stability at ambient conditions is also of concerned due to β''-Al_2O_3's reactivity with H_2O, which leads to material degradation, making this compounds not well suited for room temperature applications.

II. **Sulfides**

Sulfide based electrolytes are a good alternative to the aforementioned oxide based ones due to its increased ionic conductivity. When compared to oxygen, sulfur presents a larger ionic radius, which leads to a decreased electronegativity. For this reason, there is a smaller electrostatic force between the sodium and sulfur elements, resulting in faster sodium ions transport mechanisms when compared to oxide based electrolytes. Moreover, the overall manufacturing costs for sulfur based electrolytes are lower than oxide based ones. It is also easier to obtain good electrolyte/electrode surface contact for sulfur-based structures, with only cold pressing being needed for an intimate contact [55]. There are however some safety concerns due to sulfur's low chemical stability in the presence of air, owing to the generation of H_2S gas which is highly toxic. Therefore, handling these materials should be done in a inert gas atmosphere, increasing the complexity of the manufacturing process.

In terms of crystalline structure, sulfide electrolytes can be compartmentalized into glass and glass-ceramic structures, as seen on Fig. 2.16. The glass-type structures (Na_2SGeS_2, for example) present amorphous structures with a large number of disorders in the sub lattice. The glass-ceramic crystalline structure has been investigated in depth in recent years. One of the most studies is the Na_3PS_4 compound. Hayashi *et al.* was able to elucidate the types of phases present in the glass-structure and showed that Na_3PS_4 presents a cubic and a tetragonal phase [57]. The cubic phase presents the highest ionic conductivty at room temp, as well as the lowest activation energy, $2x10^{-4}$ S cm^{-1} and 27 kJ mol^{-1}, respectively [55].

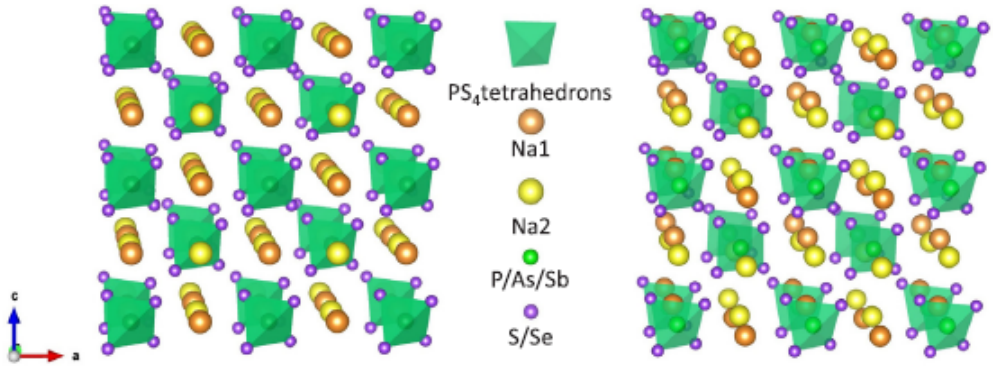

Figure 2.16: Illustration of the crystalline structure of sulfide electrolytes with (left) cubic and (right) tetragonal phases [52].

There are also strategies in place to help improve even further the ionic conductivities of the sulfur based electrolytes. By precipitation of super ionic conducting crystal from the glass precursor phase, it is possible to enhance ionic conductivity, as well as diminishing the grain-boundary resistance.

III. **NASICON**

Sodium Ionic Super Conductor (NASICON) solid state electrolyte is amongst the most promising electrolyte material for sodium based batteries. Their average ionic conductivity, before any optimizing strategy, good air stability and wide electrochemical stable window makes its use very appealing [6].

NASICON based electrolytes were first proposed back in 1976 by Goodenough *et al.* [58], and was the first reported three dimensional framework structure for sodium-ion conductors. It has the general formula of $Na_{1-x}Zr_2P_{3-x}Si_xO_{12}$ ($0 \leq x \leq 3$), with a majority of the studies being based on the formula $Na_3Zr_2Si_2PO_{12}$ due to its observed rhombohedral structure. This structure is formed of common corners formed by octahedra ZrO_6 and tetrahedra PO_4, which will compose the three dimensional framework (see Fig. 2.17) [55]. The movement of the sodium ions through the crystalline structural has also been subject to research, to figure out exactly how does the diffusion mechanism occurs. The combined octahedra and tetrahedra framework will create what are known as bottlenecks (hexagonal and octagonal), where there are vacancies that allow the sodium ions to move through, contributing to improving the ionic conductivity. In the structure, there are three types of vacancies, known as Na_1, Na_2 and Na_3, each of them connected in between themselves.

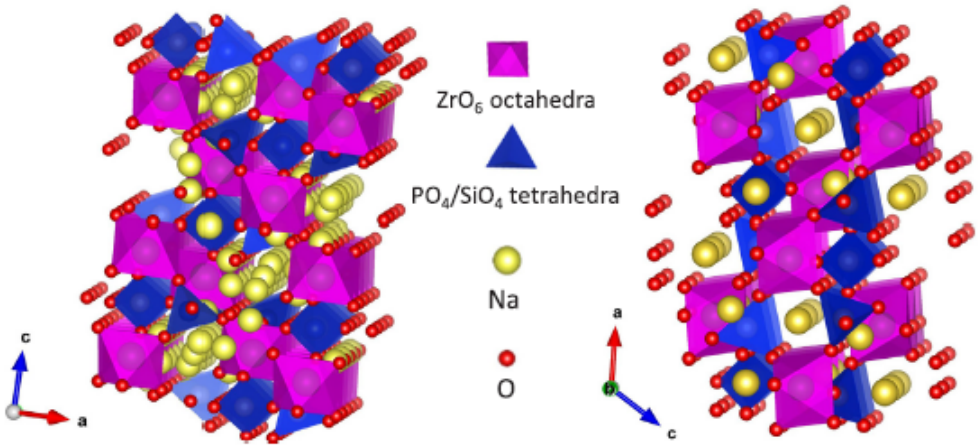

Figure 2.17: Crystalline structure of NASICON as a (right) Rhombohedral and (left) Monoclinic [52].

Bui *et al.*, using density functional theory, was able to pinpoint three different paths for the diffusion of sodium ions on NASICON type structures: pathway *a*, pathway *b* and pathway *c* [59]. Pathway *a* consists of an inner-chain process, where the sodium ions move through the aforementioned "octagonal bottleneck". Pathway *b* uses inter-chain processes, with the sodium ions moving through the "hexagonal bottleneck". Pathway *c* is a mixture of both processes.

NASICON eletrolytes present an excellent range of ionic conductivity at room temperature (10^{-4} to 10^{-3} Scm^{-1}). Monoclinic crystalline structures show a slight advantage in terms of ionic conductivity when compared to rhombohedral structures, at room temperature, due the latter's smaller unit-cell size and therefore lowered sodium ion interaction sites. It is important to note that NASICON's ionic conductivity depends not only on the crystalline structure, but also on the manufacturing methods used and the chemical composition chosen. The main issue standing in the way of the use of NASICON solid electrolytes in large-scale energy applications, when comparing to liquid electrolytes, is the ability to achieve both high ionic conductivity (>10^{-3} Scm^{-1}) and high critical current density ($\leq$1.0 mA cm^{-2}).

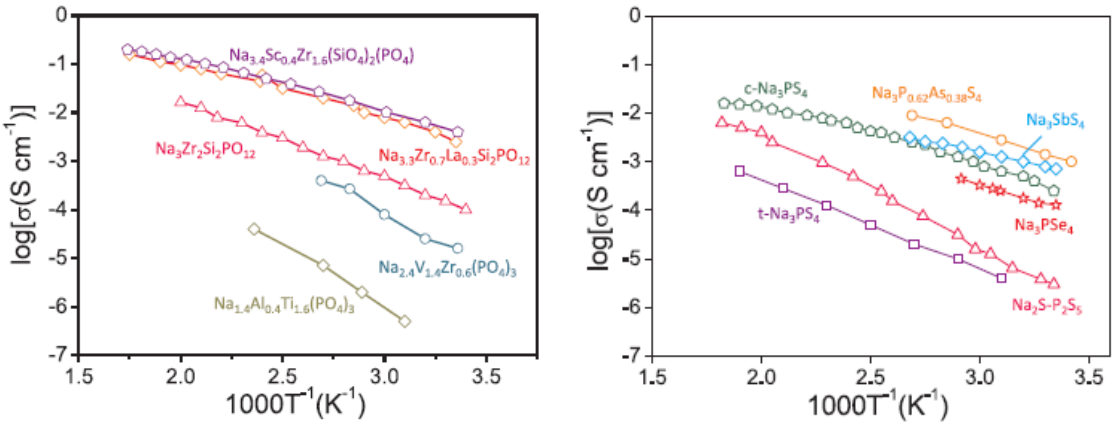

(a) (b)

Figure 2.18: Temperature dependent ionic conductivities of (a) NASICON and (b) Sulfide based materials [52].

To achieves this goals, there are strategies that can be implemented. Firstly, the sodium concentration and the atomic size of the M and M' cations in the $Na_3MM'P_3O_{12}$ formulation can be tuned to the optimal value. Another strategy is element doping, where the introduced dopants, with low solubility, can upgrade the conductivity in the electrolyte/electrode interface through the formation of a second phase [52]. For example, Shen *et al.* were able to achieve high room temperature ionic conductivity ($3.6x10^{-3}$ S cm^{-1}) with negligible electrical conductivity by substituting the Zr^{4+} and P^{5+} elements by Mg^{2+} and Si^{4+}, respectively. Moreover, the sodium content was also tuned to optimized values, yielding the formula $Na_{3.4}Mg_{0.1}Zr_{1.9}Si_{2.2}P_{0.8}O_{12}$ [6].

In this work, an undopped nasicon solid-state electrolyte was used. Features such as excellent range of ionic conductivity at room temperature and its ceramic crystalline structure makes it ideal for applications in all-solid-state batteries. The fact that it is solid and possesses good mechanical properties offers it a far superior performance in terms of providing structural stability and mechanical strength to the overall structure, when compared to electrolytes in the liquid form. Previously mentioned dopping strategies are exciting prospects to be included as future works.

Hybrid Electrolytes

As introduced in the previous sub chapters, using electrolytes composed of either only ceramic or only organic polymers brings a set of issues hard to tackle. The use of ceramics enables an electrolyte with a wide electrochemical window, good thermal stability and reasonable ionic conductivity but presents high inter-facial resistance and poor resistance to impact damages. On the other hand, organic polymers present good flexibility and low cost/weight relations but present abysmal ionic conductivity at room temperature.

A solution to this is the development of hybrid structures being composed of both ceramic and organic polymers. It has been showed that hybrid polymers can improve both the ionic conductivity at room temperature and the overall mechanical properties of the structure. For example, Kim *et al.* [60] synthesized a flexible hybrid solid electrolyte using a nasicon type powder ($Na_3Zr_2Si_2PO_{12}$) mixed with a Polyvinylidene fluoride-co-hexafluoropropylene (PVdF-HFP) polymer. The results obtained were very satisfactory, with an ionic conductivity at room temperature of $3.6x10^{-4}$ Scm^{-1} coupled with high flexibility and good cycle life. Using the same composition of nasicon powder and PVdF-HFP polymer, Cheng and colleagues [61] achieved an even higher room temperature ionic conductivity of $2.5x10^{-3}$ S cm^{-1} through a simple solution casting method followed by an immersion in a liquid electrolyte for activation purposes.

Optimization Strategies for Electrode-Electrolyte Interface Contact

Solid state electrolytes (SSE) function both as separator and ionic conductor in a full-cell configuration. The sodium ions will need to be diffused through the electrolyte and its respective interfaces with the anode and the cathode. SSE suffer from drawbacks that are not present in liquid electrolyte configurations. Volume fluctuation during the desodiation-sodiation process and insufficient area contact between electrode and electrolyte are some of the issues that plague the use of solid electrolytes in SIBs. To overcome some of these issues, strategies have been put into place to maximize the performance of solid-state batteries.

The strategy used will depend if the electrolyte is in contact with the anode or the cathode. In the latter case, due to the fact that most cathodic materials are in powder form, specific strategies are employed. Fig. 2.19 lists the most common used schemes to improve inter facial contact between the electrolyte and the electrode. The main objective is to improve the wettability of the inter face, in order to maximize the ionic flow through the contact area.

In terms of the anode/electrolyte inter phase, there is still the goal of providing and maximizing the available paths for sodium ion flow, but the main objective is shifted to the prevention of formation of dendrites when sodium metal is present. When inorganic electrolytes are in contact with sodium metal based anodes, the formation of dendrites will

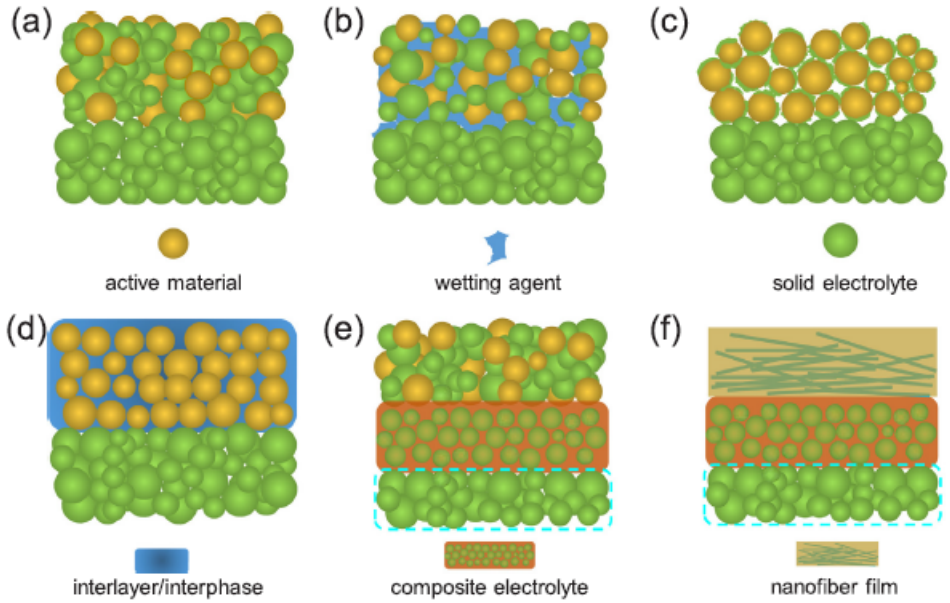

Figure 2.19: Optimization strategies for inter facial contact between cathode and electrolyte. (a) composite cathode, (b) wetting agent, (c) solid electrolyte, (d) interlayer/interphase, (e) composite electrolyte and (f) nanofibre film [52].

occur, degrading the inter phase and decreasing the electrochemical performance of the cell. For this reason, surface coating of the electrode is crucial when an inorganic solid polymer is present. In Fig. 2.20, the strategies used are displayed, and it's possible to see the attention given to the protection of the surface contact between the anode and the electrolyte.

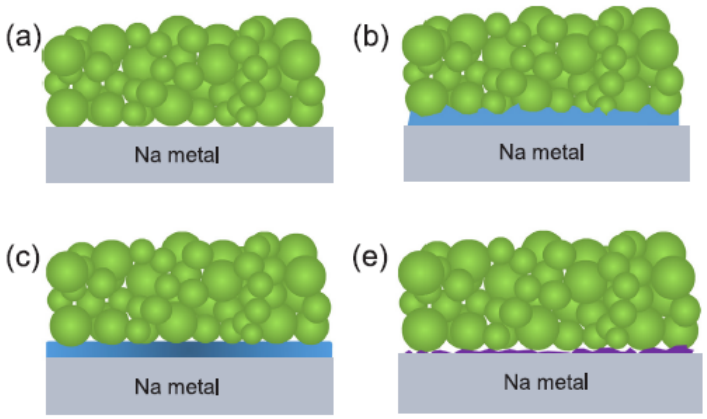

Figure 2.20: Optimization strategies for the inter facial contact between anode and electrolyte. (a) cold pressing, (b) wetting agent, (c) adding interlayer and (d) surface coating [52].

2.2.3.3 Electrolyte Mechanical Characterization

Knowing the full characteristics of the electrolyte that will be employed in a certain cell configuration is crucial to understand how the different components of the said cell will interact. Specifically for the solid state electrolytes, knowing properties such as fracture toughness, hardness and Young's modulus is of the utmost importance to know the limits in which the cell can operate safely.

As the electrolyte utilised throughout the experimental part of this work is of a ceramic nature, conventional test methods for the determination of mechanical properties are not applicable. For these reasons, other methodologies need to be employed. To achieve this, the nano/micro-indentation method can be applied. This method consists on using a diamond-based pyramidal (Berkovich-type) or spherical identer and pressing it onto the surface of the test subject. The pressing stage is done by continuously increasing the load applied through the identer onto the surface until a predefined threshold is reached, keeping the load for a certain amount time. After that, the load is gradually removed. The results obtained from this test come in the form of load-displacement curves, as seen in Fig. 2.21.

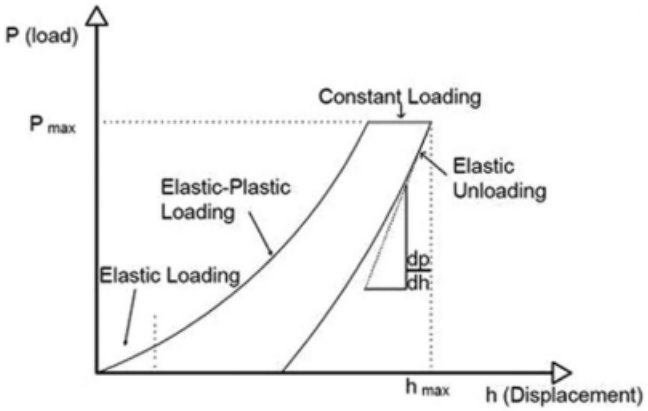

Figure 2.21: Load-Displacement curves for the nano-indentation method [62].

The type of indenter used will also affect the parameters used for the post-processing calculations. Fig. 2.22 displays the available indenter tips for the realization of a nano-indentation test, whilst Fig. 2.23 shows an up-close visualization of the dimensions and forces in place during the realization of the indentations, with the most important ones being the load applied, F, and the total indentation depth, h.

With these curves, it is possible to retrieve the material's hardness and Young's modulus. The indentation hardness (H) is defined as the load (P), divided by the contact area (A_c), or area under load. The are under load will depend on the the identer's displacement and semi-angle, h and θ, respectively. The area under load can be given by Eq. 2.6.

$$A_c = 3\sqrt{3}h^2 \tan^2 \theta \tag{2.6}$$

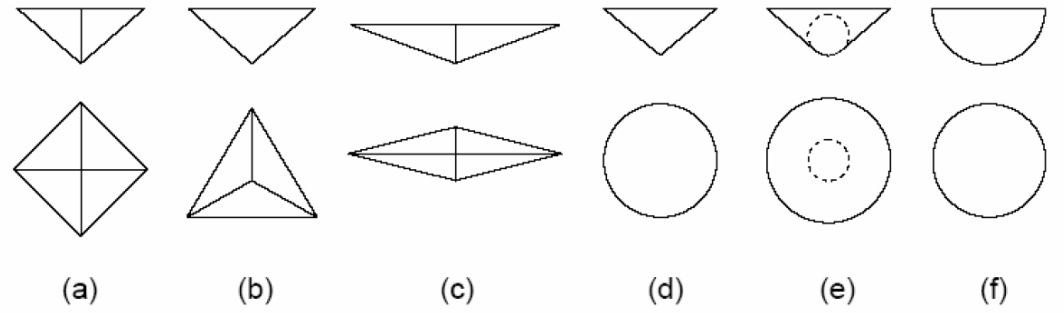

Figure 2.22: Schematics of indenter tips (a) Vickers, (b) Berkovich, (c) Knoop, (d) Conical, (e) Rockwell and (f) Spherical [63].

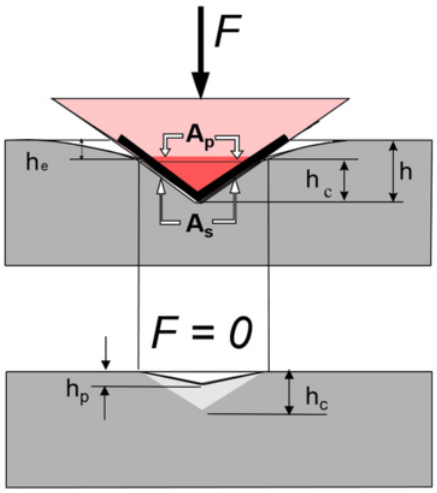

Figure 2.23: Illustration of the dimensions and loads in play for an indentation test [64].

$$H = \frac{P}{A_c} \tag{2.7}$$

To retrieve the Young's modulus, one can use the reduced modulus, E_r. The reduced modulus represents the elastic deformation suffered by both the sample and the indenter's tip. It can be given by the following formula.

$$E_r = \frac{dP}{dh}\frac{\sqrt{\pi}}{2\sqrt{A_c}} \tag{2.8}$$

Where dP/dh represents the slope of the unloading curve, also known as the stiffness. To calculate the Young's modulus, the previous equation can be converted into the following one.

$$\frac{1}{E_r} = \frac{(1-\nu_s^2)}{E_s} + \frac{(1-\nu_i^2)}{E_i} \tag{2.9}$$

Where ν represents the Poisson's ratio for the sample (ν_s) and for the indenter (ν_i) and E is the Young's modulus for the sample and indenter, respectively. Knowing the Poisson's

ration of the sample and the elastic properties of the diamond indenters E_i = 1141 GPa and ν_i = 0.07, it is possible to extract the sample's Young's modulus.

Knowing these two parameters, one can then proceed to extract the fracture toughness, in mode I, of the material in question. This is done by analysing the length of the resulting cracks from the nano/micro-indentation test [65]. Using a Scanning Electron Microscope (SEM), visual data is gathered to measure the length of the crack field and be used to calculate the material's fracture toughness.

Assuming a half-penny crack model in an elastic-plastic solid, it is possible to employ the Lawn equation (Eq. 2.10) to calculate the critical stress intensity factor (K_IC) of the material.

$$K_{IC} = \alpha \left(\frac{E}{H}\right)^{1/2} \left(\frac{P}{c^{3/2}}\right) \tag{2.10}$$

Where E is the Young's modulus, c is the total crack length and α is a constant of the material related to the shape of the indenter used (For a nasicon type material, this value is of 0.040 ± 0.004 [66]).

2.3 Structural Batteries

The previous sections have shown the faces that compose and influence the behavior of a sodium-ion battery. However, these batteries have a single primary function, that of being able to provide electrochemical energy when needed through several charge-discharge cycles. The use of sodium, as has been explained, derived from the need of improving the sustainability of these power cells. The purpose of this work was to achieve a full operating structural sodium ion solid-state battery. Structural batteries is a groundbreaking concept in the field of energy storage systems, wherein battery functionalities are integrated directly into load-bearing structures. Unlike conventional batteries that are separate entities, structural batteries employ the structure itself as a medium for storing and delivering electrical energy. This novel approach holds immense relevance in advancing various industries, particularly in the transportation and infrastructure ones. By combining the roles of energy storage and structural support, structural batteries can significantly reduce weight and increase energy efficiency and density, thereby enabling the development of lighter and more sustainable vehicles, aircraft, and buildings [67]–[69].

US Army Research Laboratory was the first entity that attempted to assemble a structural battery back in 2007, using a carbon fibre lamina as the anode and a metal coated mesh as the cathode, separated by glass fibre fabric [67]. The structure presented satisfactory mechanical performance but very poor electrochemical operational values due to a lack of electrical insulation. The inability of achieving both mechanical and electrochemical results has been one of the major hurdles to overcome in this area, with a compromise being needed in order to develop structures with satisfactory performances.

More recently, state of the art technology in structural batteries is based on employing carbon fibres as multifunctional constituents, acting as both electrode and current collectors. Asp *et al.*, using a porous solid structural polymer combined with a liquid electrolyte, were able to achieve a multifunctional structure able to possess both satisfactory energy density and mechanical properties, such as an elastic modulus of 25 GPa and a tensile strength exceeding 300 MPa [67].

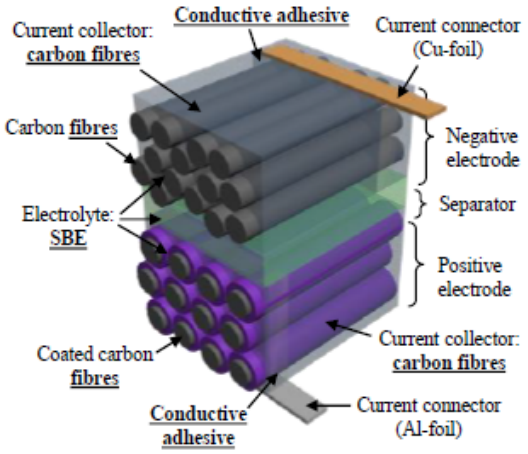

Figure 2.24: Illustration of a laminated structural battery [70].

There are two fundamental approaches to the design of structural batteries. The design can either be a coupled or decoupled system. Decoupled systems, or multifunctional systems, seek to incorporate the desired functionalities at a structural level. Inversely, coupled systems (or multifunctional materials) encompass the functionalities at a material level, where each component, such as the cathode and anode, possess multifunctional purposes.

2.3.1 Multifunctional Systems

Structural batteries designed with a multifunctional system philosophy seek to extract mechanical and electrochemical performance through the integration and storage of energy devices into composite structures, such as carbon or glass fibres.

Space and nautical structures were among the first to experiment with this type of technology. Roberts *et al.* developed a sandwich structure composed of aluminium honeycomb and carbon fibre face sheets to encompass pre-existing lithium-ion cells [71]. Since then, new approaches have been developed, with an assessment of the main influencing parameter's on the cell's manufacture and performance. Experiments conducted by Gasco and colleagues [72] demonstrated that, for all-solid-state-thin-film batteries, curing temperatures in these devices will be of paramount importance in its lifespan, with temperatures

being limited to 132 ºC. This plateau is determined by the melting points of the different constituents within the cell, such as sealants to prevent reactions within the structure.

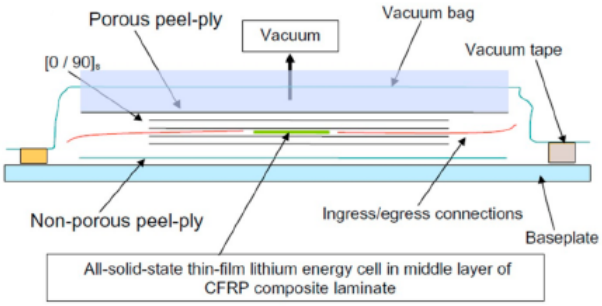

Figure 2.25: Schematic layup of a thin-film Li-ion energy cell embedding in CFRP [68].

In terms of the relationship between mechanical and electrical performance, a few studies have been conducted, mainly on lithium-ion cells. Notoriously, Shalouf *et al.* [73] organized an experiment to oversee how the cell's electrochemical performance was influenced by different loading conditions. Polymer lithium ion cells embedded on composite sandwich structures were subjected to tension, compression and bending tests, with sandwich panels without cells embedded being used as control specimens. Experimental results showed that no significant alteration of the structure's mechanical properties were observed under tensile and flexural loading. However, under compression, the panels with embedded cells demonstrated early on buckling when compared to the control specimens. In terms of electrochemical performance, it was discovered that there is a strong correlation between the structure's experienced strain and subsequent increase in the cell's internal impedance. This increased impedance leads to a notorious degradation in the (des)charging capacity of the battery, as seen in Fig. 2.26.

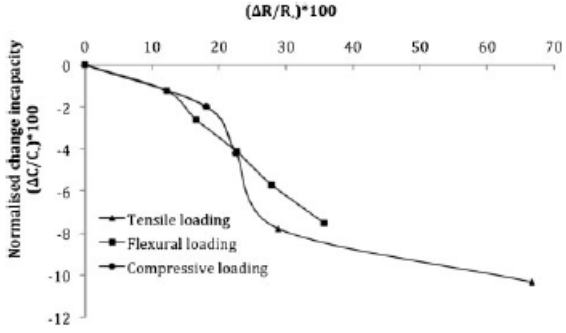

Figure 2.26: Correlation between capacity reductions with increases of internal resistance under three modes of loading [73].

Based on the obtained results, the authors were able to identify the relationship between the changes in battery storage capacities with the applied mechanical loads.

$$\varepsilon = \frac{6Plc}{Ebt_f^3} \tag{2.11}$$

Using Eq. 2.11 to define the peak compressive strain, where P is the bending load, l the span length, b the cell's length and c its thickness, of a multilayer structural battery composite, it is possible to estimate the changes in the battery's energy capacity.

$$\frac{\Delta C}{C_o} = k\|\varepsilon\| \tag{2.12}$$

Where $\Delta C/C_o$ represents the changes in energy capacity, $|\varepsilon\|$ is the aforementioned compressive strain and k is the returned linear regression from experimental results, with value of -14.3. Other methodologies have been employed to improve the mechanical behaviour of structural batteries, as for example the use of rivets (see Fig. 2.27) [74] to improve the flexural stiffness of the structure. Moreover, the study discovered that the same structure but without rivets showed a 25% drop in capacity and an unwanted increase in impedance, for the same number of cycles.

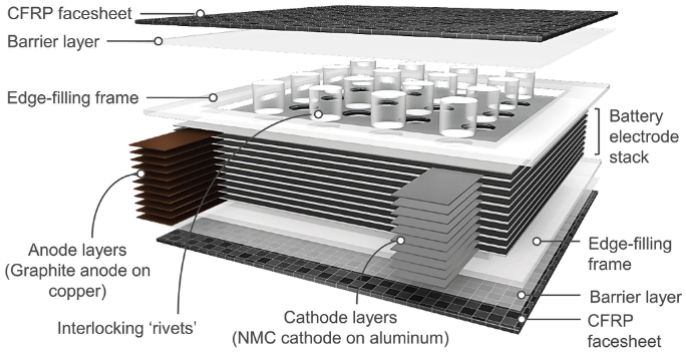

Figure 2.27: Illustration of the employment of rivets for multifunctional structural batteries [74].

2.4 Structural Solid-State Sodium Ion Cell Architecture

The described state-of-art in the field of sodium-ion structural batteries provided a helpful insight to the developed all-solid-state sodium ion structural battery. The purpose was to achieve a high-voltage all-solid-state sodium-ion structural battery.

As mentioned, the choice for the NASICON ceramic pellet employed is based on its excellent room temperature ionic conductivity and wide electrochemical stable window. Coating the nasicon solid electrolyte with a wetting polymer agent, it was possible to overcome the high interface resistance between the solid electrolyte and the electrodes, enabling the design of a hybrid solid state electrolyte.

Electrode-wise, vanadium-based phosphate was an obvious choice for cathode due to its affinity with the ceramic pellet, both sharing a nasicon-type structure. Moreover, the incorporation of a carbon coating, forming NVP-C, offers an enhanced electrical conductivity and more efficient electron transfer. For the anode, carbon-based materials were immediate due to the relative low cost and feasibility of synthesis compared to other anode for SIBs. Between the three available carbon-based anodes, and for reasons explained previously, graphite has to be scrapped from further applications. As for hard and soft carbon, the latter's amorphous nature makes it difficult to compete with the electrochemical performance of hard carbon based anodes, being therefore the more intelligent choice for anode.

To develop an all-solid-state structural battery, the incorporation of structural components is of crucial importance, as the mechanical load-bearing aspect of the battery will be equally important as the electrochemical performance. To achieve this, glass fibres will be used as embedding agents, surrounding the developed battery and providing structural stability. The fibres will have two vital functions. First, they will provide an isolating protection for the cell's components, both from and electrical standpoint, as well as protecting it from environmental agents that may cause the cell to under perform. Secondly, they will provide the ability for the battery to withstand mechanical loads without affecting the electrochemical side of the cell. Moreover, the good mechanical properties coupled with relative cheap manufacture cost, allows for the development of a facile and cost-effective battery.

The final architecture of the cell will be composed of the already mentioned electrodes, coupled with the solid-state hybrid electrolyte. Glass fibres will be then used as embedding agents, sealing the bulk of the battery using different curing methods. The only exposed component of the cell will be conductive wires used to perform the electrochemical tests.

Chapter 3

Experimental Procedures and Characterization Techniques

3.1 Electrolyte Mechanical Characterization

3.1.1 Materials and Methods

For the mechanical characterization of the solid-state ceramic electrolyte, the nano/micro-indentation method was used, with its working principles explained thoroughly on section 2.2.3.3.

The circular NASICON pellet, with a 20 mm radius, was mounted in an epoxy bio-component resin and then polished to have a total radius of resin plus pellet of no more than 24 mm and a total thickness of no more than 10 mm, as seen in Fig. 3.1 The exposed face of the ceramic pellet, where the indentations will be performed, was then cleaned with de-ionized water to remove any impurities present.

Using a Berkovich-type indenter with a diamond tip, two different sets of indentations were performed, three with a maximum load of 5 N and the remaining three with a maximum load of 10 N. The indentations were aligned vertically with a distance of 100 μm between them and no horizontal offset.

For both sets of indentations, the initial load was of 0.100 mN with a loading and unloading rate of 200 mN/s, with a dwell of 5 seconds at maximum load. The tests were performed at University of Minho's SEMAT unit.

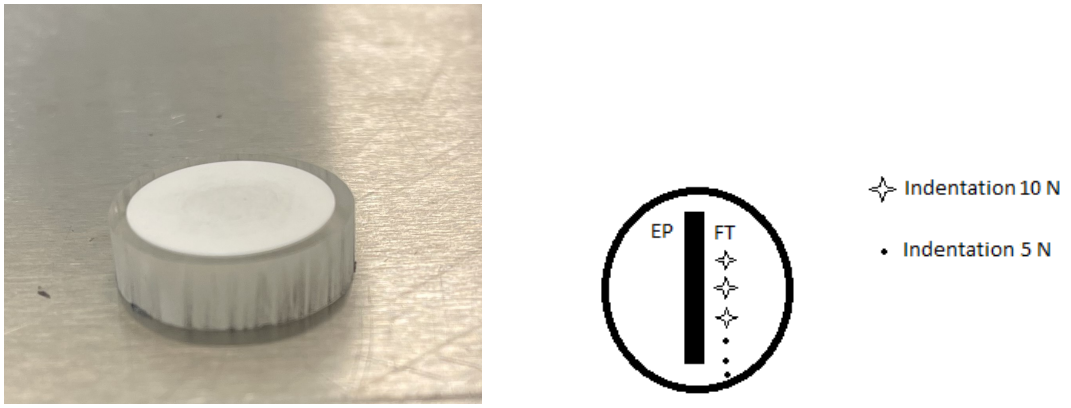

(a) (b)

Figure 3.1: (a) Sample for the nano/micro-indentation tests and (b) schematic for the indentation marks.

3.1.2 Results and Discussion

Using the theory mentioned on section 2.2.3.3, it is possible to extract the ceramic's Young's modulus from the load versus depth curves. Knowing that the indenter is a Berkovivch type with a diamond tip, whose Poisson ratio and Young's modulus are 0.07 and 1141 GPa, respectively. The sample's Poisson ratio value used was 0.27 and was retrieved from available literature [75]. The values obtained for the reduced and Young's modulus are displayed on the Table 3.1, being in accordance with current literature [75].

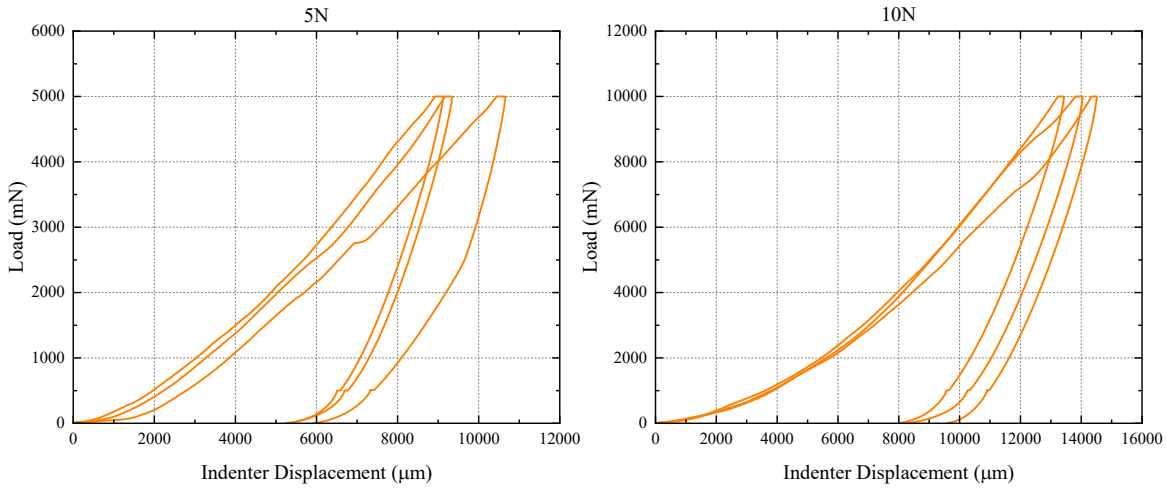

(a) (b)

Figure 3.2: Load and unload curves a maximum load of (a) 5N and (b) 10N.

Energy-dispersive X-ray spectroscopy (EDS) was also done to the sample that underwent the nano/micro indentation tests, to ensure the purity of the sample used. This technique is based on the principle that each atomic element possesses a specific signature in

Table 3.1: Values for the reduced and young's modulus for each indentation load.

Load	Ident nº	Reduced Modulus (GPa)	Young's Modulus (GPa)
5 N	1	50.633	56.905
5 N	2	50.678	43.193
5 N	3	52.116	58.378
10 N	1	51.848	50.633
10 N	2	51.892	50.678
10 N	3	53.296	52.116

its electromagnetic emission spectrum. Knowing beforehand the material's composition and analyzing the subsequent EDS spectrum, it is possible to infer whether the sample is contaminated or not.

Based on the spectrum obtained for the NASICON sample, displayed on Fig. 3.3 , it is possible to conclude that the ceramic electrolyte does not posses any impurities and its characteristic peaks in the electromagnetic emission spectrum are in accordance to values obtained in literature [6], [76], [77].

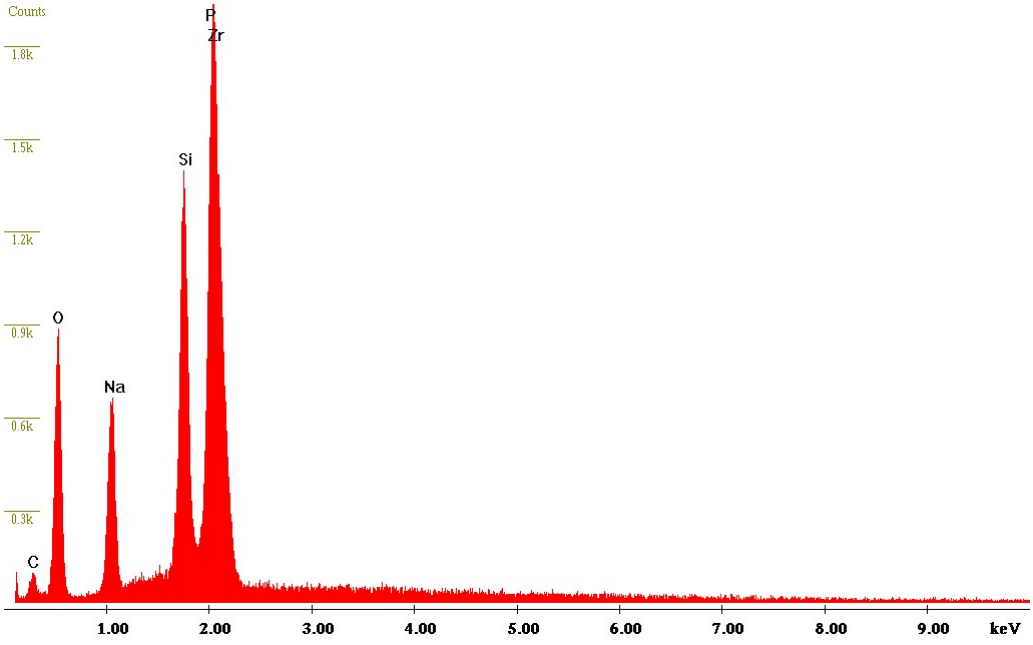

Figure 3.3: Energy-dispersive X-ray spectroscopy analysis on a NASICON sample.

Using the scanning electron microscope (SEM) technique, it was possible to obtain enhanced images of the electrolyte´s surface. This technique is based on the interaction of electrons with the sample's surface. This interaction will generate different signals according to the surface's topography, being then used to construct an image of the surface's composition. The following set of images display photographs taken from the SEM performed

on the NASICON ceramic pellet used for the nano/micro indentation tests.

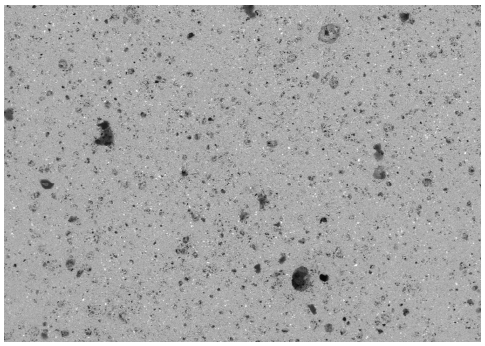

(a) 200x Zoom

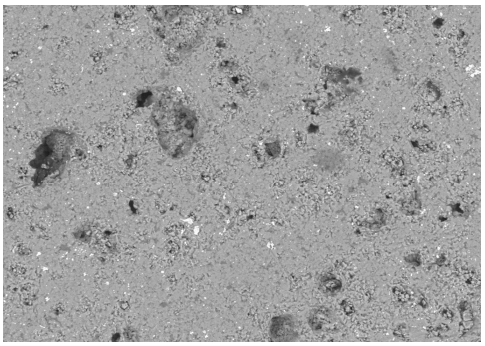

(b) 1000x Zoom

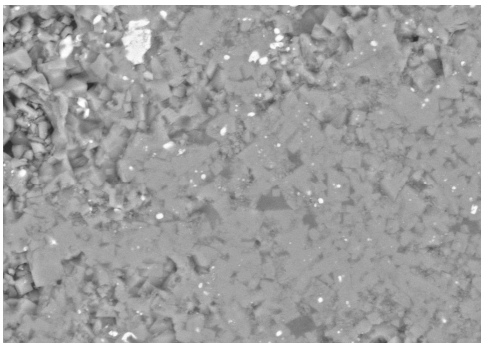

(c) 5000x Zoom.

Figure 3.4: SEM photographs obtain from the sample using different levels of amplification.

SEM images were also taken of the indentation done by the Berkovich-type indenter in order to calculate the ceramic's fracture toughness, as can be seen on Fig. 3.5. As there were three different sets of indentations made with a maximum load of 10N, three different fracture toughness can be calculated, with the material's value being an average of the indentation sets. Fig. 3.6 displays up-close images of the indentation sets and respective crack lengths.

Table 3.2 displays the retrieved crack lengths and respective fracture toughness, yielding an average value of 5.851 MPa $m^{0.5}$. The equations used to obtain these values are displayed in greater length in section 2.2.3.3, as discussed previously.

Table 3.2: Fracture toughnesss for a maximum load of 10N.

Indentation N°	**Crack length [μm]**	**K_{IC} [MPa $m^{0.5}$]**
1	41.05	6.357
2	40.32	6.844
3	51.29	4.351

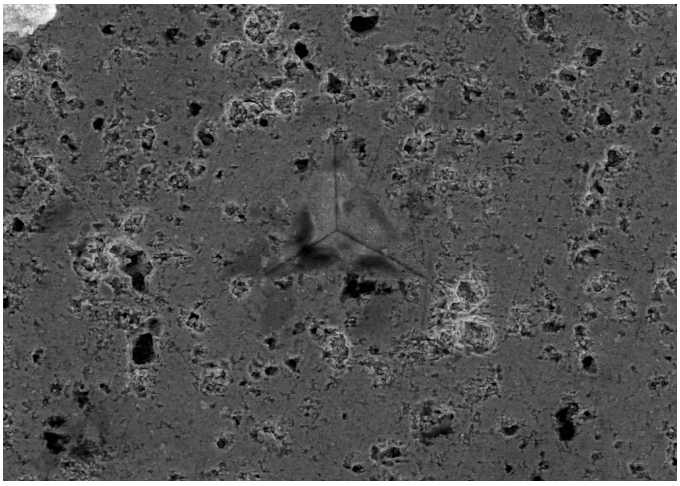

Figure 3.5: Indentation mark for a maximum load of 10N.

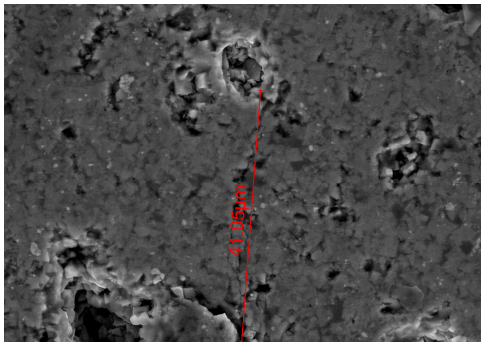

(a) 1st set.

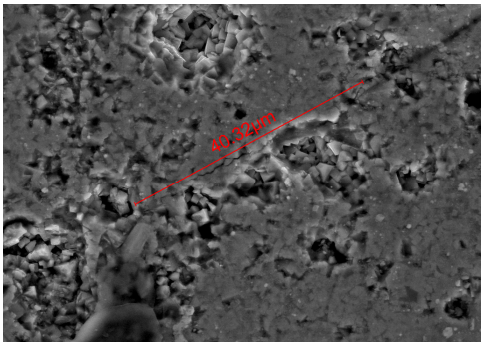

(b) 2nd set.

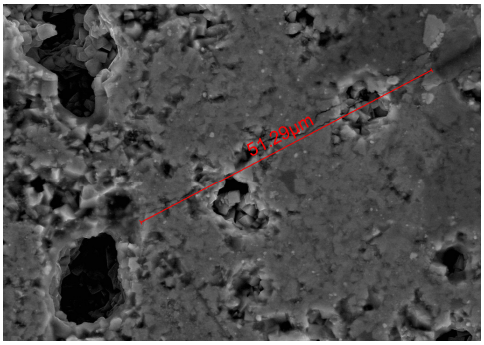

(c) 3rd set.

Figure 3.6: SEM photographs obtain for the calculation of fracture toughness.

3.2 Internal Resistance Tests: Pouch-Cell Structure

The first step towards the development of an all-solid-state battery using a NASICON-type electrolyte consists in assessing the resistance of several components utilised, focusing on the electrolyte and electrolyte/electrode interfaces. For this purpose, asymetric hybrid capacitors were conceived as test cells. These cells are composed by two different metals, with the function of testing them as current collectors, zinc, copper and carbon-felt as a porous electrode deposited on the copper current collector. Having tested different polymers as

binding agents for the NASICON solid electrolyte, within the scope of Tiago Salgueiro's master's thesis [78], the one with the highest ionic conductivity was chosen to be included in the test cells. The interface resistance with the carbon-felt and the different current collectors was tested in different test cell structures through electrochemical impedance spectroscopy, at room temperature and at different temperature levels.

3.2.1 Solid Electrolyte

3.2.1.1 Materials and Methods

Using a pouch-cell-like configuration,hybrid capacitors cell architectures were assembled to measure the internal resistance of its constituents. Having in mind both electrochemical and mechanical testing purposes, it was decided to employ two different metals who served as both electrodes and current collectors. They were placed so as to be in contact with the different electrolyte configurations. The ceramic pellet was put in between the two layers of polymer.

Electrode Configuration

For the electrodes, zinc (99.98%, ThermoFisher) was used as anode, and copper (99.9%, ThermoFisher) coupled with carbon felt (99.0%, ThermoFisher) as cathode. Foils of zinc and copper were cut to form 20x20 mm^2 contact surfaces, with a thin prong extended to serve as a location to clamp cables to perform measurements. The thickness of the copper and zinc foil was 0.254 mm and 0.25 mm, respectively. Carbon felt has a thickness of 3.18 mm.

An electrode composed of copper and carbon powder was also used. The carbon powder consisted of a mixture of pure carbon powder and ethanol. A ratio of 0.02135g of carbon and 2 ml of ethanol were mixed together thoroughly and smeared on the surface of the copper plate.

Table 3.3: Electrode configuration for solid state electrolyte.

Cell ID	Anode Material	Cathode Material
PC3	Zinc	Copper + Carbon powder
PC4	Zinc	Copper + Carbon Felt
PC5	Zinc	Copper + Carbon Felt
PC6	Zinc	Copper + Carbon Felt

Electrolyte Configuration

The $Na_3Zr_2Si_2PO_{12}$ ceramic electrolyte pellet, purchased from 4TOONE™, is of circular shape, with a radius of 20 mm and a thickness of 1 mm. It has a density of 3.0 g cm^{-3}.

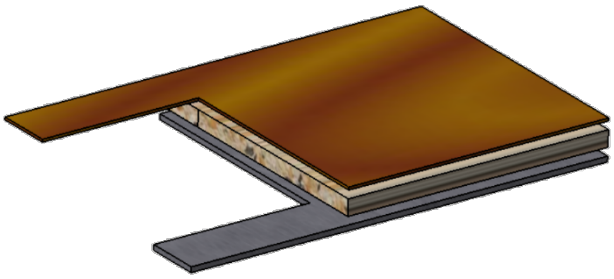

Figure 3.7: Hybrid capacitor with pouch-like configuration.

Figure 3.8: Example of a Pouch Cell.

A polymeric layer was also added to the ceramic electrolyte in order to decrease its intrinsic high inter-facial resistance and to improve the surface's wettability. For the polymeric layer coating both sides of the ceramic pellet, different compositions were tested. Commercial PVA-based glue (SuperTite™) composed of polyvinl alcohol (PVA), sodium chloride salt (Saldomar™), NASICON powder (MSE Supplies) and pure polyvinyl alcohol were incorporated in the cell using different configurations. The choice for these components was based on previous research and on review of available literature. Research conducted by Tiago Salgueiro master's thesis, allowed to infer that commercial PVA-based glue presents itself as the best candidate as polymer for electrochemical applications, while as the sodium chloride and NASICON powder were selected due to their good charge transfer properties and diffusivity effects, respectively.

In cases where more than one component was used to manufacture the polymer configuration, a pestle and a mortar were used to ensure a homogeneous mixture.

Table 3.4: Polymer configuration for solid state electrolyte.

Cell ID	Polymer Composition	Polymer Weight (g)	Electrolyte
PC3	commercial PVA-based glue (only on the side of the zinc)	0.072	NASICON Pellet
PC4	commercial PVA-based glue + NASICON Powder	0.154	NASICON Pellet
PC5	commercial PVA-based glue	0.1403	NASICON Pellet
PC6	Pure PVA	0.1085	NASICON Pellet

Fig. 3.7 displays how the different components were assembled. To avoid creating a short-circuit, a thin strip of isolating tape, around 3 mm wide, was placed on the electrode's surface in contact with the polymer, for both the cathode and the anode. The polymer mixture was then spread upon the anodic surface area and the NASICON pellet placed over it. Another layer of polymer was smeared on the top-sided surface of the pellet, with the carbon felt and finally the copper plate placed on top of the carbon felt. After assuring all interfaces were in contact properly, the assembly was sealed shut inside duct tape (tesa™) to form a pouch cell. Only the aforementioned current collector prongs were left exposed, so as to minimize the effects of outside temperature and moisture in the cell's behaviour.

After having assembled the cells, using a Gamry Interface 1010 E potentiostat, impedance spectroscopies were performed on the day of manufacture to assess the internal resistance of each pouch cell manufactured. The cells were kept at room temperature whilst the testing was performed. All the experiments were carried out with the frequencies varying from 2 MHz down to 0.1 Hz. Using the impedance obtained, it is possible to retrieve the ionic conductivity using Eq. 3.1. The ionic conductivity is dependent on the charge transfer resistance measured on the impedance spectroscopy (R), as well as the thickness (t, in cm) and surface contact area (A, in cm^2).

$$\sigma = \frac{t}{R * A} \tag{3.1}$$

The influence of temperature was also investigated. Using a *Sifamir* SIF450|50M1-2HOT hot press, the pouch cells were heated to six different predefined plateaus of temperature (20, 35, 50, 65, 80 and 95°C) and left at those plateaus for 10 minutes before conducting a EIS on each level. The tests were performed eight days after the cells were manufactured.

3.2.1.2 Results and Discussion

Despite striving for an electrolyte solution based on an all-solid-state form, different polymer-based electrolytes were tested so as to have an overview of the results achieved.

With the measurements made immediately after manufacture and at room temperature, the capacitor with the configuration of commercial PVA-based glue coupled with NASICON powder presents the best results in terms of internal resistance, with no visible second semi-circle in the Nyquist plot. This is consistent with available literature, stating the diffusive effects of the NASICON electrolyte in form of powder.

The remaining three capacitor configurations display a visible second semi-circle, due to the lack of diffusive elements in the polymer's composition, causing the resistance present in the interface of polymer/electrode to become more noticeable.

To calculate the ionic conductivity of the commercial PVA-based glue, an equivalent circuit was modeled in order to calculate parameters such as the initial charge transfer resistance and the ionic conductivity. This equivalent circuit, displayed on Fig. 3.10, will be

Table 3.5: Initial charge transfer resistance for room temperature and day of manufacture.

Cell ID	Polymer Composition	Initial R_{ct} (Ω)
PC3	commercial PVA-based glue (only on the side of the zinc)	224.24
PC4	commercial PVA-based glue + NASICON Powder	153.51
PC5	commercial PVA-based glue	186.74
PC6	Pure polyvinyl alcohol	192.04

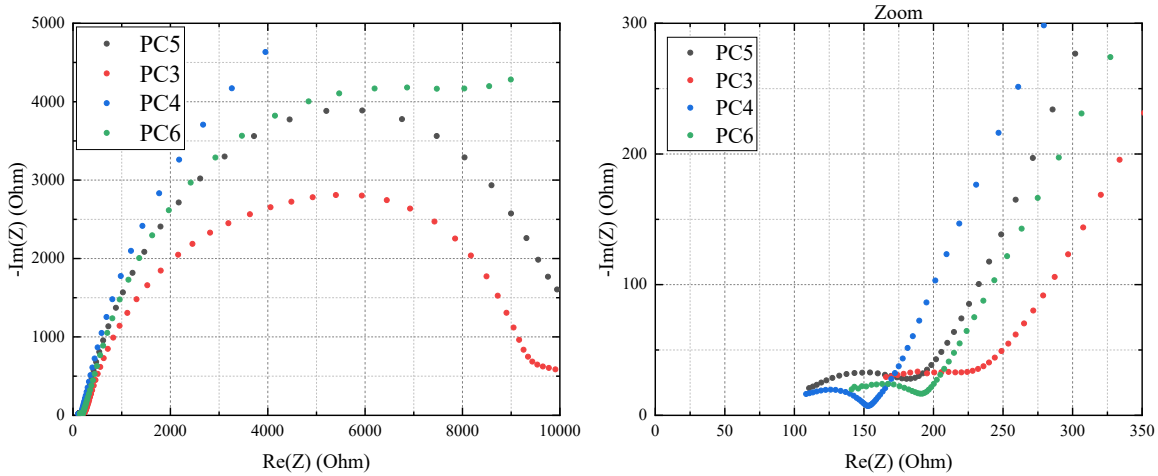

(a) Full view

(b) Zoomed view

Figure 3.9: EIS Plot at room temperature and day of manufacture.

used throughout the following sections, until active electrodes are employed in Chapter 4. The choice for this circuit relies on available literature [79].

The first resistance represents the bulk ionic and grain boundary resistance of the solid electrolyte, whilst the second resistance in parallel with the constant phase element is used to represent the interface resistance between the solid electrolyte and respective electrodes.

The ionic conductivity obtained for PC4 was $5.548 * 10^{-5}$ S cm^{-1}

In terms of the temperature influence, the results clearly show a trend of decreasing inter-facial resistance with the increase of the operating temperature, as can be seen in Fig. 3.11.

Pouch cell number four (PC4) exhibits six different resistance curves, with a consequential decrease as the temperature increases, showing that commercial PVA-based glue coupled with NASICON powder once again presents the most favourable results. The polymer composed solely of commercial PVA-based glue also exhibits, although not as clearly, a decrease of the resistance. The pure PVA-based polymer demonstrates to be influenced by the temperature, it was not however clear to see what the optimal operating temperature was, as membranes present in the compound only start to show thermal instability only in

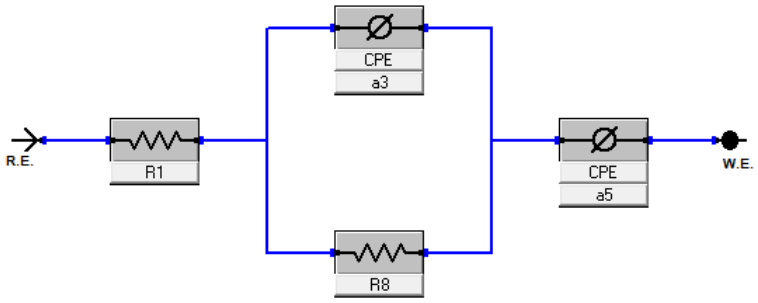

Figure 3.10: Equivalent circuit for capacitors.

regions upwards of 300ºC.

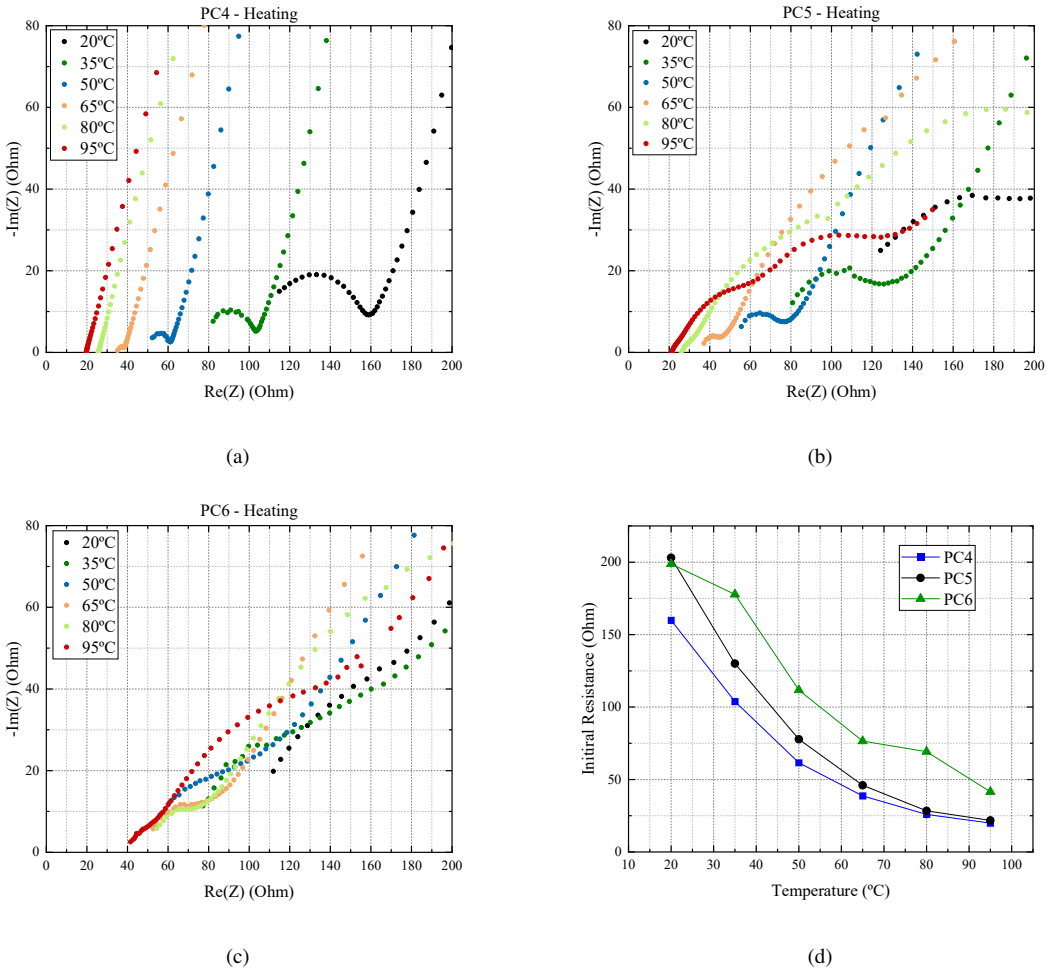

Figure 3.11: EIS Plot at the different temperature plateaus for (a) PC4, (b) PC5 and (C) PC6. (d) Evolution of initial resistance due to the effect of temperature.

Although promising results were obtained, EIS done after the cooling of the cells showed that they were ruined due to exposure to such high temperatures, despite functioning well at those temperatures. This is due to possible evaporation of some of the water content

present in both the pure polyvinyl alcohol and commercial PVA-based glue compounds. This evaporation causes the resulting mixture to become less bonding with the electrolyte's surface. Studies conducted once again in Tiago Salgueiro's thesis suggest that the maximum operating temperature conditions for these compounds is in the region of 70-80ºC.

3.2.2 Polymer Electrolyte

This section of experiments focused on isolating the influence of the ceramic electrolyte pellet, that is our ultimate goal for both structural and electrochemical safety reasons, using only the polymer layer as electrolyte. This allows to infer what is the influence of solely the polymer to the capacitor's resistance. The assembly process is exactly the same as for the solid electrolyte pouch cells, the only difference being that there will not a solid-state electrolyte present.

3.2.2.1 Materials and Methods

For the electrodes, the same metals were employed, with zinc serving as anode, and copper coupled with carbon felt or only copper itself, working as cathode.

Table 3.6: Electrode configuration for polymer electrolyte.

Cell ID	Anode Material	Cathode Material
PC9	Zinc	Copper + Carbon Felt
PC11	Zinc	Copper + Carbon Felt
PC17	Zinc	Copper

The different polymer configurations were produced by firstly weighing each component and then mixing them thoroughly using a pestle and a mortar, ensuring that the resulting substance is homogenized and grain-free.

Adding to the different polymers used to form the mixtures observed in the solid electrolytes configurations, a structural resin was also introduced to some of the capacitors. The resin, epoxy (DP490, 3M™), was used to infer what would be the influence of a component, whose main focus is structural integrity, on the cell's electrochemical behaviour, namely if and how the resistance would differ due to the presence of the structural resin. Sodium chloride was also studied, as its charge transfer properties can enhance the diffusive behaviour of the cell.

Table 3.7: Polymer electrolyte configuration.

Cell ID	Polymer Composition	Polymer Weight (g)
PC9	80% Glue + 20% NaCl	0.497 (Glue) + 0.124 (NaCl)
PC11	60% Glue + 40% NaCl	1.0664 (Glue) + 0.7292 (NaCl)
PC17	50% NASICON Powder + 25% Epoxy + 25% Glue	0.6065 (total)

3.2.2.2 Results and Discussion

As expected, the incorporation of sodium chloride as part of the electrolyte greatly reduces the initial charge transfer resistance of the manufactured hybrid capacitors. Its high ionic conductivity enabled the capacitor to achieve very low resistance values, as can be seen in

the impedance spectroscopy dislayed on Fig. 3.12, with the resistance values listed on Table 3.8.

The inclusion of the structural resin displayed very promising results. Despite showing a slightly inconvenient high charge transfer resistance, it appears that its inclusion does not affect greatly the electrochemical performance of the capacitor, making it possible to include a structural component into the cell's configuration, which was the first insight for being possible to use the resin for mechanical reinforcement. Adjusting the weight of each component in the polymer mixture can result in improved results containing the structural resin, as it will be seen in the chapters ahead.

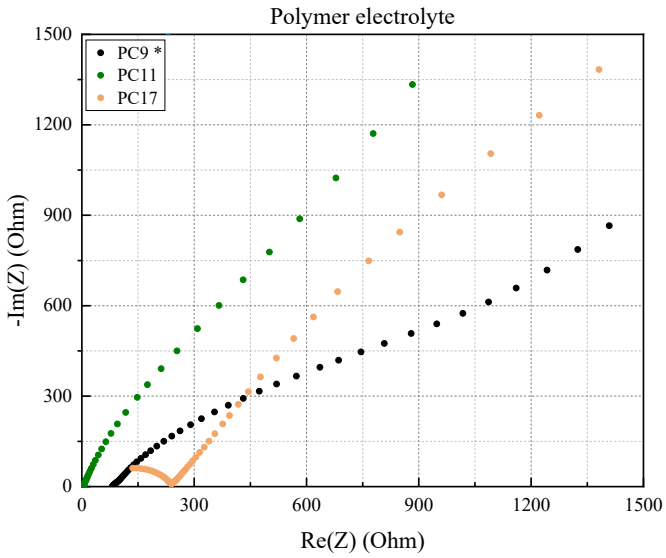

Figure 3.12: EIS plots for the polymer electrolyte capacitors (*PC9 was tested 9 days after manufacture).

Table 3.8: Initial charge transfer resistance for polymer electrolyte.

Cell ID	**Polymer Composition**	**Initial R_{ct} (Ω)**	**σ (S cm^{-1})**
PC9	80% Glue + 20% NaCl	79.47	0.00011
PC11	60% Glue + 40% NaCl	2.795	0.00299
PC17	50% NASICON Powder + 25% Epoxy + 25% Glue	245.23	3.416*10^{-5}

3.3 Internal Resistance Tests: Coin Cell and Glass Fibre Structure

The steps up until now have been able to shed some light on how the different polymers contribute to the capacitor's internal resistance and also what is the influence of temperature on the aforementioned capacitors. However, due to the intrinsic nature of a pouch cell-like configuration, it was not possible to see how the internal components of the capacitor progressed over time after manufacturing. The structure did not have the ability to be properly sealed against the effects of moisture and humidity, as well as not presenting a component capable to withstand mechanical loads and reliably assess the cell electrochemical properties.

To address this issue, capacitors were developed using a coin cell-like configuration. The objective is to observe the cell's ageing process influenced solely by its internal components and withdrawing moisture and humidity effects. Due to final goal that is the development of structural batteries and bearing in mind its great isolating and good mechanical load bearing capabilities, glass fibers were used as encapsulating agents to seal the capacitors, with identical configurations being developed for both glass fiber and coin cells and posteriorly compared between them, to assess if the glass fiber's sealing properties are as effective as the ones observed in a coin cell.

Likewise, the incorporation of a structural resin, mixed with the polymer binding agent, will once again be tested in different configurations and compared against a reference polymer. This specific resin used has a curing cycle of 24 hours at room temperature or 1 hour at 80º C. The influence of the curing process of the resin itself will also be observed.

3.3.1 Epoxy Resin as Binding Polymer

3.3.1.1 Materials and Methods

Three initial different binding polymer configurations were developed to assess the influence of the epoxy resin in the cell's internal resistance, with the most promising one being then incorporated in a coin cell-like structure.

Table 3.9 shows the binding polymer composition used.

Table 3.9: Electrolyte configuration for clamp cells.

Cell ID	Polymer Composition	Electrolyte
CG1	70% Glue + 20% Epoxy + 10% NASICON Powder	NASICON Pellet
CG2	70% Glue + 30% Epoxy	NASICON Pellet
CG3	50% Glue + 50% Epoxy	NASICON Pellet

For the assembly process, stainless steel spacers were used as electrodes. Thin conductive wires, as used previously, were fixed on top of the spacers using isolating duct tape.

The polymer mixture was then smeared on both sides of the NASICON ceramic pellet, with the spacers being placed on each surface as well. Duct tape was then wrapped around the capacitor to make sure everything was hold into place. After that, the assembly was fixed together with a clamp to simulate the pressure exerted by a coin cell.

Impedance spectroscopies were done on each of the three configurations (see Fig. 3.13), immediately after manufacturing and 24 hours after. This enables the observation of how the curing cycle of the structural resin influences the internal resistance.

3.3.1.2 Results and Discussion

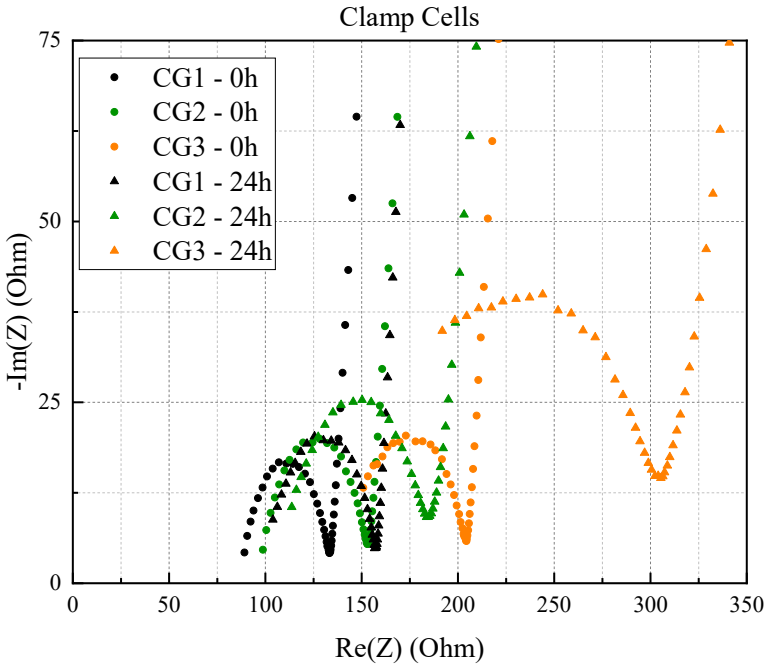

Figure 3.13: EIS - Clamp cell's evolution through the resin's curing process.

The curing process of the structural resin seems to bear rather little significance in the overall resistance of the capacitors. The rate of increase is directly linked with how much resin is present in the polymeric mix.

Comparing the three configurations, CG1 presents the most promising results, with the inclusion of the NASICON powder helping balance the resistive nature of the resin. As the content of resin increases, the mixture becomes evermore viscous, leading to higher inter facial resistance. The optimal content of structural resin is reached at 30%. Values higher than this leads to a spike in the inter facial resistance after curing, as can be seen in capacitor CG3.

As CG1's composition had the best results, it will be redone inside the coin cell and its ageing process compared to a capacitor composed of only PVA-based glue in the polymer mixture.

Table 3.10: Initial charge transfer resistance for clamp cell configuration.

Cell ID	Polymer Composition	Initial R_{ct} (Ohm)	σ (S cm^{-1})
CG1 - 0h	70% Glue + 20% Epoxy + 10% NASICON Powder	133.44	9.555*10^{-5}
CG1 - 24h	70% Glue + 20% Epoxy + 10% NASICON Powder	156.60	8.142*10^{-5}
CG2 - 0h	70% Glue + 30% Epoxy	157.10	8.116*10^{-5}
CG2 - 24h	70% Glue + 30% Epoxy	183.83	6.936*10^{-5}
CG3 - 0h	50% Glue + 50% Epoxy	207.61	6.142*10^{-5}
CG3 - 24h	50% Glue + 50% Epoxy	306.95	4.154*10^{-5}

3.3.2 Coin Cell Encapsulation

3.3.2.1 Materials and Methods

Using a CR2032-type coin cell (components from Nanografi), two different capacitors were developed. Both of them had the same manufacturing process, with a spacer and the positive case serving as current collectors. A spring was allocated between the spacer and negative case to ensure that pressure was distributed uniformly. The NASICON pellet was coated on both sides with the different polymer binding agents. One of the cells had only the commercial PVA-based glue serving as polymer, with the other using the polymer compound which presented the best results in the clamp cell's testing phase. The process of assembly was done by stacking vertically each component in the following order: negative case, spring, spacer, polymer, pellet, polymer and positive case. In Fig. 3.14 it is possible to see the aforementioned components, with the negative case, positive case, spacer and spring being displayed in a clockwise direction, beginning on the upper left corner. The crimping of the coin cells components were done using a MSK-160D Digital Pressure Controlled Electrical Crimper from MTI Corp.

Figure 3.14: Components of a CR2032 coin cell [80].

Table 3.11: Electrolyte configuration for coin cells.

Cell ID	Polymer Composition	Electrolyte
CC8	70% Glue + 20% Epoxy + 10% NASICON Powder	NASICON Pellet
CC9	100% Glue	NASICON Pellet

After the cells were correctly assembled, impedance spectroscopies were conducted after manufacturing and throughout the following days to assess the ageing process. They remained stored in a dry environment to ensure that tests were conducted in the most neutral environment possible.

3.3.2.2 Results and Discussion

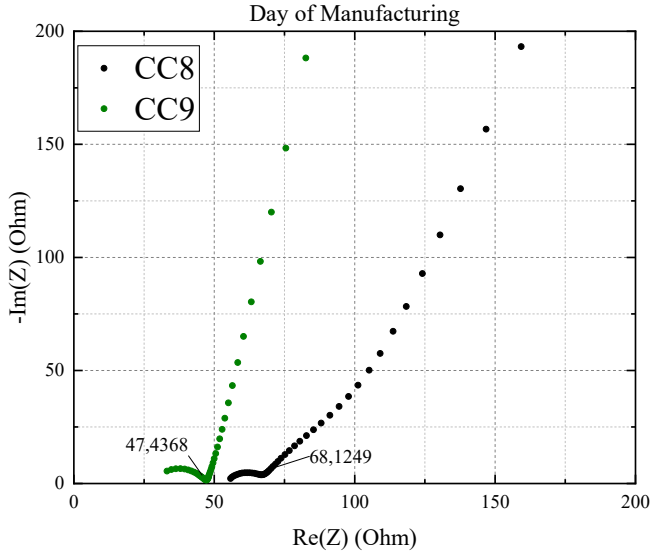

Figure 3.15: EIS - Comparison between CC8 and CC9

The EIS conducted on the day of manufacturing (DOM) shows that the configuration involving the structural resin presents a 30% decrease in resistance when compared to only PVA-based glue as polymer. A possible explanation can be due to the incorporation of NASICON powder and the good ratio of epoxy and PVA-based glue, allowing for a better wettability of the electrolyte's surface.

In terms of ageing, the impedance spectroscopies conducted throughout the following days showed that CC9, composed of structural resin, exhibited virtually no ageing, maintaining a constant value of initial resistance. CC8 showed fluctuations of resistance values, which can be traced to the differences in ambient temperature during the testing phase.

It is known that PVA-based glue can be prone to be influenced by the ambient temperature during testing. The incorporation of the structural resin, and subsequent curing, seems

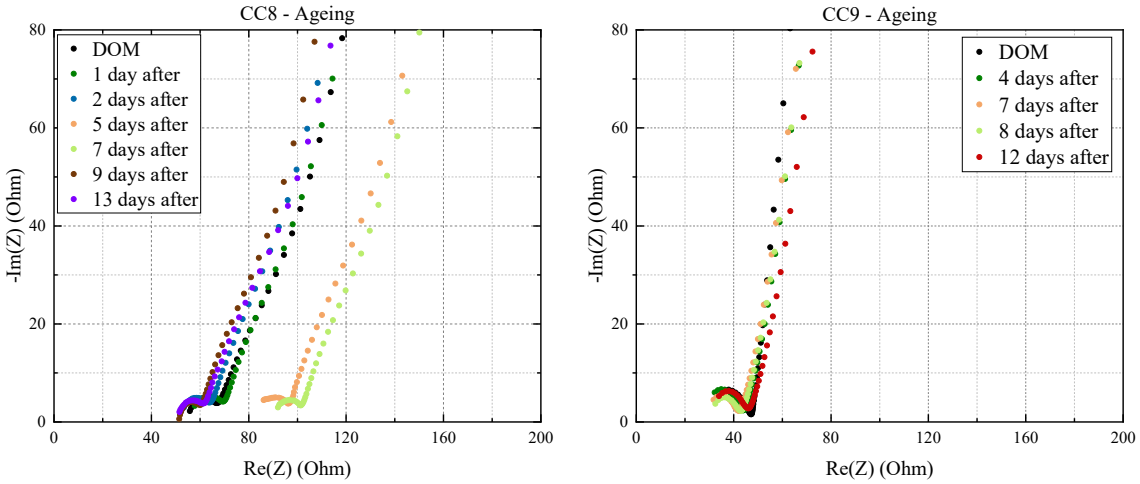

(a) CC8 (b) CC9

Figure 3.16: EIS - Ageing process of the coin cell configurations.

to be a solution to this issue. Whilst PVA-based glue remains a viscous liquid after curing, epoxy resin turns into a solid. This solid phase may help to form an impermeable layer around the interface of electrode/electrolyte, explaining the lack of ageing and effect of ambient temperature. Fig. 3.17 helps to illustrate the reduced ageing of the coin cell's composition. The two peaks observed on CC8 are due to differences in the ambient temperature during measurements, after 5 and 7 days respectively, as has been mentioned before.

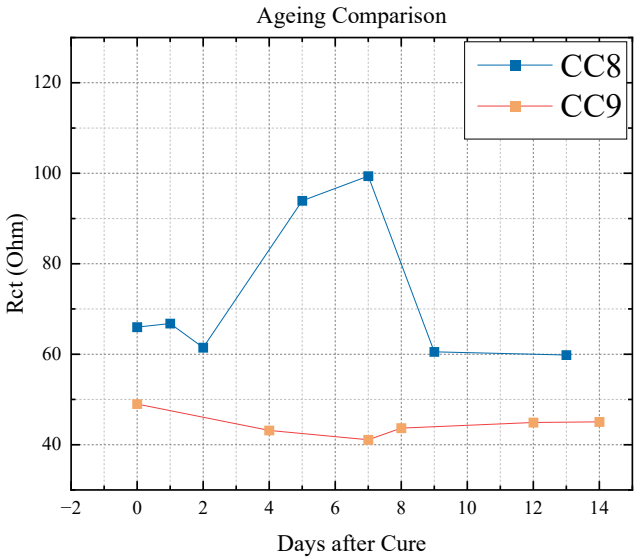

Figure 3.17: Evolution of R_{ct} after manufacture in coin cells.

3.3.3 Glass Fibre Encapsulation

3.3.3.1 Materials and Methods

Symmetric capacitors using a solid-state electrolyte and with similar configuration used in the last chapter were developed and encapsulated inside glass fibers. The objective was to assess if this form of encapsulation was able to return results similar to the ones observed using a coin cell-like configuration. If successfully implemented, this enables the creation of an embedded system, focusing both on the mechanical and electrochemical aspects of the cell.

The cells were embedded using a 25 g/m^2 undirectional glass fibre reinforced plastic supplied by NTPT (TP736LT). The material is supplied in the form of pre-preg and the resin system is a proprietary high toughness epoxy (736LT)s. For the capacitors GF1, GF2, GF4 and GF5, a total number of 40 layers were used with a stacking orientation of $[0^\circ/90^\circ]$ to enclose the capacitors in a symmetric plane laminate. For the following capacitors, the total number of layers used was 16 with a orientation of $[0^\circ_2/90^\circ_2]_2$. The curing process was done using the aforementioned hot plate and placing an aluminium mold on top of the capacitors in order to ensure uniform distribution of temperature and pressure throughout. No vacuum bag was used and the capacitors were cured for 8 hours at 80ºC in compliance with the manufacturer specification. The mold contained a 25x25 mm^2 orifice in the middle to accommodate the bulk of the capacitors.

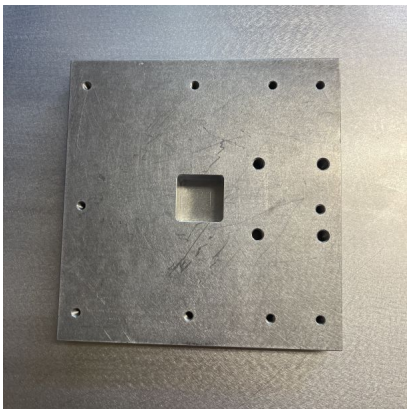

Figure 3.18: Aluminium mold used for the curing of glass fibers in the hot press.

The first step consisted on inspecting the best method to connect the thin conductive copper wires to the surface of the current collectors. Two technologies were employed, one consisting on using isolating duct tape, and the other by spot welding the wires onto the metal's surface. After curing the fibers in the press, it was discovered that the welding connection suffered from corrosion and therefore the use of duct tape was best suited for this type of application, as can be seen in Fig. 3.19.

The configuration of the polymer mixtures used were identical to the ones used in the coin cell stage. One was based purely on the PVA-based PVA-based glue, with the second

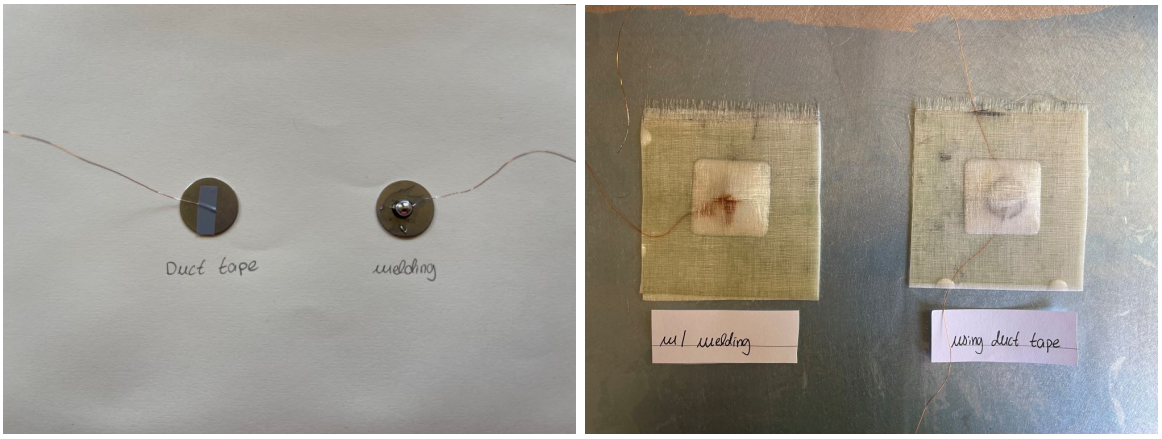

(a) (b)

Figure 3.19: Connection of the conductive wires to the current collector's surface (a) before and (b) after curing.

configuration being composed of PVA-based glue, structural resin and NASICON powder.

Table 3.12: Polymer configuration for glass fiber cells.

Cell ID	Polymer Composition	Electrolyte
GF4, GF6	70% Glue + 20% Epoxy + 10% NASICON Powder	NASICON Pellet
GF1, GF2, GF5, GF7, GF8	100% Glue	NASICON Pellet

Another aspect that was looked into was of how to optimize the seal process of the capacitors from the environment and also how to prevent the polymer mixture from reacting with the resin of the pre-preg. The use of duct tape and oversized current collectors as isolating agents were investigated. In a first step, stainless steel coin spacers were used as current collectors and placed directly upon the fibers, before curing.

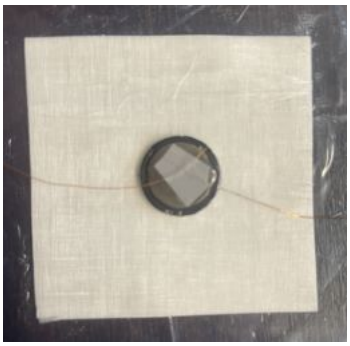

Figure 3.20: Capacitor using only fibers as sealing agent, before curing.

American-style duct tape, from Tesa™, was used to seal the cells, forming a protective pouch within the capacitor. The resulting pouch cells were then placed in-between the glass fibres cured in the hot press.

(a) (b)

Figure 3.21: Duct tape as sealing agent (a) before and (b) after curing.

Another strategy used to improve the sealing process of the capacitors was the use of oversized copper current collectors. The objective was to employ copper foil with dimensions superior to the circular ceramic electrolyte pellet in order to prevent the polymer mix to get in contact with the fibers. This method was tried out with (GF8) and without (GF7) duct tape wrapping the copper foil, with the copper having dimensions of 2.1x2.1 cm and 2.5x2.5 cm, respectively. As was the case in section 3.2.1.1, isolating tape was used on the edges of the copper foils to prevent a possible short circuit. Table 3.13 summarises the different encapsulation configurations investigated within this work.

Table 3.13: Glass fiber configuration

Cell ID	Current Collector	Seal Strategy	Wire connection
GF1	stainless steel	only fibers	welded
GF2	stainless steel	only fibers	isolating tape
GF4	stainless steel	only fibers	isolating tape
GF5	stainless steel	fiber + duct tape	isolating tape
GF6	stainless steel	fiber + duct tape	isolating tape
GF7	copper	bigger dimensions	isolating tape
GF8	copper	bigger dimensions + duct tape	isolating tape

3.3.3.2 Results and Discussion

After the cells were cured and impedance spectroscopies done, they were opened to assess the state of the polymer at the interfaces. Capacitors whose seal strategy did not involve duct tape displayed little, or none, remaining polymer in the electrode/electrolyte interface. It appears that the polymeric mixture, both only PVA-based glue and with structural resin, reacted with the fiber's resin, causing the wetting agents to be removed from the inter facial locations. This in turn caused the EIS done to show massive resistance, caused by lack of wetting agent. When the capacitor was sealed off with duct tape, as seen in Fig. 3.21a, the

polymer mixture was impeded to react with the fibers, maintaining a good wettability in the electrode/electrolyte interface.

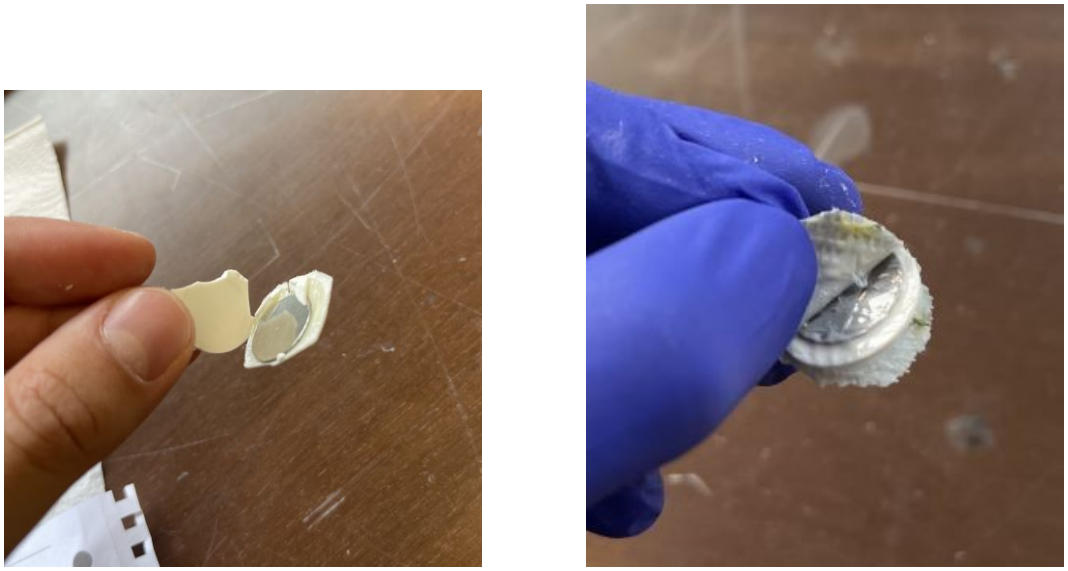

(a) Only fibers (b) Using duct tape

Figure 3.22: State of wetting agent after cure.

As the seal strategy composed of using duct tape presented the best results, they will be analysed more in detail.

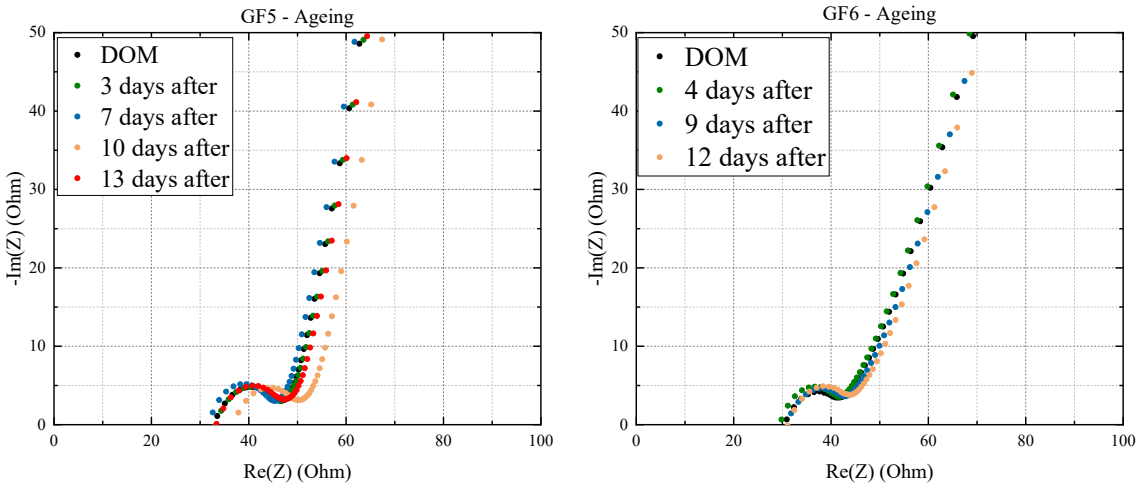

(a) GF5 (b) GF6

Figure 3.23: EIS - Ageing process of the glass fiber configurations.

Impedance spectroscopies done through the course of the following days after the day of manufacture (DOM) show that there was, once again, virtually no sign of ageing of the capacitors. The use of duct tape inside the glass fibre encapsulation provided an optimal sealing strategy, making the capacitors unbothered by the effects of outside temperature

and moisture, with no visible spiked in impedance measurements, as happened in the coin cells.

Similarly to what was observed in the coin cells, the configuration that was composed of the structural resin showed even smaller variations in ageing and lower initial resistance values.

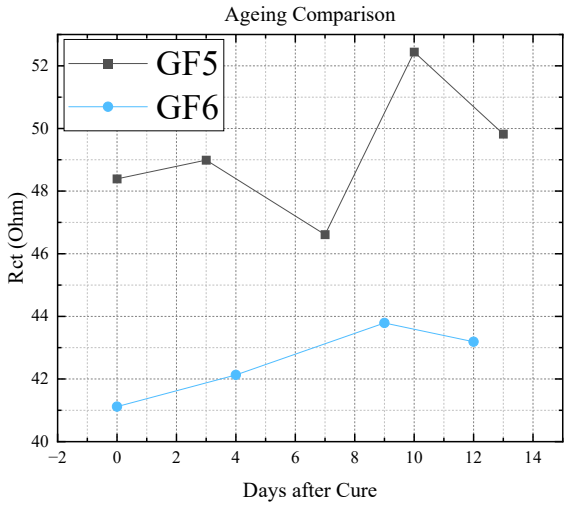

Figure 3.24: Evolution of R_{ct} after manufacture in glass fiber cells.

Fig. 3.25 shows impedance spectroscopy plots of identical capacitor configurations using either coin cell or glass fiber structures to seal off the components. CC8 and GF5 possess a PVA-based glue based polymer, with CC9 and GF6 incorporating structural resin, as has been mentioned before. When comparing the plots, the results demonstrate that the glass fiber cell exhibits lower initial charge transfer resistance immediately after manufacturing. This shows that there seems to be no significant drawback in incorporating a component with structural capabilities as a sealing agent. The results allow for the creation of multifunctional systems who present enhanced performance compared to conventional non-structural configurations.

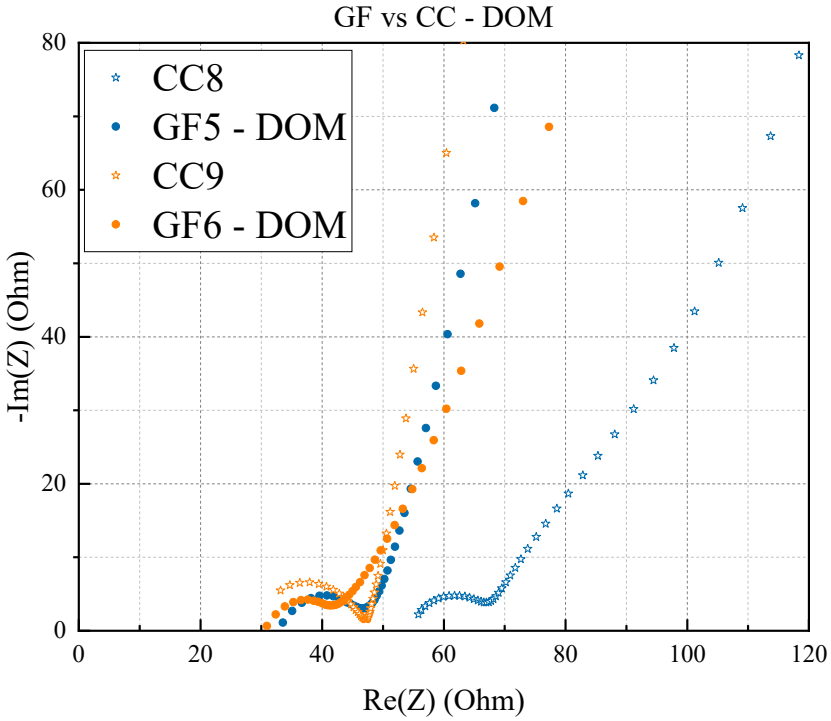

Figure 3.25: EIS - Comparison between glass fiber and coin cell capacitors on the day of manufacture.

Chapter 4

Full Cell Development

Using the knowledge gathered from the previous steps, full solid state sodium ion structural cells were developed with active electrodes and embedded within glass fibres. The electrodes developed in the following subsection will be employed on all full cells ensuring common ground for the discussion of the obtained results.

4.1 Materials and Methods

4.1.1 Cathode Preparation

For the cathodic material, $Na_3V_2(PO_4)_3$ (NVP-C) was employed due to its promising results analysed on Chapter 2. NVP was synthesized using a one-stage carbothermal reduction strategy. The objective of this process was control thoroughly the carbon content of the NVP material, preventing possible short-circuits in future steps.

The protocol for the synthesis of pure NVP was based on Zhao and colleagues' article [81] and developed and optimized on the context of the aforementioned master's thesis developed by Tiago Salgueiro. It consisted on dissolving 2 mmol of NH_4VO_3 and 2.8 mmol of $C_2H_2O_4$ into 30 mL of deionized water at a temperature of 80ºC. 3 mmol of NaH_2PO_4 was then added to the solution and evaporated into a gel at 80ºC. It was then dried overnight for 12 h at 120ºC.

With the pure NVP prepared, it was then possible to move onto the manufacturing of the cathode itself. A mass ratio of 80:10:10 composed of the NVP, carbon black and polyvinylidene fluoride (PVDF), respectively, was used as cathode. Using a pestle and a

mortar, the three components were mixed vigorously, forming a grain-free slurry. After that, the slurry was coated onto stainless steel coin cell spacers being used as current collectors. Finally, the whole assembly was dried for 8 h at 120ºC under vacuum.

Figure 4.1: Cathode after being dried overnight in vacuum.

The cathode's weight was measured by first weighing the spacers where the cathode would be placed. After the cathode was dried, the assembly of spacer plus cathode was weighed again and the cathode's weight was measured by subtracting the measured values. Table 4.1 displays the weights obtained.

Table 4.1: Weight measurements for the cathode.

Cell ID	**Cathode Weight (g)**
FC4	0,0062
FC6	0,0039
FC7	0,0085
FC9	0,0065
ATC1	0,0152
ATC2	0,0122
ATC4	0,0139
ATC6	0,014

As mentioned previously, the choice of NVP-C as cathode for the all-solid-state sodium-ion structural battery developed is based on this compound's very high sodium-ion mobility and firm structural stability. The use of carbon coating is employed as an optimizing strategy due to NVP's relative low theoretical capacity.

The crystalline structure of the NVP-C cathode presents a three-dimensional open framework structure, were three Na^{+} in the molecular form are located either in a M1 or M2 site. These M represent a transition metal element and are part of the crystalline structure. The vanadium present in the NVP-C structure presents four oxidation states and can, in theory, be oxidized from V^{3+} to V^{4+} and possibly V^{5+}. It can also be reduced from V^{3+} to V^{2+} by intercalation of the sodium ion.

During the de/intercalation process, it is expected that some electrochemical reactions occur in the NVP-C structure. Two voltage plateaus are expected to appear at 3.4 V and 1.6 V, owing to the redox pairs of V^{3+}/V^{4+} and V^{3+}/V^{2+}, respectively, which points to a two-phase transformation [5]. The high voltage plateau presented in the first redox pair makes the use of this material very attractive as cathodes for sodium-ion batteries. The eletrode reaction occurring during the charge and discharge of the NVP-C cathode can be represented using Eq. 4.1.

$$\begin{aligned} Na_3V_2^{3+}(PO_4)_3 &\leftrightarrow Na_{3-x}V_{2-x}^{3+}V^{4+}(PO_4)_3 + xNa^+ + xe^- \\ Na_3V_2^{3+}(PO_4)_3 + xNa^+ + xe^- &\leftrightarrow Na_{3+x}V_{2-x}^{3+}V_x^{2+}(PO_4)_3 \end{aligned} \tag{4.1}$$

4.1.2 Anode Preparation

For the negative electrode, a hard carbon based anode was used due to its low cost and easy synthesis process. The preparation process is similar to the one observed for the cathode [13].

A first step consisted on mixing polyvinylidene fluoride (PVDF) with an NMP (N-Methyl-2-pyrrolidone) solvent until a viscous liquid is formed. Subsequently and using a 80:10:10 mass ratio, hard carbon (TMAX), super P and the mixed PVDF slurry are bundled together using a pestle and a mortar. The resultant mixture should not contain any visible grains.

The next step consist on smearing the anodic material onto two different surfaces. The first one used is identical to the one used for the cathodes, that is, the stainless steel coin cell spacers. Another material investigated was heated carbon felt, where using a paint brush, the hard carbon anode was coated onto the carbon felt. The anodes were then left to dry overnight at 80ºC under vacuum.

Figure 4.2: Anode material "slurry" after being mixed.

4.1.3 Electrolyte and Cell Assembly

The electrolyte employed was still the solid-state NASICON ceramic pellet. The choices for wetting agents were based on results achieved up until this point, with two different configurations being used. The first one is composed exclusively of commercial PVA-based glue, with the second one being a conglomerate of commercial PVA-based glue, epoxy and nasicon powder, with 70:20:10 mass ratios, respectively.

In terms of the assembly itself, the process consisted first on doing the layup process of the glass fibres used. The cells were encapsulated in-between two plates of glass fibre (TP736LT, 25g/m^2), each of them consisting of a total of 16 layers with 70x70 mm^2 dimensions and with a layup orientation of $[0^\circ_2/90^\circ_2]_2$. A piece of duct tape was placed on top of the upper layer of the bottom plate of fibres, with the constituents of the battery placed on top of the duct tape. Thin conductive wires, identical to the ones used on section 3.3.3.1, were connected to the surface of the coin cell spacers using isolating duct tape.

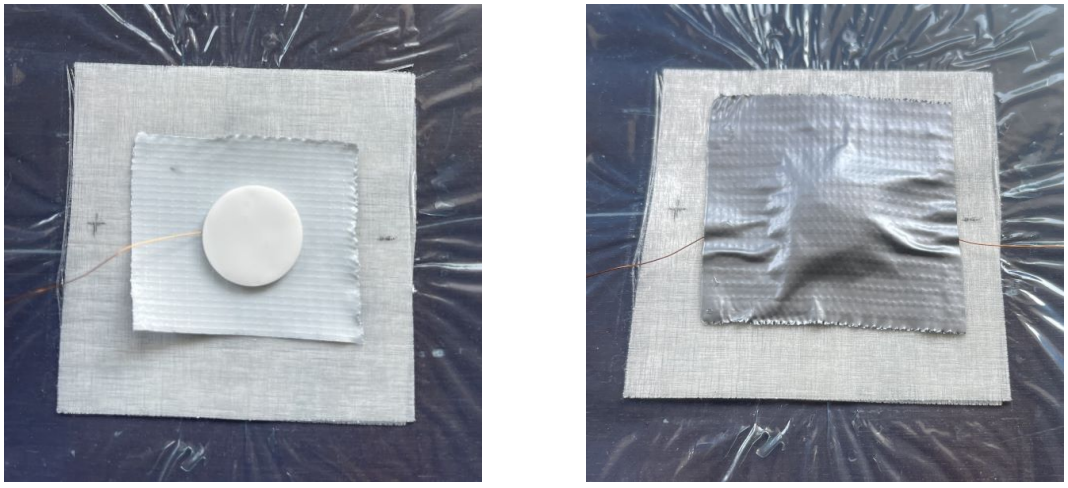

(a) Before sealing

(b) After sealing

Figure 4.3: Assembly process of full cells during the duct tape sealing step.

The stacking sequence begins with the current collector plus anode combination being placed at the bottom, in contact with the duct tape. The polymer mixture is then smeared on both sides of the ceramic pellet, with the electrolyte being placed on top of the anodic surface. The cathode and stainless steel spacer is then placed on top of the ceramic pellet. After ensuring the constituents are stacked correctly, a second piece of duct tape is placed on top of the battery and connected to the duct tape previously in place, as seen in Fig. 4.3. This ensures good sealing against foreign agents. This process is done for cells containing both stainless steel spacers only and for the ones where carbon felt is employed (see Fig. 4.4).

The final stage of the assembly process is the closing of the fibres by placing the second plate of glass fibre on top and ensuring proper bonding between the fibres, when they are in

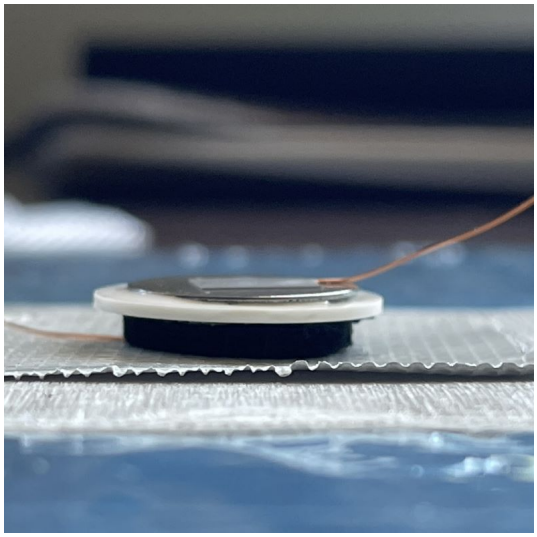

Figure 4.4: Side view of the assembly process containing carbon felt smeared with the anodic material

touch, as seen in Fig. 4.5. With this step done, the whole assembly then needs to undergo some sort of temperature and pressure cycle in order for the fibres to cure.

Two different methods were used for the curing of the fibres. The hot press mentioned on section 3.2.1.1 was used for curing by heating the cells for 8 h at 80ºC under a pressure of 40 bar, distributed by the already mentioned aluminum mold on the region where the glass fibre only is present, with no pressure being applied in the cell region. The second method consisted on using an autoclave oven for the curing of the cells. The curing cycle was done at 80º C for 8 hours with a pressure of 6 bar, with the cells being under vacuum.

Table 4.2 lists the binding polymer agent used in the different full cells developed.

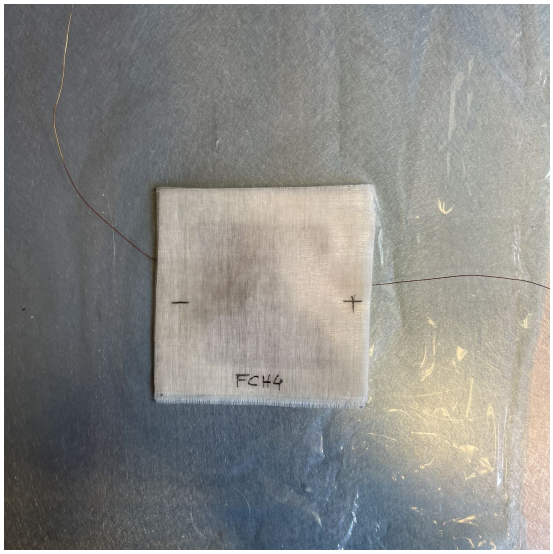

Figure 4.5: Full cell before undergoing the curing cycle.

Table 4.2: Configuration for full cells.

Cell ID	Electrolyte	Curing Type	Anodic Surface
FC4	Pellet + 100% commercial PVA-based glue	Hot Press	Spacer
FC6	Pellet + (70% commercial PVA-based glue + 20% Epoxy + 10% NP)	Hot Press	Spacer
FC7	Pellet + (100% commercial PVA-based glue)	Hot Press	Spacer
FC9	Pellet + 100% commercial PVA-based glue	Hot Press	Carbon felt
ATC1	Pellet + 100% commercial PVA-based glue	Autoclave	Spacer
ATC2	Pellet + (70% commercial PVA-based glue + 20% Epoxy + 10% NP)	Autoclave	Spacer
ATC4	Pellet + 100% commercial PVA-based glue	Autoclave	Carbon felt
ATC6	Pellet + (70% commercial PVA-based glue + 20% Epoxy + 10% NP)	Autoclave	Carbon felt

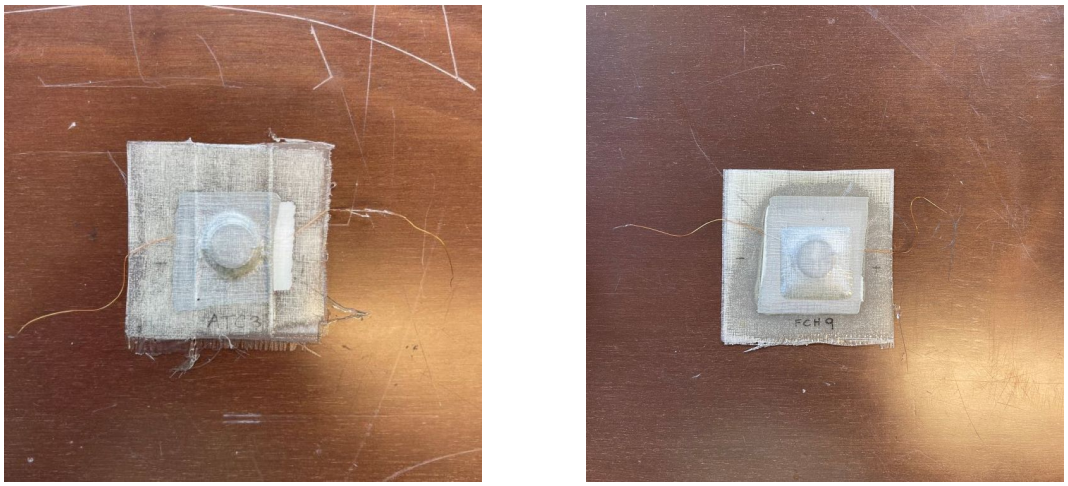

(a) Autoclave

(b) Hot Press

Figure 4.6: Full Cells after curing process.

For the analysis of the impedance spectroscopies performed, the equivalent model displayed on Fig. 4.7 was developed. It was based on available literature [9], where the two loops of resistances and constant phase elements correspond to each electrode's interface. The final constant phase element is used to modulate the non-ideal diffusive behaviour of the cells. The EIS presented on section 4.2 were all performed after the cell underwent the respective charge and discharge cycle for the capacitance calculation.

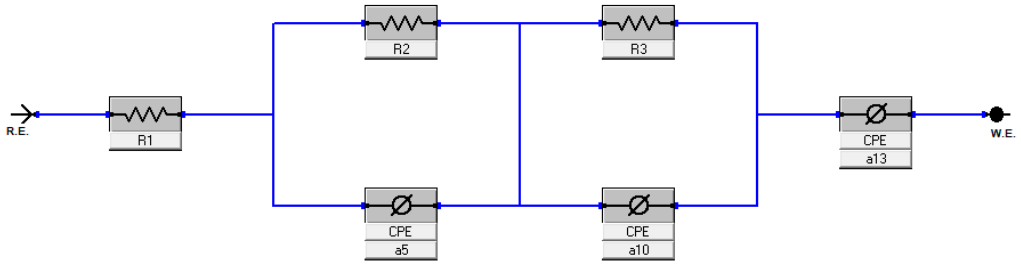

Figure 4.7: Equivalent circuit for full cells.

Charge and discharge cycles were also performed in order to quantify the cyclability and capacity retention of the cell throughout a number of cycles. Predefined time and tension

plateaus were defined for the electrochemical tests, with parameters such as coulombic efficiency and capacity being calculated from experimental data. The capacity can be obtained through Eq. 4.2.

$$C = \frac{I * \Delta T}{\mathrm{m_{cat}}} \tag{4.2}$$

where I represents the discharge current, ΔT the discharge time before the cut-off time, and m_{cat} is the total mass of the cathodic material. The same cut-off time was used for all experiments for comparison reasons.

All cells were subjected to charge and discharge cycles to determine capacity values and impedance spectroscopies after said cycles. ATC4 cell also underwent prolonged cyclic charge and discharge tests.

4.2 Results and Discussion

4.2.1 Hot-Press Cured All-Solid-State Structural Batteries

Impedance spectroscopies performed after the capacity-determination tests display that its values will differ in accordance to the charge profile implemented on the cell. Optimal values of the testing parameters should be implemented to achieve best possible capacity values, as the results suggest to be very influential on the final results. When done correctly, they are in line with expectations, with two distinct semi-circles and a diffusive region for the lower frequencies. The two semi-circles represent the inter-facial resistance in each of the electrode/electrolyte inter-facial zone.

The results obtained for the cells cured in the hot press demonstrated the benefits of incorporating carbon felt as coating for the hard carbon based anode. Using this method, it was possible to verify an increase of 124% in the capacity, when compared to coating on stainless steel spacers. The incorporation of the structural resin in the polymeric mixture seems to provoke more resistance in the charging process. Nonetheless the capacity obtained was 44% higher compared to its commercial PVA-based glue only counterpart.

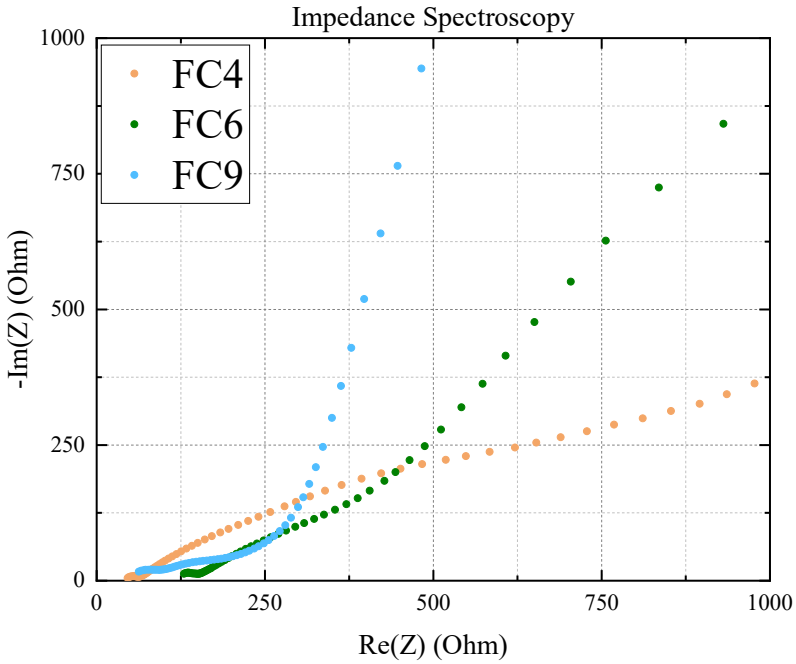

Figure 4.8: Impedance spectroscopy after charge and discharge. NVP-C and Hard Carbon were the used cathode and anode, respectively, on the three cells tested.

For the energy density, the calculation was based on ref. [82], where the maximum capacity obtained was multiplied by the mid-point voltage during the discharge process.

The charge plateau seems to be stabilizing in the region of [1.8-2.5] V, with detrimental effects when the cell overshoots these regions. This indicates that the vanadium-based cathode is not achieving the V^{3+}/V^{4+} redox couple. This is expected to occur, due to the considerably different internal resistance between solid and liquid electrolytes. After the first operational full cell, the optimization of each of the cell's components will be the subject of future work.

Despite the low capacity experienced, it is possible to see in Fig. 4.9f a discharge plateau being formed in cell nº 7. A discharge current of 10 μA allowed the cell to form this steady plateau at 0.6 V.

Table 4.3: Capacity and Coulombic efficiency for hot press cells.

Cell ID	Electrolyte	Capacity [mAh/g]	Energy Density [Wh kg^{-1}]
FC4	Pellet + 100% commercial PVA-based glue	6.079	4.13
FC6	Pellet + (70% commercial PVA-based glue + 20% Epoxy + 10% NP)	8.777	4.54
FC7	Pellet + 100% commercial PVA-based glue	3.931	2.31
FC9	Pellet + 100% commercial PVA-based glue	13.614	5.90

Experimental evidence also suggests that the weight and thickness of the cathodic film is of paramount importance. A correlation between the positive electrode's weight and performance was observed, where the cells with a weight above 0.01 g presenting very poor results.

Using the equivalent circuit from Fig. 4.7, it is possible to extract the values of R1, R2 and R3 from the hot press cells. It seems that the success of the results obtained are directly linked to the resistance values observed. A poorly executed charge or discharge process is the result of an increased inter-facial resistance.

Table 4.4: Resistance values for hot press full cells.

Cell ID	Electrolyte	R1 (Ω)	R2 (Ω)	R3 (Ω)
FC4	Pellet + 100% commercial PVA-based glue	42.26	60.64	1034
FC9	Pellet + 100% commercial PVA-based glue	43.76	27.94	251.80

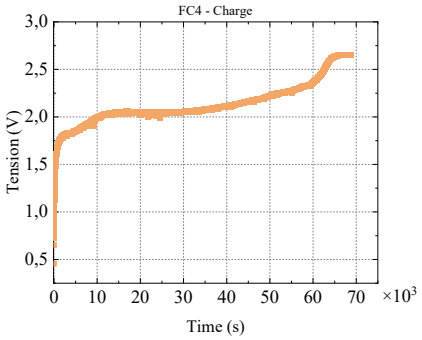

(a) FC4 - Charge at 75 μA

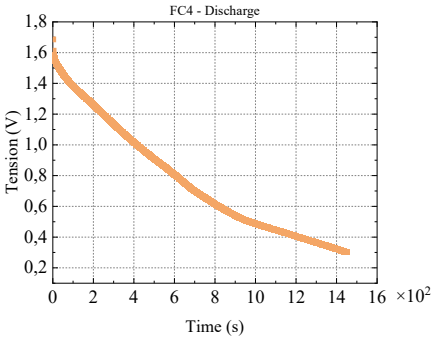

(b) FC4 - Discharge at 75 μA

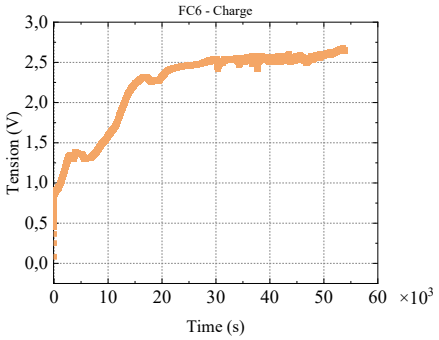

(c) FC6 - Charge at 75 μA

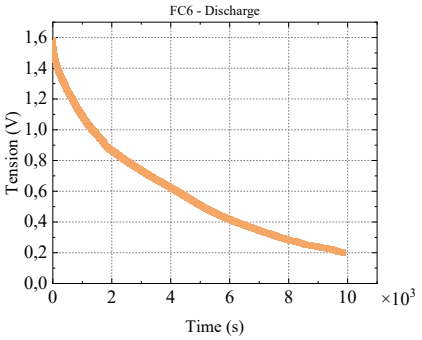

(d) FC6 - Discharge at 10 μA

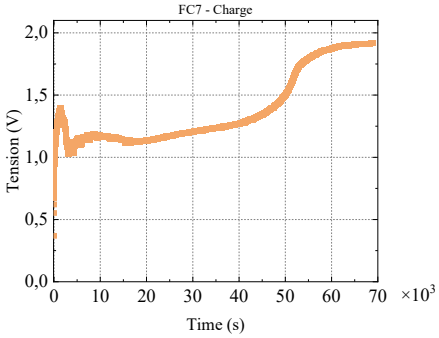

(e) FC7 - Charge at 75 μA

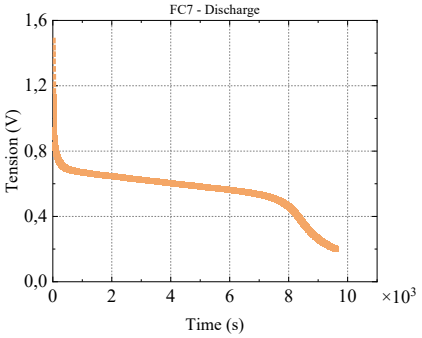

(f) FC7 - Discharge at 10 μA

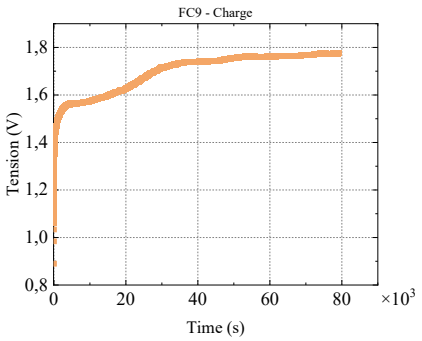

(g) FC9 - Charge at 75 μA

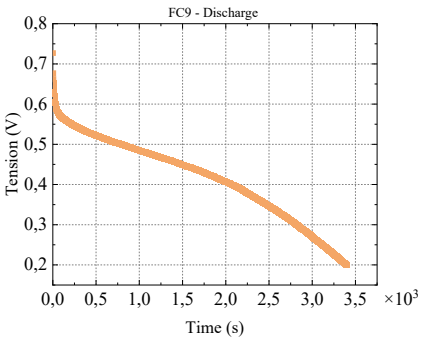

(h) FC9 - Discharge at 75 μA

Figure 4.9: Charge and discharge profiles of full cells developed in the hot press, with the respective charge and discharge currents.

4.2.2 Autoclave Cured All-Solid-State Structural Batteries

As observed in the cells manufactured in the hot press, the inclusion of carbon felt greatly improves the electrochemical performance of the cell. Furthermore, the curing in the autoclave also seems to produce a further improvement in comparison with the hot press.

This is most likely due to the more evenly distributed pressure used in the autoclave, as even the bulk of the battery is under pressure, something that wasn't possible when using the aluminum mold in the hot press. This distribution of pressure has two effects. First, it presents an almost perfect seal against foreign environmental effects. Secondly, it ensures all the different components of the battery are in contact with each other, improving therefore the wettability of each interface and decreasing resistance.

Table 4.5: Capacity and Coulombic efficiency for autoclave cells.

Cell ID	Electrolyte	Capacity [mAh/g]	Energy Density [Wh kg^{-1}]
ATC1	Pellet + 100% commercial PVA-based glue	2.770	2.25
ATC2	Pellet + (70% commercial PVA-based glue + 20% Epoxy + 10% NP)	3.354	1.90
ATC4	Pellet + 100% commercial PVA-based glue	23.651	22.35
ATC6	Pellet + (70% commercial PVA-based glue + 20% Epoxy + 10% NP)	11.468	12.844

Configurations that include carbon felt in its composition display charging times more prolonged and steadier profiles, demonstrating the anode's capability to hold charge. In terms of capacity, and comparing to the same electrolyte composition, increases in the order of 754% were observed for cells whose anode is coated in carbon felt. It was possible to develop a cell with a capacity of 23.651 mAh g^{-1} for the electrolyte composed of the ceramic pellet and commercial PVA-based glue, and a capacity of 11.468 mAh g^{-1} for the cell with the structural resin in its composition.

Overall, after assessing all parameters, it appears clear that curing using the autoclave is the best option for the fabrication of the cells. The vacuum allows the contact surfaces to be as much in touch as possible, as well as preventing foreign agents from mining the cell's performance.

Autoclave cell number four (ATC4) also underwent cycles of charge and discharge to infer how efficient its cyclability was and if it was capable to maintain its efficiency throughout the cell's cycle numbers. The cycling rate chosen was 2C, with charge and discharge currents of 100 μA. It is important to point out that the capacity depends on the discharge current and lower currents may generate higher capacity values, however losing in this case performance in terms of cell power.

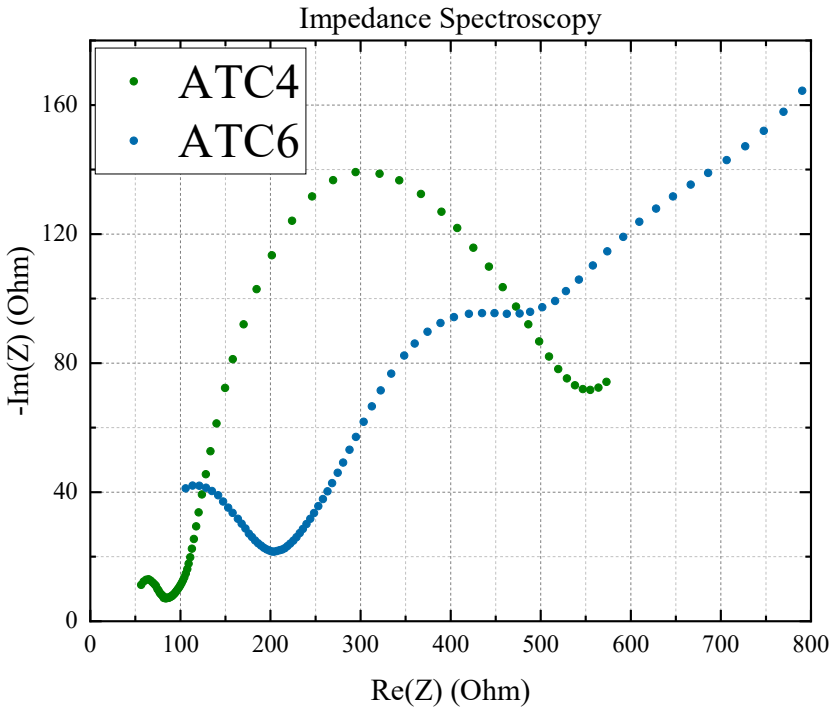

Figure 4.10: Impedance spectroscopies for full cells developed using the autoclave.

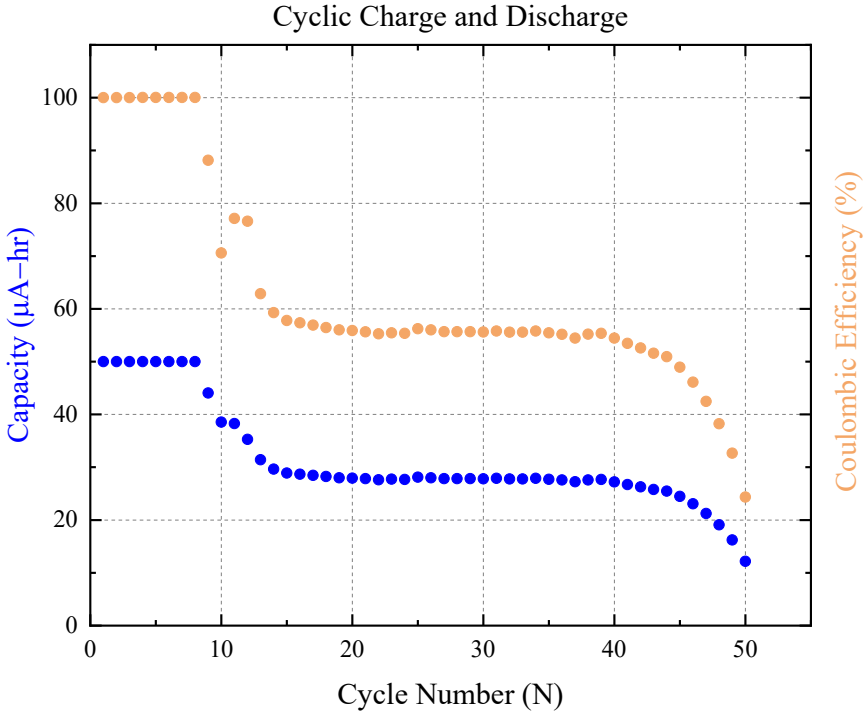

Figure 4.12: Capacity by cycle number for ATC4.

As can be seen on Fig. 4.12, the cell was able to withhold, through the first 8 cycles, a maximum coulombic efficiency value of no less than 99.99%. The coulombic efficiency is obtained by simply dividing the discharge's capacity by the charge's capacity, for each cycle.

A second plateau of capacity was then formed and maintained until around 50 cycles, showing a remarkable cycling capability for a solid-state battery encapsulated in fibre glass, where through the first 45 cycles the effiiency obtained was no less than 50.93%.

Impedance spectroscopies, after charging and discharging, were also done to the cells number four and six, to have a visual comparison of the effect of incorporating the structural resin in the cell's configuration. The resistances were retrieved using the equivalent circuit modelled in the hot-press section.

ATC4 displays a more pronounced second semi-circle on the nyquist plot, with no visible diffusion slope for the measured frequencies (≥ 0.1 Hz), whilst for the battery containing the structural resin, ATC6, the second semi-circle evolves to a diffusive behaviour, explaining its low R1 and R2 values but more pronounced R3 measurements, when compared to ATC4.

Table 4.6: Resistance values for autoclave full cells.

Cell ID	**Electrolyte**	**R1 (ω)**	**R2 (ω)**	**R3 (ω)**
ATC4	Pellet + 100% commercial PVA-based glue	44.57	98.33	347.60
ATC6	Pellet + (70% commercial PVA-based glue + 20% epoxy + 10% NP)	46.63	48.46	701.10

It is challenging to compare the results obtained in these configurations to existent data present in current available literature. The capacity here obtained is not as high as some of the work currently available, with lithium/sodium-ion or lithium/sodium-metal batteries with liquid electrolytes, neither is the cycling stability and impedance values. However, and taking into account the advanced strategies being put into place throughout this work, it is easy to understand possible disparities between the results here achieved and current state-of-art. To the best of the author's knowledge, there has not been yet put forward a fully solid sodium ion structural battery, with a good ionic conductor solid electrolyte pellet, and using metal-free electrodes, capable of achieving satisfactory capacity values for acceptable discharge currents.

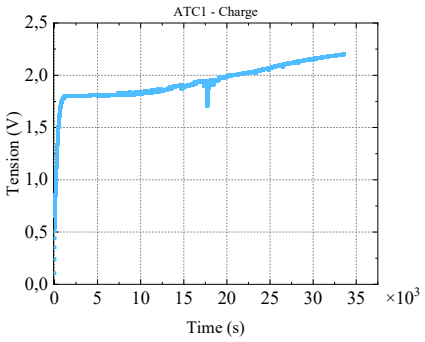

(a) ATC1 - Charge at 100 μA

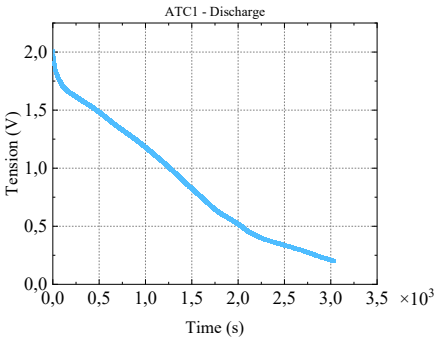

(b) ATC1 - Discharge at 50 μA

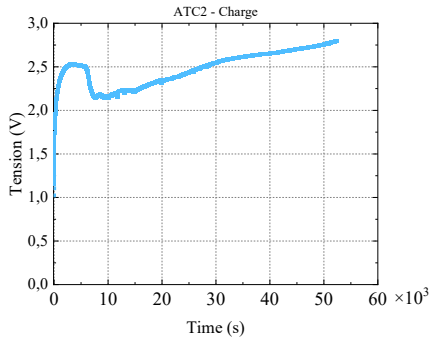

(c) ATC2 - Charge at 100 μA

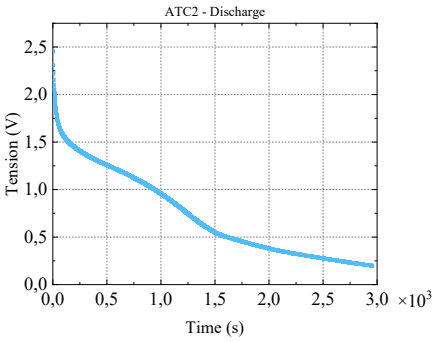

(d) ATC2 - Discharge at 50 μA

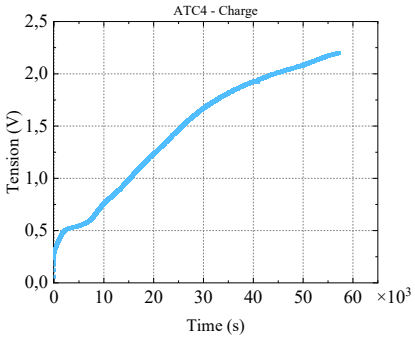

(e) ATC4 - Charge at 100 μA

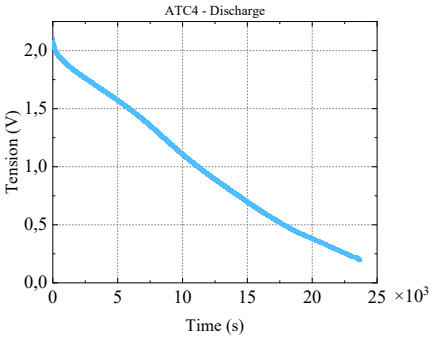

(f) ATC4 - Discharge at 50 μA

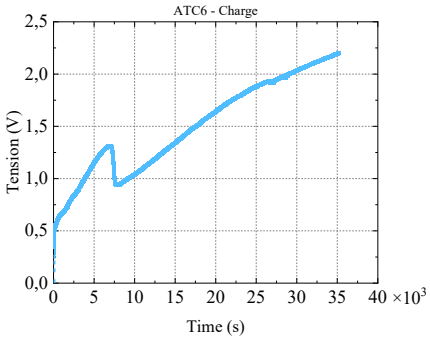

(g) ATC6 - Charge at 100 μA

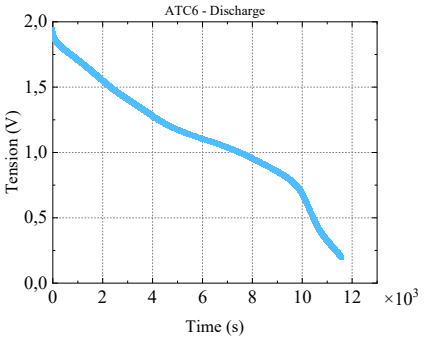

(h) ATC6 - Discharge at 50 μA

Figure 4.11: Charge and discharge profiles of full cells developed in the autoclave.

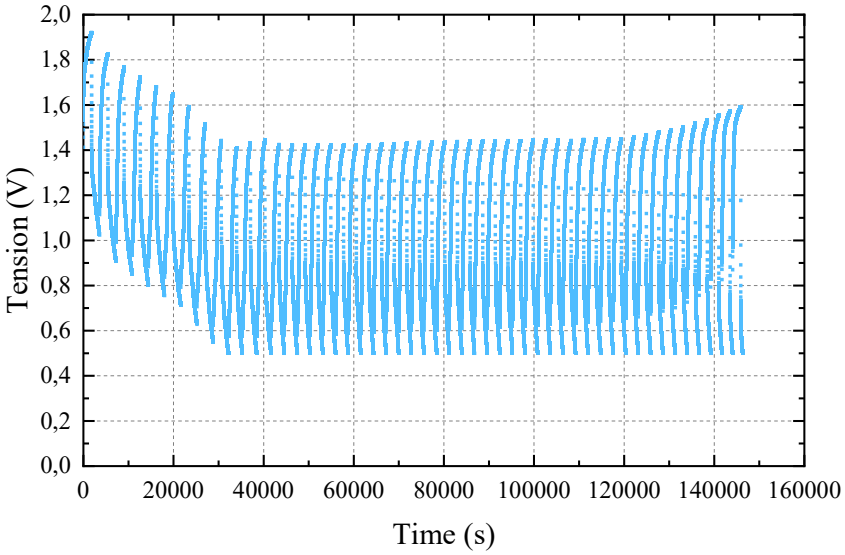

Figure 4.13: Charge and discharge cycles plotted sequentially in the time domain for ATC4 cell.

Chapter 5

Conclusion and Future Work

This thesis was kicked off with the goal of developing a novel and innovative all-solid-state sodium ion structural battery, incorporating electrodes that do not contain any form of metallic sodium with the hopes of achieving a high voltage cell, therefore addressing prominent challenges present in the existing structural energy storage devices, such as the safety threats posed from the use of liquid components in batteries.

Beginning with a thorough review of the field's latest technologies and through extensive experimental work, it was possible to develop a multi-functional structural battery with of 23.651 mAh g^{-1} and good cycling capability with a energy density of 22.35 Wh Kg^{-1} for a 100 μA discharge current using an all-solid-state electrolyte ceramic pellet coupled with a wetting agent composed of polyvinyl alcohol. These results become even more striking when one bears in mind the non-existence of metallic sodium in the cell's configuration, with all the sodium ions having been originated from the cathode. Moreover, it was also successfully implemented the incorporation of a structural resin in the cell's polymeric mixture, without significant drawbacks in the battery's electrochemical performance. The resin provides enhanced structural stability, as well as enforcing a better adhesion between the electrode and electrolyte, leading to more robust and durable devices, including a 17% decrease of initial resistance in glass fiber structure and a 30% decrease when in a coin cell structure. Finally, the fact that these results were obtained at room temperature constitutes another advantageous feature when considering possible use in real-world applications.

The overall structural integrity of the structural battery was also addressed through the encapsulation of the cells using glass fibres. Using an autoclave for the curing phase, it was possible to develop systems whose sealing and ageing properties were even better than the

widely used coin cell casings. Providing not only an isolating layer to external environmental factors, the use of glass fibres as encapsulating agent provides an modern strategy to improve the global safety and stability of the energy storage device, making it attractive for real-world practical applications.

Notwithstanding the promising results achieved, it is important to address the limitations discovered during the experimental phase. The use of duct tape as sealing agent is not ideal from the mechanical standpoint, as it could be a source of a possible delamination with repeated use. The same argument can be directed to the use of coin cell spacers as current collectors, with its lack of adhesion to the glass fibres being a cause for concern when employed in structural applications. Moreover, the heavily influential nature of the cathode's weight in the cell's electrochemical performance needs to be further studied to pinpoint the exact values that extract the best performance, as well as addressing the issue of the non-existent second redox couple reaction in the charging and discharging process.

These limitations can however be viewed as potential focal points for innovations. Innovative solutions such as the incorporation of carbon fibres as both current collectors and sealing agent have been demonstrated for use in lithium ion batteries and can be a basis for future works regarding the development of solid-state sodium ion structural batteries. The effect of different environmental conditions one might find in real-world applications is also a potential source for research, as it is imperative that the reaction of the energy storage device to adverse conditions is well documented to ensure the safety of operations. Finally, after achieving the goal of this work, the first operational operating full cell, the optimization of each of the cell's components will naturally be the objective of future work.

In conclusion, the path leading to the final structural electrochemical cell configuration was paved with challenges and hardships, as is usual when dealing with ground-breaking technology that has not yet been fully comprehended. Despite this, the rewards make it worthwhile, as the achievements made in the field of structural stability, integrity and durability during the development of this thesis will hopefully enable the field of structural batteries to make a leap forward, and lead the way in the endeavour to improve sustainability efforts and contribute to a more suitable world to future generations.

Bibliography

[1] S. Shafiee and E. Topal, "When will fossil fuel reserves be diminished?" *Energy Policy*, vol. 37, no. 1, pp. 181–189, 2009, ISSN: 0301-4215. DOI: https://doi.org/10.1016/j.enpol.2008.08.016. [Online]. Available: https://www.sciencedirect.com/science/article/pii/S0301421508004126.

[2] Iea, *Global ev outlook 2021 – analysis*. [Online]. Available: https://www.iea.org/reports/global-ev-outlook-2021.

[3] F. Danzi, M. Valente, S. Terlicka, and M. H. Braga, "Sodium and potassium ion rich ferroelectric solid electrolytes for traditional and electrode-less structural batteries," *APL Materials*, vol. 10, no. 3, p. 031 111, 2022. DOI: 10.1063/5.0080054. eprint: https://doi.org/10.1063/5.0080054. [Online]. Available: https://doi.org/10.1063/5.0080054.

[4] L. G. Simpkins and M. Krivic, *The side effects of lithium mining*, Sep. 2021. [Online]. Available: https://wellcomecollection.org/articles/YTdnPhIAACIAGuF3.

[5] Y. Zhu, H. Xu, J. Ma, P. Chen, and Y. Chen, "The recent advances of nasicon-na3v2(po4)3 cathode materials for sodium-ion batteries," *Journal of Solid State Chemistry*, vol. 317, p. 123 669, 2023, ISSN: 0022-4596. DOI: https://doi.org/10.1016/j.jssc.2022.123669. [Online]. Available: https://www.sciencedirect.com/science/article/pii/S0022459622007940.

[6] L. Shen, J. Yang, G. Liu, M. Avdeev, and X. Yao, "High ionic conductivity and dendrite-resistant nasicon solid electrolyte for all-solid-state sodium batteries," *Materials Today Energy*, vol. 20, p. 100 691, 2021, ISSN: 2468-6069. DOI: https://doi.org/10.1016/j.mtener.2021.100691. [Online]. Available: https://www.sciencedirect.com/science/article/pii/S2468606921000563.

[7] G. Instruments, *Basics of electrochemical impedance spectroscopy*, https://www.gamry.com/application-notes/EIS/basics-of-electrochemical-impedance-spectroscopy/, Accessed on March 15, 2023, 2021.

[8] W. Choi, H.-C. Shin, J. M. Kim, J.-Y. Choi, and W.-S. Yoon, "Modeling and applications of electrochemical impedance spectroscopy (eis) for lithium-ion batteries," *Journal of Electrochemical Science and Technology*, vol. 11, no. 1, pp. 1–13, 2020.

[9] P. Vadhva, J. Hu, M. J. Johnson, *et al.*, "Electrochemical impedance spectroscopy for all-solid-state batteries: Theory, methods and future outlook," *ChemElectroChem*, vol. 8, no. 11, pp. 1930–1947, 2021.

[10] J.-Y. "Hwang, S.-T. Myung, and Y.-K. Sun, ""sodium-ion batteries: Present and future",," *"Chem. Soc. Rev."*, vol. "46", "3529–3614", "12" "2017". DOI: "10.1039/C6CS00776G". [Online]. Available: http://dx.doi.org/10.1039/C6CS00776G.

[11] L. Liu, Y. Tian, A. Abdussalam, M. R. H. S. Gilani, W. Zhang, and G. Xu, "Hard carbons as anodes in sodium-ion batteries: Sodium storage mechanism and optimization strategies," *Molecules*, vol. 27, no. 19, 2022, ISSN: 1420-3049. DOI: 10.3390/molecules27196516. [Online]. Available: https://www.mdpi.com/1420-3049/27/19/6516.

[12] "Plant-derived hard carbon as anode for sodium-ion batteries: A comprehensive review to guide interdisciplinary research," *Chemical Engineering Journal*, vol. 447, p. 137 468, 2022, ISSN: 1385-8947. DOI: https://doi.org/10.1016/j.cej.2022.137468. [Online]. Available: https://www.sciencedirect.com/science/article/pii/S1385894722029564.

[13] S. Senthilkumar, M. Abirami, J. Kim, W. Go, S. M. Hwang, and Y. Kim, "Sodium-ion hybrid electrolyte battery for sustainable energy storage applications," *Journal of Power Sources*, vol. 341, pp. 404–410, 2017.

[14] Y. Wang, W. Zhu, A. Guerfi, C. Kim, and K. Zaghib, "Roles of ti in electrode materials for sodium-ion batteries," *Frontiers in Energy Research*, vol. 7, 2019, ISSN: 2296-598X. DOI: 10.3389/fenrg.2019.00028. [Online]. Available: https://www.frontiersin.org/articles/10.3389/fenrg.2019.00028.

[15] C. Chen, Q. Zhang, X. Li, *et al.*, "Na+ intercalation pseudocapacitance in graphene-coupled titanium oxide enabling ultra-fast sodium storage and long-term cycling," *Nano Energy*, vol. 36, pp. 46–53, 2017.

[16] J. "Xu, C. Ma, M. Balasubramanian, and Y. S. Meng, ""understanding na2ti3o7 as an ultra-low voltage anode material for a na-ion battery",," *"Chem. Commun."*, vol. "50", "12564–12567", "83" "2014". DOI: "10.1039/C4CC03973D". [Online]. Available: http://dx.doi.org/10.1039/C4CC03973D.

[17] Y. Tian, G. Zeng, A. Rutt, *et al.*, "Promises and challenges of next-generation "beyond li-ion" batteries for electric vehicles and grid decarbonization," *Chemical Reviews*, vol. 121, no. 3, pp. 1623–1669, 2021, PMID: 33356176. DOI: 10.1021/acs.chemrev.0c00767. eprint: https://doi.org/10.1021/acs.chemrev.0c00767. [Online]. Available: https://doi.org/10.1021/acs.chemrev.0c00767.

[18] S. Komaba, T. Mikumo, N. Yabuuchi, A. Ogata, H. Yoshida, and Y. Yamada, "Electrochemical insertion of li and na ions into nanocrystalline fe3o4 and fe2o3 for rechargeable batteries," *Journal of The Electrochemical Society*, vol. 157, no. 1, A60, Nov. 2009. DOI: 10.1149/1.3254160. [Online]. Available: https://dx.doi.org/10.1149/1.3254160.

[19] S. Liu, Y. Wang, Y. Dong, Z. Zhao, Z. Wang, and J. Qiu, "Ultrafine fe3o4 quantum dots on hybrid carbon nanosheets for long-life, high-rate alkali-metal storage," *ChemElectroChem*, vol. 3, no. 1, pp. 38–44, 2016. DOI: https://doi.org/10.1002/celc.201500410. eprint: https://chemistry-europe.onlinelibrary.wiley.com/doi/pdf/10.1002/celc.201500410. [Online]. Available: https://chemistry-europe.onlinelibrary.wiley.com/doi/abs/10.1002/celc.201500410.

[20] M. M. "Rahman, A. M. Glushenkov, T. Ramireddy, and Y. Chen, ""electrochemical investigation of sodium reactivity with nanostructured co3o4 for sodium-ion batteries"," *"Chem. Commun."*, vol. "50", "5057–5060", "39" "2014". DOI: "10.1039/C4CC01033G". [Online]. Available: http://dx.doi.org/10.1039/C4CC01033G.

[21] X. "Xie, D. Su, J. Zhang, S. Chen, A. K. Mondal, and G. Wang, ""a comparative investigation on the effects of nitrogen-doping into graphene on enhancing the electrochemical performance of sno2/graphene for sodium-ion batteries"," *"Nanoscale"*, vol. "7", "3164–3172", "7" "2015". DOI: "10.1039/C4NR07054B". [Online]. Available: http://dx.doi.org/10.1039/C4NR07054B.

[22] H. "Liu, F. Cao, H. Zheng, *et al.*, ""in situ observation of the sodiation process in cuo nanowires"," *"Chem. Commun."*, vol. "51", "10443–10446", "52" "2015". DOI: "10.1039/C5CC03734D". [Online]. Available: http://dx.doi.org/10.1039/C5CC03734D.

[23] A. Darwiche, C. Marino, M. T. Sougrati, B. Fraisse, L. Stievano, and L. Monconduit, "Better cycling performances of bulk sb in na-ion batteries compared to li-ion systems: An unexpected electrochemical mechanism," *Journal of the American Chemical Society*, vol. 134, no. 51, pp. 20 805–20 811, 2012, PMID: 23194439. DOI: 10.1021/ja310347x. eprint: https://doi.org/10.1021/ja310347x. [Online]. Available: https://doi.org/10.1021/ja310347x.

[24] B. Chen, M. Liang, Q. Wu, S. Zhu, N. Zhao, and C. He, "Recent developments of antimony-based anodes for sodium-and potassium-ion batteries," *Transactions of Tianjin University*, pp. 1–27, 2021.

[25] G. Wang, M. Guo, Y. Zhao, *et al.*, "Recent advances in antimony sulfide-based nanomaterials for high-performance sodium-ion batteries: A mini review," *Frontiers in Chemistry*, vol. 10, p. 870 564, 2022.

[26] B. Peng, Y. Xu, K. Liu, X. Wang, and F. M. Mulder, "High-performance and low-cost sodium-ion anode based on a facile black phosphorus-carbon nanocomposite," *ChemElectroChem*, vol. 4, no. 9, pp. 2140–2144, 2017. DOI: https://doi.org/10.1002/celc.201700345. eprint: https://chemistry-europe.onlinelibrary.wiley.com/doi/pdf/10.1002/celc.201700345. [Online]. Available: https://chemistry-europe.onlinelibrary.wiley.com/doi/abs/10.1002/celc.201700345.

[27] Y. Liu, N. Zhang, X. Liu, C. Chen, L.-Z. Fan, and L. Jiao, "Red phosphorus nanoparticles embedded in porous n-doped carbon nanofibers as high-performance anode for sodium-ion batteries," *Energy Storage Materials*, vol. 9, pp. 170–178, 2017, ISSN: 2405-8297. DOI: https://doi.org/10.1016/j.ensm.2017.07.012. [Online]. Available: https://www.sciencedirect.com/science/article/pii/S240582971730243X.

[28] Y. Liu, N. Zhang, L. Jiao, and J. Chen, "Tin nanodots encapsulated in porous nitrogen-doped carbon nanofibers as a free-standing anode for advanced sodium-ion batteries," *Advanced Materials*, vol. 27, no. 42, pp. 6702–6707, 2015. DOI: https://doi.org/10.1002/adma.201503015. eprint: https://onlinelibrary.wiley.com/doi/pdf/10.1002/adma.201503015. [Online]. Available: https://onlinelibrary.wiley.com/doi/abs/10.1002/adma.201503015.

[29] H. Kim, J. Hong, Y.-U. Park, J. Kim, I. Hwang, and K. Kang, "Sodium storage behavior in natural graphite using ether-based electrolyte systems," *Advanced Functional Materials*, vol. 25, no. 4, pp. 534–541, 2015. DOI: https://doi.org/10.1002/adfm.201402984. eprint: https://onlinelibrary.wiley.com/doi/pdf/10.1002/adfm.201402984. [Online]. Available: https://onlinelibrary.wiley.com/doi/abs/10.1002/adfm.201402984.

[30] Y. Li, Y.-S. Hu, X. Qi, *et al.*, "Advanced sodium-ion batteries using superior low cost pyrolyzed anthracite anode: Towards practical applications," *Energy Storage Materials*, vol. 5, pp. 191–197, 2016, ISSN: 2405-8297. DOI: https://doi.org/10.1016/j.ensm.2016.07.006. [Online]. Available: https://www.sciencedirect.com/science/article/pii/S2405829716301994.

[31] E. Stauffer, J. A. Dolan, and R. Newman, "Chapter 4 - chemistry and physics of fire and liquid fuels," in *Fire Debris Analysis*, E. Stauffer, J. A. Dolan, and R. Newman, Eds., Burlington: Academic Press, 2008, pp. 85–129, ISBN: 978-0-12-663971-1. DOI: https://doi.org/10.1016/B978-012663971-1.50008-7. [Online]. Available: https://www.sciencedirect.com/science/article/pii/B9780126639711500087.

[32] D. A. Stevens and J. R. Dahn, "High capacity anode materials for rechargeable sodium-ion batteries," *Journal of The Electrochemical Society*, vol. 147, no. 4, p. 1271,

Apr. 2000. DOI: 10.1149/1.1393348. [Online]. Available: https://dx.doi.org/10.1149/1.1393348.

[33] S. Qiu, L. Xiao, M. L. Sushko, *et al.*, "Manipulating adsorption–insertion mechanisms in nanostructured carbon materials for high-efficiency sodium ion storage," *Advanced Energy Materials*, vol. 7, no. 17, p. 1 700 403, 2017. DOI: https://doi.org/10.1002/aenm.201700403. eprint: https://onlinelibrary.wiley.com/doi/pdf/10.1002/aenm.201700403. [Online]. Available: https://onlinelibrary.wiley.com/doi/abs/10.1002/aenm.201700403.

[34] Y. Cao, L. Xiao, M. L. Sushko, *et al.*, "Sodium ion insertion in hollow carbon nanowires for battery applications," *Nano Letters*, vol. 12, no. 7, pp. 3783–3787, 2012, PMID: 22686335. DOI: 10.1021/nl3016957. eprint: https://doi.org/10.1021/nl3016957. [Online]. Available: https://doi.org/10.1021/nl3016957.

[35] P. Bai, Y. He, X. Zou, X. Zhao, P. Xiong, and Y. Xu, "Elucidation of the sodium-storage mechanism in hard carbons," *Advanced Energy Materials*, vol. 8, no. 15, p. 1 703 217, 2018. DOI: https://doi.org/10.1002/aenm.201703217. eprint: https://onlinelibrary.wiley.com/doi/pdf/10.1002/aenm.201703217. [Online]. Available: https://onlinelibrary.wiley.com/doi/abs/10.1002/aenm.201703217.

[36] A. M. Skundin, T. L. Kulova, and A. B. Yaroslavtsev, *Sodium-ion batteries (a review)*, 2018. DOI: 10.1134/S1023193518020076. [Online]. Available: https://www.wizdom.ai/publication/10.1134/S1023193518020076/title/sodium_ion_batteries_a_review.

[37] Z. Li, C. Bommier, Z. S. Chong, *et al.*, "Mechanism of na-ion storage in hard carbon anodes revealed by heteroatom doping," *Advanced Energy Materials*, vol. 7, no. 18, p. 1 602 894, 2017. DOI: https://doi.org/10.1002/aenm.201602894. eprint: https://onlinelibrary.wiley.com/doi/pdf/10.1002/aenm.201602894. [Online]. Available: https://onlinelibrary.wiley.com/doi/abs/10.1002/aenm.201602894.

[38] D. Ni, W. Sun, Z. Wang, *et al.*, "Heteroatom-doped mesoporous hollow carbon spheres for fast sodium storage with an ultralong cycle life," *Advanced Energy Materials*, vol. 9, no. 19, p. 1 900 036, 2019. DOI: https://doi.org/10.1002/aenm.201900036. eprint: https://onlinelibrary.wiley.com/doi/pdf/10.1002/aenm.201900036. [Online]. Available: https://onlinelibrary.wiley.com/doi/abs/10.1002/aenm.201900036.

[39] F. Xie, Z. Xu, A. C. S. Jensen, *et al.*, "Hard–soft carbon composite anodes with synergistic sodium storage performance," *Advanced Functional Materials*, vol. 29, no. 24, p. 1 901 072, 2019. DOI: https://doi.org/10.1002/adfm.201901072. eprint: https://onlinelibrary.wiley.com/doi/pdf/10.1002/adfm.201901072.

[Online]. Available: https://onlinelibrary.wiley.com/doi/abs/10.1002/adfm.201901072.

[40] Y. Lu, C. Zhao, X. Qi, *et al.*, "Pre-oxidation-tuned microstructures of carbon anodes derived from pitch for enhancing na storage performance," *Advanced Energy Materials*, vol. 8, no. 27, p. 1 800 108, DOI: https://doi.org/10.1002/aenm.201800108. eprint: https://onlinelibrary.wiley.com/doi/pdf/10.1002/aenm.201800108. [Online]. Available: https://onlinelibrary.wiley.com/doi/abs/10.1002/aenm.201800108.

[41] W. Zuo, A. Innocenti, M. Zarrabeitia, D. Bresser, Y. Yang, and S. Passerini, "Layered oxide cathodes for sodium-ion batteries: Storage mechanism, electrochemistry, and techno-economics," *Accounts of Chemical Research*, vol. 56, no. 3, pp. 284–296, 2023, PMID: 36696961. DOI: 10.1021/acs.accounts.2c00690. eprint: https://doi.org/10.1021/acs.accounts.2c00690. [Online]. Available: https://doi.org/10.1021/acs.accounts.2c00690.

[42] B. Xie, B. Sun, T. Gao, Y. Ma, G. Yin, and P. Zuo, "Recent progress of prussian blue analogues as cathode materials for nonaqueous sodium-ion batteries," *Coordination Chemistry Reviews*, vol. 460, p. 214 478, 2022, ISSN: 0010-8545. DOI: https://doi.org/10.1016/j.ccr.2022.214478. [Online]. Available: https://www.sciencedirect.com/science/article/pii/S001085452200073X.

[43] L. Wang, J. Song, R. Qiao, *et al.*, "Rhombohedral prussian white as cathode for rechargeable sodium-ion batteries," *Journal of the American Chemical Society*, vol. 137, no. 7, pp. 2548–2554, 2015, PMID: 25615887. DOI: 10.1021/ja510347s. eprint: https://doi.org/10.1021/ja510347s. [Online]. Available: https://doi.org/10.1021/ja510347s.

[44] L. Lander, J.-M. Tarascon, and A. Yamada, "Sulfate-based cathode materials for li- and na-ion batteries," *The Chemical Record*, vol. 18, no. 10, pp. 1394–1408, 2018.

[45] P. Barpanda, M. Ati, G. Rousse, *et al.*, "A 3.8-v earth-abundant sodium battery electrode," *Nature Communications*, vol. 5, p. 4358, 2014. DOI: 10.1038/ncomms5358.

[46] M. S. "Islam, R. Dominko, C. Masquelier, C. Sirisopanaporn, A. R. Armstrong, and P. G. Bruce, ""silicate cathodes for lithium batteries: Alternatives to phosphates?"" *"J. Mater. Chem."*, vol. "21", "9811–9818", "27" "2011". DOI: "10.1039/C1JM10312A". [Online]. Available: http://dx.doi.org/10.1039/C1JM10312A.

[47] S. Li, J. Guo, Z. Ye, *et al.*, "Zero-strain na2fesio4 as novel cathode material for sodium-ion batteries," *ACS Applied Materials & Interfaces*, vol. 8, no. 27, pp. 17 233–17 238, 2016, PMID: 27305627. DOI: 10.1021/acsami.6b03969. eprint: https://doi.org/10.1021/acsami.6b03969. [Online]. Available: https://doi.org/10.1021/acsami.6b03969.

[48] Y. Fang, J. Zhang, L. Xiao, X. Ai, Y. Cao, and H. Yang, "Phosphate framework electrode materials for sodium ion batteries," *Advanced Science*, vol. 4, no. 5, p. 1 600 392, 2017. DOI: https://doi.org/10.1002/advs.201600392. eprint: https://onlinelibrary.wiley.com/doi/pdf/10.1002/advs.201600392. [Online]. Available: https://onlinelibrary.wiley.com/doi/abs/10.1002/advs.201600392.

[49] L.-m. Zhang, X.-d. He, S. Wang, *et al.*, "Hollow-sphere-structured na4fe3(po4)2(p2o7)/c as a cathode material for sodium-ion batteries," *ACS Applied Materials & Interfaces*, vol. 13, no. 22, pp. 25 972–25 980, 2021, PMID: 34038077. DOI: 10.1021/acsami.1c04035. eprint: https://doi.org/10.1021/acsami.1c04035. [Online]. Available: https://doi.org/10.1021/acsami.1c04035.

[50] X. Zhang, X. Rui, D. Chen, *et al.*, "Na 3 v 2 (po 4) 3: An advanced cathode for sodium-ion batteries," *Nanoscale*, vol. 11, no. 6, pp. 2556–2576, 2019.

[51] L. Fan, S. Wei, S. Li, Q. Li, and Y. Lu, "Recent progress of the solid-state electrolytes for high-energy metal-based batteries," *Advanced Energy Materials*, vol. 8, no. 11, p. 1 702 657, 2018.

[52] W. Hou, X. Guo, X. Shen, K. Amine, H. Yu, and J. Lu, "Solid electrolytes and interfaces in all-solid-state sodium batteries: Progress and perspective," *Nano Energy*, vol. 52, pp. 279–291, 2018, ISSN: 2211-2855. DOI: https://doi.org/10.1016/j.nanoen.2018.07.036. [Online]. Available: https://www.sciencedirect.com/science/article/pii/S221128551830524X.

[53] D. Fenton, "Complexes of alkali metal ions with poly (etylene oxide)," *polymer*, vol. 14, p. 589, 1973.

[54] S. S. Sekhon, S. Singh, and M. Singh, "Ionic conductivity of polyethylene oxide (peo)-based polymer electrolytes," *Journal of Applied Polymer Science*, vol. 112, no. 1, pp. 364–371, 2009. DOI: 10.1002/app.29170.

[55] J.-J. Kim, K. Yoon, I. Park, and K. Kang, "Progress in the development of sodium-ion solid electrolytes," *Small Methods*, vol. 1, no. 10, p. 1 700 219, 2017.

[56] T. L. Kulova and A. M. Skundin, "Electrode/electrolyte interphases of sodium-ion batteries," *Energies*, vol. 15, no. 22, p. 8615, 2022.

[57] A. Hayashi, K. Noi, A. Sakuda, and M. Tatsumisago, "Superionic glass-ceramic electrolytes for room-temperature rechargeable sodium batteries," *Nature communications*, vol. 3, no. 1, p. 856, 2012.

[58] J. Goodenough, H.-P. Hong, and J. Kafalas, "Fast na+-ion transport in skeleton structures," *Materials Research Bulletin*, vol. 11, no. 2, pp. 203–220, 1976, ISSN: 0025-5408. DOI: https://doi.org/10.1016/0025-5408(76)90077-5. [Online]. Available: https://www.sciencedirect.com/science/article/pii/0025540876900775.

[59] K. M. Bui, V. A. Dinh, S. Okada, and T. Ohno, "Na-ion diffusion in a nasicon-type solid electrolyte: A density functional study," *Physical Chemistry Chemical Physics*, vol. 18, no. 39, pp. 27 226–27 231, 2016.

[60] J.-K. Kim, Y. J. Lim, H. Kim, G.-B. Cho, and Y. Kim, "A hybrid solid electrolyte for flexible solid-state sodium batteries," *Energy & Environmental Science*, vol. 8, no. 12, pp. 3589–3596, 2015.

[61] M. Cheng, T. Qu, J. Zi, *et al.*, "A hybrid solid electrolyte for solid-state sodium ion batteries with good cycle performance," *Nanotechnology*, vol. 31, no. 42, p. 425 401, Jul. 2020. DOI: 10.1088/1361-6528/aba059. [Online]. Available: https://dx.doi.org/10.1088/1361-6528/aba059.

[62] E. Özçelikci, H. İlcan, G. Yıldırım, and M. Şahmaran, "11 - nanoscale characterization of cementitious composites," in *Recent Advances in Nano-Tailored Multi-Functional Cementitious Composites*, ser. Woodhead Publishing Series in Civil and Structural Engineering, M. Şahmaran, F. Shaikh, and G. Yıldırım, Eds., Woodhead Publishing, 2022, pp. 375–406, ISBN: 978-0-323-85229-6. DOI: https://doi.org/10.1016/B978-0-323-85229-6.00006-8. [Online]. Available: https://www.sciencedirect.com/science/article/pii/B9780323852296000068.

[63] N. Lecture, "Basic principle, by do kyung kim," *Dept. of Material Science and Engineering KAIST, Korea*, 1.

[64] *Instrumented indentation test (iso 14577)*, https://www.zwickroell.com/industries/materials-testing/hardness-testing/instrumented-indentation-test-iso-14577/, Accessed: 31st of july 2023.

[65] A. Datye, U. D. Schwarz, and H.-T. Lin, "Fracture toughness evaluation and plastic behavior law of a single crystal silicon carbide by nanoindentation," *Ceramics*, vol. 1, no. 1, pp. 198–210, 2018.

[66] R. Hill, J. Hempel, Y.-T. Cheng, *et al.*, "Structural and mechanical characterization of nasicon solid electrolytes upon cycling in molten sodium.," Sandia National Lab.(SNL-NM), Albuquerque, NM (United States), Tech. Rep., 2021.

[67] L. E. Asp, K. Bouton, D. Carlstedt, *et al.*, "A structural battery and its multifunctional performance," *Advanced Energy and Sustainability Research*, vol. 2, no. 3, p. 2 000 093, 2021.

[68] F. Danzi, R. M. Salgado, J. E. Oliveira, A. Arteiro, P. P. Camanho, and M. H. Braga, "Structural batteries: A review," *Molecules*, vol. 26, no. 8, p. 2203, Apr. 2021, ISSN: 1420-3049. DOI: 10.3390/molecules26082203. [Online]. Available: http://dx.doi.org/10.3390/molecules26082203.

[69] L. E. Asp, M. Johansson, G. Lindbergh, J. Xu, and D. Zenkert, "Structural battery composites: A review," *Functional Composites and Structures*, vol. 1, no. 4, p. 042 001, 2019.

[70] D. Carlstedt, "Computational modelling of structural battery composites," Ph.D. dissertation, Chalmers Tekniska Hogskola (Sweden), 2022.

[71] S. C. Roberts and G. S. Aglietti, "Structural performance of a multifunctional spacecraft structure based on plastic lithium-ion batteries," *Acta Astronautica*, vol. 67, no. 3, pp. 424–439, 2010, ISSN: 0094-5765. DOI: https://doi.org/10.1016/j.actaastro.2010.03.004. [Online]. Available: https://www.sciencedirect.com/science/article/pii/S0094576510000846.

[72] F. Gasco and P. Feraboli, "Manufacturability of composite laminates with integrated thin film li-ion batteries," *Journal of Composite Materials*, vol. 48, no. 8, pp. 899–910, 2014. DOI: 10.1177/0021998313480195. eprint: https://doi.org/10.1177/0021998313480195. [Online]. Available: https://doi.org/10.1177/0021998313480195.

[73] S. M. Shalouf, J. Zhang, and C. H. Wang, "Effects of mechanical deformation on electric performance of rechargeable batteries embedded in load carrying composite structures," *Plastics, Rubber and Composites*, vol. 43, no. 3, pp. 98–104, 2014. DOI: 10.1179/1743289813Y.0000000064. eprint: https://doi.org/10.1179/1743289813Y.0000000064. [Online]. Available: https://doi.org/10.1179/1743289813Y.0000000064.

[74] P. Ladpli, R. Nardari, F. Kopsaftopoulos, and F.-K. Chang, "Multifunctional energy storage composite structures with embedded lithium-ion batteries," *Journal of Power Sources*, vol. 414, pp. 517–529, 2019, ISSN: 0378-7753. DOI: https://doi.org/10.1016/j.jpowsour.2018.12.051. [Online]. Available: https://www.sciencedirect.com/science/article/pii/S0378775318314022.

[75] J. Wolfenstine, W. Go, Y. Kim, and J. Sakamoto, "Mechanical properties of nasicon: A brief review," *Ionics*, vol. 29, no. 1, pp. 1–8, 2023.

[76] J. Miao, C. Yu, J. Xia, *et al.*, "New nasicon-based all-solid-state reference electrode towards a ph sensor for the electrochemical measurement of harsh environments," *Ionics*, vol. 28, no. 5, pp. 2437–2445, 2022.

[77] X. Yu and A. Manthiram, "Sodium-sulfur batteries with a polymer-coated nasicon-type sodium-ion solid electrolyte," *Matter*, vol. 1, no. 2, pp. 439–451, 2019.

[78] T. B. Salgueiro, "All solid state sodium-ion batteries with nasicon-type materials: Electrolyte and cathode integration," Ph.D. dissertation, 2023.

[79] S. Saffirio, M. Falco, G. B. Appetecchi, F. Smeacetto, and C. Gerbaldi, "Li1.4al0.4ge0.4ti1.4(po4)3 promising nasicon-structured glass-ceramic electrolyte for all-solid-state li-based batteries: Unravelling the effect of diboron trioxide," *Journal of the European Ceramic Society*, vol. 42, no. 3, pp. 1023–1032, 2022, ISSN: 0955-2219. DOI: https://doi.org/10.1016/j.jeurceramsoc.2021.11.014. [Online]. Available: https://www.sciencedirect.com/science/article/pii/S0955221921008128.

[80] *CR2032, CR2025, CR2016, CR2430 Coin Cell Case Sets (SS304)*, https://www.landtinst.com/cr2032-cr2025-cr2016-cr2430-coin-cell-case-sets-ss304/, Accessed on July 15, 2023, 2023.

[81] Q. Zhao, W. Yang, Q. Zhang, *et al.*, "Facile synthesis of pure na3v2 (po4) 3 powder via a two-stage carbothermal reduction strategy," *Journal of Sol-Gel Science and Technology*, vol. 103, no. 1, pp. 205–213, 2022.

[82] I. Hasa, *How do i determine the energy density (wh/kg) of the li ion battery?* Dec. 2015.